NASA CR-156641

(NASA-CR-156641) RADAR SYSTEMS FOR A POLAR MISSION, VOLUME 3, APPENDICES A-D, S, T Final Report (Kansas Univ.) 143 p HC A07/MF A01 CSCL 17I

N78-10345

Unclas G3/32 52326

[redacted]

THE UNIVERSITY OF KANSAS CENTER FOR RESEARCH, INC.
2291 Irving Hill Rd.—Campus West Lawrence, Kansas 66044

THE UNIVERSITY OF KANSAS SPACE TECHNOLOGY CENTER
Raymond Nichols Hall
2291 Irving Hill Drive—Campus West Lawrence, Kansas 66045
Telephone:

RADAR SYSTEMS FOR A POLAR MISSION
FINAL REPORT

Remote Sensing Laboratory
RSL Technical Report 291-2
Volume III

(This Volume contains Appendices A-D and S-T. Appendices D, S, and T should be considered as addenda to Volume IV of TR 295-3, "Radar Systems for the Water Resources Mission - Final Report," CONTRACT NAS 5-22384, which was published in June, 1976.)

R. K. Moore
J. P. Claassen
R. L. Erickson
R. K. T. Fong
B. C. Hanson
M. J. Komen
S. B. McMillan
S. K. Parashar

June, 1976

Supported by:
NATIONAL AERONAUTICS AND SPACE ADMINISTRATION
Goddard Space Flight Center
Greenbelt, Maryland 20771
CONTRACT NAS 5-22325

THE UNIVERSITY OF KANSAS SPACE TECHNOLOGY CENTER
Raymond Nichols Hall
2291 Irving Hill Drive—Campus West Lawrence, Kansas 66045

Telephone:

STATE OF THE ART — RADAR MEASUREMENT OF SEA ICE

RSL Technical Report 291-1
Remote Sensing Laboratory

S. K. Parashar

December 1975

Supported by:

NATIONAL AERONAUTICS AND SPACE ADMINISTRATION
Goddard Space Flight Center
Greenbelt, Maryland 20771

CONTRACT NAS 5-22325

TABLE OF CONTENTS

	Page
ABSTRACT	ii
1.0 INTRODUCTION	1
2.0 CHARACTERISTICS OF SEA ICE	2
2.1 Formation of Sea Ice	2
2.2 Classification of Sea Ice Forms	4
2.3 Physical Properties	5
2.3.1 Salinity and Temperature Profiles	5
2.3.2 Surface Roughness	7
2.4 Electrical Properties of Sea Ice	7
3.0 SEA ICE PARAMETERS OF INTEREST	9
3.1 Utility of Radar Systems	10
3.2 Imaging Radar (SLAR)	10
4.0 STATE OF THE ART — RADAR MEASUREMENT OF SEA ICE	11
5.0 SPECIFICATION OF PARAMETERS FOR ICE MAPPING RADAR	19
6.0 CONCLUSIONS AND RECOMMENDATIONS	23

ABSTRACT

A review of the state of the art and radar measurement of sea ice indicates that imaging radar systems have demonstrated the ability to observe many useful parameters of sea ice. Many workers in North America and the U.S.S.R. have reported success in monitoring such features of sea ice as concentration, floe size, leads and other water openings, drift, topographic features such as pressure ridges and hummocks, fractures, and a qualitative indication of age and thickness. Scatterometer measurements made north of Alaska show a good correlation with a scattering coefficient with apparent thickness as deduced from ice type analysis of stereo aerial photography.

Although the information on frequency dependence of sea ice radar return is meager, indications are that frequencies from 9 GHz upward seem to be better for the purpose than the information gathered at 0.4 GHz by a scatterometer. Some information indicates that 1 GHz is useful, but not as useful as higher frequencies. Either form of like-polarization can be used and it appears that cross-polarization may be more useful for thickness measurement. Resolution requirements have not been fully established, but most of the systems in use have had poorer resolution than 20 meters.

The radar return from sea ice is much different than that from lake ice, but the only quasi-operational systems that have been reported are the sea ice work by the U.S.S.R. and the lake ice work by NASA Lewis Research Center.

State of the Art — Radar Measurement of Sea Ice

by

S. K. Parashar

1.0 INTRODUCTION

The first attempt to map sea ice by a side-looking airborne radar (SLAR) was made in the early 1960's when U.S. Army Cold Regions Research and Engineering Laboratory (CRREL) conducted experiments over the Arctic pack ice by utilizing the Westinghouse AN/APQ-56 radar system. Since then a number of studies have been especially directed towards radar measurement of sea ice. It is largely through such efforts that the ability of radar to map sea ice has been demonstrated to the point of practicality. Studies to date have proven the capability and utility of radar to measure and discriminate sea ice, but these studies have helped little in the understanding of the physical phenomenon of radar return from sea ice. Past studies have also lacked in producing optimum design criteria for future operational radar systems of general utility. These drawbacks in most of the past research efforts have been largely due to the inability to collect complete "ground truth" information along with the experimental radar data. Because of this it never had been possible to properly correlate radar measurements with the sea ice parameters with a high degree of confidence. There is also a lack of even qualitative experimental data available corresponding to different frequencies, polarizations, and angles, yet this is needed in the design of future experiments and systems. On the other hand, a complete understanding of the physical phenomenon and a knowledge of the optimum system parameters is not really essential for the design of an operational system. This has been demonstrated by the Russians who are already using the side-looking airborne radar (SLAR) "Toros" for operational ice surveillance.

The current state of the art in radar measurement of sea ice is presented in this report. This is achieved through a thorough review of the past studies, both experimental and theoretical. An attempt is made to specify design parameters for future operational systems. Also included in the report is a section on formation of sea ice, on physical and electrical properties of sea ice, and on sea ice parameters of

interest. This material is included here with the hope that it will help the reader to understand the nature and complexity of the problem. In the final section recommendations are made for the need to conduct future experiments.

2.0 CHARACTERISTICS OF SEA ICE

The two major forms of ice in the Arctic and Antarctic regions of the oceans are sea ice and glacier ice. Glacier ice is formed on the land and is a fresh water structure. Glacier ice breaks away into the ocean and is found in the form of icebergs or ice islands. Sea ice is formed from sea water which contains salt. The properties of sea ice and glacier ice are thus different. Fresh-water ice formed in the rivers may also be found in the ocean.

The physical and electrical properties of sea ice alone are discussed in this section. Also included here is a section on the formation of sea ice.

2.1 Formation of Sea Ice

The formation of sea ice is a complex process and depends on a number of factors. The main factors which influence the formation of sea ice are the brine content of the surface water (surface salinity, density of brine in the water), the vertical distribution of the salinity, surface temperature, and the depth of water. The other factors which influence the formation of sea ice are wind, currents, sea state, and the intensity or rate of cooling (16).

Sea ice starts to form earlier on the surface of shallow than on deep water, so under similar conditions the ice begins to form near the coast first. Water with a density of brine greater than 24.7 percent has to be cooled to lower temperatures, from top to bottom, than the normal freezing temperature of water before the surface starts freezing. The temperature of maximum density in sea water with a salinity of less than 24.7 percent lies above the freezing temperature. The temperature of maximum density in pure water is $+3.98^{\circ}$ C. Thus, when a layer of sea water with a salinity of less than 24.7 percent is subjected to cooling, the density at the surface increases resulting in free convection. As water is further subjected to cooling, this convection continues until the temperature of maximum density of the convective column is reached. The amount of brine present in water only affects the initial

independent of the salinity of the water. The process of freezing can be delayed if the winds produce ocean currents which carry the warmer water to the surface.

The first sign of freezing varies according to different conditions to which the water is subjected. A calm sea surface subjected to rapid cooling results in the formation of small, needle like crystals. According to Weeks and Assur (31), the first crystals of pure ice to form are minute spheres which rapidly change their shape to circular disks. After a disk has grown to a critical diameter - which is dependent on the salinity - form of the disk becomes unstable and it changes to a dendritic hexagonal star (31). The critical diameter for these disks is on the order of 2 to 3 mm for fresh water but decreases with increasing salinity. These crystals grow rapidly and close together to form a more or less uniform sheet of ice, known as young ice.

On the other hand, when waves or strong currents disturb the sea surface, the first sign of freezing is an oily, opaque appearance of water. This is known as grease ice. Upon further freezing, grease ice develops into nilas or ice rind. This development again depends on wind exposure, waves and salinity. Nilas appear as an elastic crust with a matte surface; whereas ice rind has a brittle, shiny crust.

At this stage, except in wind sheltered areas, the thickening ice usually separates into masses as a result of the irregular motion of the surface water. The freezing occurs in separate centers from which it spreads outwards, forming circular flat disks with raised edges. These disks are 1 to 3 inches in diameter and this type of ice is called pancake ice. When freezing continues because of continued low temperatures, the cake pieces freeze together,after repeated breaking from continued motion and from chafing and collisions, to form a continuous sheet. This sheet of ice is normally less than one foot thick. The thickness of ice may grow to four or five inches within 48 hours, after which the growth is slower.

Under the influence of wind, currents, waves and pressure the sea ice may break up and drift from its original location to disperse in some regions and crowd in others. Because of this shifting of ice, pressure may cause the ice to pile up as ridges and hummocks. Another effect of pressure; the overriding of one piece onto another, is known as rafting. Rafting causes the ice thickness to become double that of the original piece. According to Weeks and Assur (31), the main body of an ice sheet grows in a columnar form with vertical ice crystals. The orientation of the crystallographic c-axis of the ice crystal is perpendicular to the growth axis but otherwise random. During the growth of the sea ice, the impurities in the form of brine are partially rejected to the water underneath. That is why the salinity of sea ice is

always less than the salinity of the original sea water from which it was formed. The distribution of impurities such as brine pockets and air bubbles has some effect on electrical and mechanical properties of sea ice.

Sea ice seldom becomes more than two meters thick during the first winter, but may assume far greater vertical dimensions because of piling-up of broken ice in the form of hummocks (5). In the spring and summer, snow cover and sea ice start melting. This continuing thawing produces passages and holes in which the surface water drains. In the next winter, this ice again starts freezing, growing to a thickness of more than two meters. It may attain greater thickness through ridges and hummocks. Thus, first year ice (ice of one winter's growth) is always less thick than multi-year ice (ice of more than one winter's growth which has gone through at least one summer's melt). First year sea ice is more salty than multi-year sea ice. First year sea ice, which is less than one year old, melts more readily than old ice.

2.2 Classification of Sea Ice Forms

There are several systems of classification of ice forms. The most widely used system is the terminology suggested under the auspices of the World Meteorological Organization (WMO). Sea ice can be classified according to age, concentration, and the way it is formed. Some of the terms are described below:

New Ice: A general term for recently formed ice, which includes fragil ice, grease ice, slush, and slinga. These types of ice are composed of thin pointed ice crystals which are only weakly frozen together and have a definite form only while they are afloat.

Nilas: A thin elastic crust of ice, easily bending on waves and swell and under pressure, thrusting in a pattern of interlocking "fingers" known as finger rafting. It has a matte surface and is up to 10 cm thick.

Young Ice: Ice in the transition stage between nilas and first-year ice, 10-30 cm in thickness.

First-year Ice: Sea ice of not more than one winter's growth developing from young ice and 30 cm - 2 m in thickness.

Old Ice or Multi-year Ice: Sea ice which has survived at least one summer's melt and includes second-year ice. It is up to 3 m or more thick with most topographic features smoother than on first-year ice. The ice at the top is almost salt free.

Concentration: The concentration of sea ice can be described in terms of the ratio in tenths of the sea surface actually covered by ice to the total area of sea surface (both ice covered and ice-free) at a specific location or over a defined area.
Floe: Any relatively flat piece of sea ice 20 m or more across in horizontal extent.
Polynya: Any non-linear shaped opening enclosed in ice.
Lead: Any fracture or passage-way through sea ice which is navigable to surface vessels.
Open Water: A large area of freely navigable water in which sea ice is present in less than one-tenth concentration.

2.3 Physical Properties

2.3.1 Salinity and Temperature Profiles

Sea ice differs from fresh water ice in that it has impurities contained in its ice matrix. The impurities present are in the nature of liquid brine inclusions and are commonly called brine pockets of sea ice (31). The amount of salt or the percent brine volume initially trapped in the sea ice is dependent on the salinity of the original water and the rate of cooling. More brine is trapped if the water is cooled rapidly. Ice crystals can be readily distinguished from the brine pockets and normally have a platty substructure with brine pockets located along it.

The amount of brine present at a given temperature can be found from the phase diagram given in Figure 1. A decrease in temperature results in the decrease of the relative volume of brine. Sea ice at equilibrium at a given temperature consists of pure ice and brine of a specified composition as shown in the phase diagram (Figure 1).

Apart from brine the other component of the void volume of air present in the sea ice and to use the brine folume computed from the phase diagram.

The equations for determining the brine volume of sea ice from the phase diagram as given by Frankenstein and Garner (13) are as follows:

$$V_b = S\left(\frac{52.56}{T} - 2.28\right), \quad -0.5^{\circ} \leqslant T \leqslant -2.06\ ^{\circ}C$$

$$V_b = S\left(\frac{45.917}{T} + 0.930\right),\ -2.06^\circ \leqslant T \leqslant -8.2^\circ\ C$$

$$V_b = S\left(\frac{43.795}{T} + 1.189\right),\ -8.2^\circ \leqslant T \leqslant -22^\circ\ C$$

where,

V_b = brine volume in parts per thousand

S = salinity of ice in parts per thousand

T = absolute value of the ice temperature in $^\circ C$.

The following equation can be used for the cases in which less accuracy is desired:

$$V_b = S\left(\frac{49.185}{T} + 0.532\right),\ -0.5^\circ \leqslant T \leqslant -22.9^\circ\ C.$$

The standard error and the correlation coefficients are 0.1545 and 0.9995 respectively.

The typical salinity profiles for different thicknesses of sea ice as given by Weeks and Assur (31) are shown in Figures 2 and 3. As seen from these figures, sea ice is quite salty when it is first formed; the salinity of a given segment of ice gradually decreases with time, and the vertical salinity profile at any given time has a characteristic 'c' shape. The low values of the salinity at the top of the 200 cm profile indicate that it has been through a summer's melt. The salinity and temperature profiles for both first year and multi-year ice as measured experimentally by McNeill and Hoekstra (22) are shown in Figures 4 and 5 respectively. Cox and Weeks (8) pointed out that the salinity distribution in multi-year ice is dependent on the ice topography and cannot be adequately represented by a single average profile. From the measurements it was found that there existed distinct differences between the profiles obtained from hummocks and depression (Figures 6 and 7).

The relationship between the average salinity $\bar{S}$ of the ice, and the ice thickness h can be represented by the two linear equations for the measurements made from cool sea ice at the growth season

$$\bar{S} = 14.24 - 19.39h, \quad h < 0.4m$$
$$S = 7.88 - 1.59h, \quad h > 0.4m$$

The linear relationship for the data collected during the melt season is given by

$$\bar{S} = 1.58 + 0.18h$$

2.3.2 Surface Roughness

Thick first year ice is generally rougher than the multi-year ice. The major difference is due to the fact that the multi-year ice has undergone at least one cycle of erosion whereas the first year ice has not. The deterioration effects on the sea ice surface caused by the ice having gone through a summer's melt (5) are the following: a) the weathering, rounding and subdividing of normally sharp, high-standing pressure ridges; b) the ablation of small pressure ridges through weathering, creating isolated hummocks on the ice; c) the creation of fresh water puddles or melt pools and their subsequent refreezing and d) the presence of a subdued drainage pattern on the ice surface.

There is a lack of general quantitative information available on the surface roughness parameters of sea ice. No such information is available on the micro-wavelength scales. This information is needed to compute radar return from sea ice utilizing theoretical scattering models. A very general idea of the roughness parameters and the spatial variations in roughness (such as size, number and frequency of ridges) can be obtained from (37), (38), and (39).

2.4 Electrical Properties of Sea Ice

It is evident from above that the physical properties of sea ice change significantly with time and age. The physical properties in turn determine and influence the electrical properties of sea ice. The radar scattering from sea ice depends on the surface roughness, subsurface structure, and electrical properties. The electrical properties of pure ice and freshwater ice have been investigated by many workers (Auty and Cole, 1952 (7); Cummings, 1952 (9); Dorsey, 1940 (10); Murphy, 1934 (24); and are quite well established. The most interesting properties of pure ice are its high static dielectric constant (about 100) and its long relaxation time (about 10^{-4} seconds).

For frequencies much greater than 1 MHz, the dielectric constant drops to about 3. The dielectric behavior of ice and water as a function of frequency is given in Figure 8.

As is evident from section 2.2 the physical properties of sea ice are different from those of pure ice because of the presence of impurities in the sea ice. These impurities are in the nature of brine pockets and air bubble (Fukino (14), Addison (1), Hoekstra (17)). A number of different workers have tried to measure the dielectric properties of sea ice experimentally by means of cored samples. The measurements made by Fukino (14) are in the frequency range 100 Hz to 50 kHz in various temperature ranges. Addison and Pounder (3) measured the electrical properties of sea ice in the frequency range from 20 Hz to 100 MHz. The electrical properties of sea ice presented by Wentworth and Cohn (32) are in the frequency range of 0.1 to 30 MHz and those presented by Addison (2) are 20 Hz to 100 MHz. Ragle, et al., (24a) have quoted some electrical properties of sea ice above 100 MHz. It was only in 1971 that an attempt was made by Hoekstra and Cappillino (17) to determine the complex dielectric constant of sea ice in the frequency range from 100 MHz to 23 GHz. Byrd, et al., (7) have reported the variation of loss tangent with salinity in natural sea ice, at the frequency of 34 GHz.

It is evident from above that little data about the electrical properties of sea ice are available. There is clearly a need to make more measurements, especially in the frequency region about 100 MHz. To fully use the theoretical radar scattering models, the knowledge of electrical parameters is essential in the microwave range of the frequency spectrum (33).

The electrical properties of sea ice as reported in the literature have one feature in common: the complex dielectric constant of sea ice is dependent on both temperature and brine volumes. The brine volume in turn depends on salinity and temperature. Salinity and temperature change with thickness and depth of sea ica, so the electrical properties of sea ice are a function of ice thickness and depth. The electrical properties of sea ice as reported by Hoekstra and Cappillino (17) are presented here.

In Figure (9a) the dielectric loss of sea ice samples as a function of temperature for different salinity is given at a frequency of 400 MHz. The dielectric loss at a frequency of 9.8 GHz is given in Figure 9b. The dielectric loss and dielectric constant at a frequency of 2.3×10^{10} Hz are given in Figure 9c. As is evident from these figures the dielectric loss of sea ice increases with an increase in salinity and temperature. The dielectric loss is more at 400 MHz than at 9.8 GHz. The dielectric constant increases with an increase in the temperature. As a result electromagnetic waves at the same wavelength are liable to penetrate the first year ice less than multi-year ice. Also, in the winter the relative penetration of waves is going to be more than in summer because of lower temperatures and thus lower loss tangent.

The complex dielectric constant in general determines the strength of the scattered or reflected signal and the penetration or attenuation of the electromagnetic wave inside the medium. An attempt was also made by Hoekstra and Cappillino (17) to compute theoretically the dielectric properties of sea ice and the results reported are shown to be in general agreement with the experimental results in certain frequency ranges.

The dielectric constant of brine varies from 80 at 10^8 Hz to approximately 34 at 2.3×10^{10} Hz. The dielectric constant of pure ice in this frequency range remains at about 3.5. Thus, the dielectric constant of inclusions (brine) is several times larger than the dielectric constant of the continuum (ice). The dielectric constant of the mixture thus depends on the amount and the shape of the inclusions.

It is hoped that the electrical and physical properties of sea ice presented above will help the reader to interpret the radar data from sea ice and to understand the nature of radar return.

3.0 SEA ICE PARAMETERS OF INTEREST

The two parameters of interest in the study of ice cover of the Arctic ocean are the variations of ice thickness and the roughness or topographic relief of the ice cover. The distribution of ice thickness in the Arctic ocean is needed to correctly model the mechanics of ice interaction so that the drift and the dynamics of Arctic ice pack can be predicted (40). Measures and variations of ice thickness are also needed to accurately calculate the mass budgets of the ice packs as an input to

climatic models (41). In addition, accurate information on variations in ice thickness is required for a wide variety of applications and operations such as those involving ice-breaking by ships and the transport of heavy equipment over ice. This information will help in economical route selection and safe load predictions.

The knowledge of the surface roughness characteristics is important for determining the momentum the wind imparts to the ice cover. This momentum is usually the most important driving force in the ice drift. Recently a program is underway to develop a large air cushion vehicle to traverse the Arctic pack. In the design of such a system the knowledge of the surface roughness is necessary (39).

Sea ice covers a large area. Thus, the usual sure method of determining sea ice thickness and roughness by direct measurement is extremely time-consuming, expensive and has several other limitations. A need also exists to know these parameters on a continuous and regular basis. This can only be provided by means of remote measurement techniques.

3.1 Utility of Radar Systems

Large areas of sea ice have been mapped in the past primarily by the use of conventional photographic methods from aircraft using black and white, color, and infrared films. More recently space photography has also been used. It was demonstrated by Anderson (5) that low-altitude photographs can be interpreted and different types of sea ice can be identified. By identifying different ice types a rough estimate of the thickness of ice can be obtained. It is also possible to obtain a crude measure of surface roughness from stereoscopic aerial photography. The fact remains that photographic methods are not reliable in bad weather conditions and lack of enough incident light. This is a great handicap as the regions of large sea ice cover suffer from uncertain weather conditions throughout the year and are in darkness for many months. As the performance of radar systems is not affected by the bad weather conditions and lack of incident light, these systems hold a great potential for remote measurement of significant parameters of sea ice.

3.2 Imaging Radar (SLAR)

Side-looking airborne imaging radar (SLAR) is designed to "look" to the side to permit better resolution than otherwise possible. It is an active system as it transmits

its own electromagnetic energy and measures the energy reflected back from a target. The SLAR transmits a beam in a fixed direction perpendicular to the line of flight. Coverage of ground features is accomplished by the forward motion of the vehicle carrying the radar, which causes successive transmitted beams to cover new areas. These continuous line scans result in a composite coverage of a wide swath of the surface. The energy reflected back to the radar from the targets is recorded on a photographic film. The amount of backscatter returned by ground features is determined by the radar frequency, angle of incidence, surface roughness on the radar wavelength scale, dielectric properties of the target, and aspect angle.

The ability of a radar to image an individual target depends on the range to the target, the radar backscatter of the target and the sensitivity of the receiver. The ability of radar to discriminate two closely spaced targets is a function of the system resolution, since resolution in general is defined as the ability to distinguish between two adjacent objects on the ground. In the imaging radar each area of the size of the resolution cell produces one point on the image.

In the noncoherent, real aperture, radar system, the resolution in the across-track is achieved by transmitting a short pulse. Shorter pulses mean shorter resolution cells in the across-track direction. In the along-track or azimuth direction the resolution is achieved by the antenna beamwidth. The narrower the beamwidth, the shorter is the size of resolution cell. A narrower beamwidth can be obtained by increasing the size of the antenna or increasing the frequency. In the synthetic-aperture radar the length of the antenna is increased synthetically. Azimuth resolution which is equal to half the antenna length and independent of the wavelength can in theory be obtained by synthetic-aperture techniques. Synthetic-aperture techniques will definitely have to be used to obtain fine resolutions from satellite altitudes (Skolnik, 26)).

The image produced by a radar is somewhat similar, although not identical to an optical photograph. This difference lies because of the use of longer wavelengths in the case of radar, and because distortions have different causes.

4.0 STATE OF THE ART — RADAR MEASUREMENT OF SEA ICE

SLAR was developed in the early 1950's primarily for military use. It was first used to map sea ice in the early 1960's when the U.S. Army Cold Regions Research and

Engineering Laboratory (CRREL) conducted experiments over the Arctic pack ice utilizing the existing AN/APQ-56 radar system. The capability of a radar imager to map large areas of sea ice in short periods of time was shown then. It was shown by Anderson (4) through the analysis of the obtained images that major sea ice types can indeed be identified on the radar imagery. He showed that the sea ice imagery is interpretable to the extent that winter ice (only one season old) can be differentiated from the thicker, older, polar ice. The concentration and distribution of sea ice can also be determined. The rough-surfaced polar ice, generally from 2.5 to 4 meters thick, with pressured ice areas being much thicker, gave a light tone on the images. The relatively dark-toned areas consisted of relatively smooth refrozen leads and polynyas with younger, thinner ice. Open water gives still darker tones. This experiment was conducted in winter. No quantitative analysis which would help in the design of future radar systems was done by him. The AN/APQ-56 radar system used in collecting the data is a real aperture system operating at 8.6 mm wavelength.

It is pointed out by Bradie (42) that one hindrance to interpretation of ice features on radar is the great tonal variance between open water, young ice, grease ice and slush ice.

During September 1969, the U.S. Coast Guard, in conjunction with the Manhattan tanker test, conducted ice-mapping experiments in the Northwest Passage using a modified Philco-Ford AN/DPD-2 SLAR, operating in the Ku-band (16.5 GHz frequency). In addition to the research effort to determine its feasibility as an ice observational technique, the SLAR was also used as a routine aid to the Manhattan. This experiment was conducted to assess the performance of SLAR in mapping and identifying sea ice. As shown by Johnson and Farmer (18), the results of this experiment indicated that SLAR can readily be used to detect ice concentration, floe size and number, and water openings.

It is also possible to identify, through careful image interpretation, ice age, ice drift, surface topography, fractures, and pressure characteristics. Young ice gives even dark tone and may have bright straight lines indicating ridging. Dark-gray to black and smooth tone is given by first year ice and ridging indicated by light straight lines. Second year ice gives even graytone and may have ridging. Ridges are more jagged than in first year ice and also higher than first year ice. An even tone is given by relatively smooth topography. Multi-year ice gives mottled tones of gray probably caused by high weathered ridges and interconnecting melt holes. Old multi-year drainage

channels can also be traced sometimes. Dark areas of no radar return signify presence of open water. The parameter which can be most easily determined on the radar imagery is ice concentration along with the size of floe. The most difficult characteristic of the ice to determine from SLAR imagery, other than its actual thickness, is probably its categorical age. Another important feature that can be interpreted is whether or not ice is or has been under pressure. It is also possible to identify topographic features such as pressure ridges, hummocks, and cracks.

It is pointed out by Johnson and Farmer (18) that the all-weather, day-night operational capability and the broad areal coverage provided by SLAR make it an effective means of observing sea ice characteristics and for many purposes it provided observations superior to information obtained by a visual ice observer. The same experimental data was used to determine the drift of sea ice. The results were presented by Johnson and Farmer in another paper (19) and reveal that single ice floes, as well as general ice masses, could be tracked to an accuracy of nearly one nautical mile. In the study conducted at Biache by Bradie (43) of the SLAR imagery obtained in the Mahnattan experiment, it is pointed out that major ice types, cracks and leads can be identified.

Ketchum and Tooma (20) presented the results obtained from the radar experiment conducted by the U.S. Naval Oceanographic Office during April, 1968. This experiment was conducted over the sea-ice fields north of Alaska; the four-frequency radar system of the Naval Research Laboratory was used. The results presented (20) indicate that the shorter-wavelength X-band radar appears to have the greatest potential for sea ice study when more definitive information such as mapping, distributions of stages of ice development, and fracture pattern analysis is required. The X-band radar imagery can be used to discriminate old (second year ice) from the young ice, the old ice giving higher return or backscatter. Young ice (first year ice and younger) is smooth and could not be discriminated from open water in this experiment. Pressure-ridge patterns could sometimes be identified when they were present on a low-backscatter background. There were no notable differences between horizontally and vertically polarized X-band imagery. The potential value of L-band radar is not for mapping the aerial distribution for surface topography. Various ice types do not give discriminatory graytone at this wavelength, whereas the more topographic features such as ridges and hummocks can be discriminated. Only the most prominent features, such as large floes and fractures, could be identified on the P-band (400 MHz) radar imagery. It was pointed out that for

motion studies in which reidentification of specific features is necessary, the X-band or preferably K-band radars, would be the best choice. This was the only known multi-frequency study of radar images of sea ice.

In studies conducted by Raytheon company (27, 29) and Photographic Interpretation Corporation (28), it was shown that SLAR is a useful tool to map changing nature of sea ice. Data acquired by the U.S. Coast Guard of the Baffin Bay and Beaufort Sea areas in February and March of 1971 were analyzed by Raytheon Company (29). Major ice types such as new ice, young, ice, first-year ice and multi-year ice could be identified on the imagery. It was not possible to make a finer delineation of the categories. SLAR imagery did permit the determination of surface configuration and it was much easier to delineate edge of the floe on the SLAR imagery than the photo. The effects of snow cover on sea ice could not be determined. Sea ice images did not exhibit any masking because of snow cover except for the return from ridges. The identification of the ice age could be accomplished, whether covered by thick or thin ice cover.

The same data were also analyzed by Photographic Interpretation Corporation (27). In their report an attempt was made to determine winter sea-ice parameters and to compare winter sea-ice pattern "keys" with the summer pattern "keys". It was pointed out that interpreters must not rely entirely on radar keys for their work but should properly assess all of the imagery parameters such as tones, textures, spatial relationships, imagery limitations, ice environment and season, and ice stress patterns. By doing this a very detailed description of sea ice can result and the predictions about the ice can be made with more reliability. Multi-year ice can be separated from other ice types more rapidly on the radar image than through use of aerial photos and stress zones can also be quickly delineated. Snow cover does not present any detrimental masking effect of sea ice conditions on the Ku-band radar imagery.

Glushkov and Komarov (15) and Loshchilov (21) demonstrated the use of SLAR imagery (wavelength = 20 mm) obtained from the TOROS* in determining the ice conditions and ice drift. The use of optical techniques to analyze the sea ice imagery was reported by Zagorodnikov and Loshchilov (34).

---

*The TOROS was developed for ice reconnaissance use. The word "toros" is Russian for "ice ridge".

The TOROS experiments were started in 1968 and have been carried out extensively since that time. Moore (45) was shown ice images from various seasons and multi-year coverage of ice islands during a visit to the Arctic and Antarctic Institute in Leningrad in June, 1973. At that time he was shown an ice coverage map of the north coast of the USSR prepared in May, 1973, for the use of shipping. He was led to believe that the TOROS was by that time coming into operational use for mapping ice to permit optimal ship routing for convoys along the USSR's northern sea route.

To evaluate the capabilities of a SLAR system as an ice reconnaissance tool, a SLAR test project was organized and carried out in April, 1972 by the Canadian Department of National Defence and the Atmospheric Environment Service of Canada. The SLAR system used for the experiment was a Morotola AN/APS94D unit operating at a wavelength of 3.2 cm. The results of the experiment are presented in a report by the Canadian Department of Atmospheric Environment (35). The results indicate that it is generally possible to identify open water by low radar returns and uneven boundaries with surrounding ice that show good contrast in tone. It is difficult to distinguish new ice from open water because the surface is generally smooth and the profile of any rafting present is low. Variation in returns from large floes is apparent in the larger scale imagery. It is possible to determine floe size and concentration and to distinguish first year ice, fast ice and multi-year ice. Floes showing good radar returns can be classed as rough first year ice. Note that the AN/APS-94D has a resolution along-track of 7.5m/km and a swath to one side of 40 km. Thus, the resolution is crude at the far range, and the incidence angle is quite near grazing over much of the swath.

It is evident from the material presented above that a radar system is capable of remotely sensing sea ice. Despite this knowledge there is a lack of fundamental research in this area. No systematic studies for relating radar returns or backscatter to sea ice were undertaken until 1967. A joint mission over sea ice in the Arctic was conducted in May, 1967 by National Aeronautics and Space Administration (NASA), Navy Oceanographic Office, U.S. Army Cold Regions Research and Engineering Laboratory (CRREL), the Arctic Institute of North America, and the University of Kansas with the objective of verifying the ability of a 2.25 cm wavelength radar scatterometer to identify sea ice types. The reason for not using radar imagers was that a more quantitative

study of radar backscatter could be undertaken from scatterometer data since scatterometers permit more detailed observation of radar scattering behaviour than imagers. The radar scatterometer used is an instrument designed to measure the radar backscattering coefficient σ^o (radar cross-section normalized to the illuminated area) as a function of the illuminated incidence angle θ (angle measured from the vertical) and by design is a calibrated system (23). The radar return power and thereby the graytone on the radar image, is directly proportional to σ^o. σ^o is an important parameter in the design of a radar system and it depends on frequency, polarization, angle, and electrical and physical properties of the target such as complex electric permittivity, surface roughness and subsurface structure. All of the SLAR's in operation today are uncalibrated systems. As a result it is not possible to compare images obtained from two different systems or to compare images produced by the same system at different times. Moreover, it is impossible to obtain quantitative information which would help in the design of future systems. Because radar scatterometers are calibrated systems, the data obtained from them is of great value in understanding the nature of radar return from different targets and in the design of future systems.

An analysis of the scatterometer data obtained from the May, 1967 mission was carried out by Rouse (25). It was shown that a 2.25 cm wavelength scatterometer can be used to discriminate ice types. It was seen that multi-year ice gives higher return at all angles than the first year ice. Open water can be distinguished easily. This experiment was limited to a single frequency (13.3 GHz) and vertical polarization.

In April 1970, another experiment was conducted jointly by NASA, Naval Oceanographic Office, and the University of Kansas. This experiment was designated Mission 126 and was carried out in the vicinity of Pt. Barrow, Alaska. Large amounts of data were gathered by this mission so that a systematic study of radar return from sea ice could be undertaken. This study was conducted by Parashar (33). The ability of radar to discriminate sea ice types and their thickness was presented. Radar backscatter measurements at 400 MHz (HH, VV, VH and HV polarizations) and 13.3 GHz (VV polarization) were analyzed in detail. The scatterometer data were separated into seven categories of sea ice according to age and thickness as interpreted from low-altitude stereo aerial photographs. There is a reversal of character of radar return from sea ice less than 18 cm thick at the two frequencies. Multi-year ice (sea ice greater

than 180 cm thick) gives strongest return at 13.3 GHz. First-year ice (30 to 90 cm thick) and open water give strongest return at 400 MHz. Open water can be differentiated at both the frequencies. Although 400 MHz is not found to be as satisfactory for ice identification as 13.3 GHz, combining a 13.3 GHz and a 400 MHz system definitely eliminates the ambiguity regarding very thin ice.

Four-polarization 16.5 GHz radar imagery was also analyzed. The results (33) show that open water and three categories of sea ice can be identified on the images. The results of the imagery analysis are consistent with the radar scatterometer results. There is some indication that cross-polarization return may be better in discriminating sea ice types and thus thickness, but the quality of the images was not sufficient to guarantee the validity of this conclusion.

An attempt was also made to formulate a theory for polarized radar backscatter cross-section σ^{o} for sea ice by taking into account the amount of brine entrapped, temperature, and surface roughness. The computed results from the theory are shown to be in general agreement with the experimental results.

Automatic classification techniques were applied to scatterometry data. Using the four categories (as in the SLAR analysis) 85 percent agreement can be achieved between the radar and stereo-photo interpretations.

A review of the material presented above shows that radar is indeed a valuable tool in the measurement of sea ice. Past research efforts have clearly demonstrated the ability and utility of radar to map the changing nature of sea ice. It has been shown that radar can be used for operational ice surveillance, and apparently the Soviet Union is using SLAR for this purpose. Despite numerous research efforts, however, there still exists a lack of information in terms of understanding the nature of radar return and optimum parameters for ice-mapping imaging radars. For example the optimum parameters such as frequency, polarization angle, and resolution for ice discrimination still need to be established. The effect of snow cover has to be ascertained completely. A general technique for interpreting sea-ice imagery and for identifying different important features needs to be formulated. A need also exists to evaluate different automatic classification techniques which will facilitate handling large amounts of sea-ice data. The changes in image because of changes in weather and/or seasonal conditions have still to be studied.

The current state of the art in the radar measurement of sea ice can be summarized as below:

1. Radar can be used to measure the following parameters of sea ice:

a. Concentration: It is most easily determined.

b. Floe Size: It can be readily observed.

c. Water openings: They are quite easily determined as black areas of no radar return.

d. Drift: It can be determined by the repeated radar coverage of the same area and by identifying similar features. Single ice floes, as well as general ice masses, can be tracked to an accuracy determined by repetition period, resolution, and navigational accuracy.

e. Topographic features: The ability to detect individual pressure ridges is limited by the sensor resolution. Pressure ridges are noted by their white or light gray linear images. Hummocks can be detected on good SLAR imagery.

f. Fractures: Fractures are quite often imaged as alternate dark and light returns, depending on their width and orientation to the radar beam. Careful scrutiny of the imagery is necessary when interpreting this feature.

g. Pressure: SLAR imagery can be used to interpret whether or not ice is or has been under pressure.

h. Ice age: It is probably the most difficult characteristic that can be determined from SLAR imagery. The resolution of the SLARs used previously generally restricts their ability to discriminate between individual minute surface features, such as puddles and drainage channels, that are characteristic of certain stages of development. However it is possible to determine categorical age by identifying certain other features such as size, shape, and texture of the imaged ice; its location as compared to the surrounding ice; place where imagery was taken and time of the year. It is also possible to discriminate and identify different ice types from the relative gray tones of the image. Normally at X-band and higher frequencies, multi-year ice gives the strongest return. New ice which is rough, sometimes gives as bright a return as given by multi-year ice, but it can be discriminated from multi-year ice because it does not have any sharp edges. More research is needed before a general set of guidelines can be developed for interpreting ice age or category age from the radar imagery. The effects of frequency, polarization, angle, polarization, resolution and seasonal variation have still to be fully understood.

i. Ice thickness: It is not possible to get a direct measure of the ice thickness from a radar image. It is possible, though, to get a rough measure of the ice thickness by associating a mean thickness with an ice category with brightness on a radar image or value of σ^o on scatterometer data. This can only provide a rough estimate but still is useful information. It is also possible to obtain an empirical relationship between the brightness on a radar image, or between σ^o on scatterometer data and ice thickness.

2. Frequency: X- or Ku-band appears to be best in discriminating sea ice types, at least on the basis of the few frequencies used to date. There is evidence, though, that a two frequency system may be best in delineating different ice types. Combining

a 13.3 GHz and a 400 MHz system definitely eliminates the ambiguity regarding very thin ice. There is a reversal of angular character of radar return from sea ice less than 18 cm thick at these two frequencies. The resolution achievable at a low frequency of 400 MHz may not be suitable for most purposes. The best frequency or combination of frequencies still needs to be established.

3. Polarization: There appears to be no difference between the like polarizations in their ability to discriminate sea ice, on the basis of limited evidence. There is some indication that cross-polarization may be better in discriminating sea ice types and thus thicknesses.

4. Resolution: No quantitative study has been undertaken to see the effect of resolution in discriminating ice type. All the systems used so far in the radar measurement of sea ice had different resolutions. The best resolution probably was on the order of 20 meters (DPD-2 system), with the exception of the single experiment with the NRL 4-frequency system.

5. Snow Cover: The masking effect of snow cover has still to be determined. There is a preliminary indication that the waves at K-band can penetrate snow cover so that they are not affected by it, which suggests that snow cover would not be a problem at lower frequencies.

6. Seasonal Variation: The changes produced in the appearance of ice on a radar image due to the seasonal variations have to be studied. Preliminary indication is that the same set of guidelines can be used in interpreting winter and summer radar imagery of sea ice.

7. Automatic classification of ice: It has been shown that automatic classification techniques can be used in discriminating sea ice types in analyzing scatterometer data. An agreement of about 85 percent has been achieved in identifying and classifying four categories of sea ice as established from stereo-photo interpretation. Such automatic classification schemes have yet to be tried on the radar images of sea ice. These classification techniques can also be used in establishing optimum discriminatory parameters such as frequency, polarization, and angles.

5.0 SPECIFICATION OF PARAMETERS FOR ICE MAPPING RADAR

In this section the parameters which can be specified from the past research efforts for ice mapping radars are identified. To design an optimum ice-mapping radar system, the

effect of polarization, frequency, and angle in discriminating sea ice has to be considered and clearly understood. This can be only achieved if the radar scattering data corresponding to different frequencies, polarizations, and angles are available. It is almost impossible to collect such a large amount of data.

Thus, it is desirable to have a scattering model which would predict the radar scattering at a particular frequency, angle, and polarization. Such an analytical scattering model was developed for sea ice by considering surface roughness, amount of entrapped brine, and temperature. The computed results obtained from this model have been shown to be in general agreement with the experimental results (33), but more research is required for testing the theoretical model. Theoretical models are helpful in the sense that they can be used in inter- or extra-polating experimental results and in understanding the nature of radar return.

Some of the parameters which are recommended are given below along with the reason for choosing them:

Frequency: X- or K-band appears to be the best choice for the frequency. Most of the radars in operation today operate at these bands. Radar imagery at these frequencies do provide sufficient information to delineate and identify major categories of ice. It may be difficult at these frequencies to identify surface patterns which generally aid the interpretation process. There should not be any masking effect of snow at this frequency. The utility of a two-frequency combination system should be explored. A suitable second frequency can be L-band, since this is easier to implement than P-band, and probably it exhibits the same reversal of thin ice return relative to Ku- and X-bands found at 400 MHz. More research is definitely required before an optimum frequency or a combination of frequencies can be selected; interpolation using a theory tested only at 13.3 GHz and 400 MHz is too risky to permit specifying what might happen, say, at C-band.

Polarization: There appears to be no difference in VV or HH (like) polarizations in their ability to discriminate ice types. There is some indication (33) that cross-polarized signals (VH or HV) may be best in discriminating ice types and thus sea ice thickness. This result could not be validated before (44) because of poor quality of radar images and lack of cross-polarized scatterometry data at the designed frequency. A preliminary analysis of the cross-polarized scatterometry data by the Canadian Center of Remote Sensing (44) indicated that it confirms that HV or VH polarization may be better than VV or HH polarization in discriminating sea ice. The final confirmation of this results must wait till the analysis of all the data is completed. More research is definitely required before the utility of cross-polarized signals in discriminating ice types is

clearly established. Since the cross-polarized signals are much weaker than like-polarized signals, more power would be needed with a cross-polarized system, so the benefits should be carefully evaluated.

Angles: There appears to be no indication from the past research efforts that one set of the angles normally used for SLAR is better than the other in discriminating ice types. Scatterometer data at 13.3 GHz (33) indicate that incident angles more than 20 degrees should be used.

Spatial Resolution and Scale: Most of the radar systems which have been used in the past to collect sea ice data have moderate resolutions upwards of 20 meters. The DPD-2 system used by U.S. Coast Guard has a spatial resolution of about 20 meters in both the along-track and the cross-track direction at mid-range. Johnson and Farmer (18) state that the resolution of SLAR generally restricts its ability to discriminate between individual minute surface features, such as puddles and drainage channels, that are characteristic and indicative of certain stages of development of ice growth. The ability of radar to map pressure ridges and fractures is also restricted by the resolution of the radar.

The type of resolution required depends on the purpose of the ice imagery. It is possible to examine sea ice on a variety of spatial scales that range over 10 orders of magnitude (36). In the smallest scale, the microscale, the effects of the growth conditions on the structure of resulting ice and the controlling effect of these structural variations on its small scale (< 10 m) property variation become important.

The micro-structural properties of the ice become of less importance as the scale length increases. These are replaced by effects produced by ensembles of ice features such as floes, leads and pressure ridges. These observations are considered on the meso-scale (100 m - 50 km). On the macroscale (> 100 km) remote sensing techniques can only be used to obtain random samples of the ice of interest or to prepare maps of general coverage.

When the ice imagery has to be used only for detecting open water or thin ice areas for navigational purposes, the resolution requirement needs to be established on the basis of smallest passage through which a ship can safely navigate. The resolution should be of the order of the width of the ship. On the other hand, long leads might be detected with poorer resolution if the ships involved were strong enough to penetrate narrow leads.

On the basis of the above discussion it is clear that the resolution required by an all-purpose ice mapping radar should be of the order of 100 m or better.

Dynamic range of σ^o: The mean σ^o vs. θ curve at 13.3 GHz, VV polarization, obtained from radar scatterometer measurements (33) made in NASA Mission 126 is shown in Figure 10. The solid line is the actual curve obtained and the vertical bar gives $\pm$ one standard deviation at each angle. As is evident from this figure, the value of σ^o did not decrease monotonically as the incidence angle increased and thus there are kinks in the curve. This could possibly be due to the antenna pattern or to sampling variability. A visually-smoothed curve is given by the dashed line. These same data were separated into 7 categories of sea ice according to thickness; category 1 being open water, category 2 being ice under 2 inches (5 cm) thick, category 3 being ice 2 - 7 inches (5-18 cm) thick, category 4 being ice 7 - 12 inches (18 - 90 cm) thick, category 5 being ice 1 - 3 feet (30 - 90 cm) thick, category 6 being ice 3 - 6 feet (90 - 180 cm) thick, and category 7 being ice 6 - 12 feet (180 - 360+ cm) thick. The σ^o vs. θ curve at 13.3 GHz, VV polarization for each of the seven categories is shown in Figure 10a. The maximum value of σ^o obtained was about 20 dB at 0 degrees (extrapolated from 5°) and minimum a value of -20 dB at 60 degrees. As is evident from these curves for a radar imager operating at angles above 30 degrees, a dynamic range of about 30 dB will be required.

σ^o vs. θ curves at 400 MHz, VV polarization for the same seven categories obtained from Mission 126 are shown in the Figures 11, 12 and 13. A dynamic range of about 30 dB would be required for a system operating at angles above 30 degrees. The mean of all categories is shown in Figures 14, 15 and 16.

σ^o vs. θ curves for each category at 13.3 GHz and 400 MHz frequency computed by using the theoretical model of (33) are shown in Figure 17, 18 and 19. Results obtained from the theoretical model show that the contribution to the value of σ^o at both 13.3 GHz and 400 MHz is more from the surface roughness term than from the inhomogeneity. The most dominant contribution at 13.3 GHz frequency at all angles is from the surface roughness. In the case of 400 MHz at angles above 40 degrees the inhomogeneity contribution becomes more significant. It is evident from Figure 9 that as the salinity and temperature increase the permittivity also increases thereby increasing the value of σ^o for ice having smooth surface.

Minimum Signal: The radar system should be sensitive enough to measure at least as small as -20 dB.

Gray-tone Resolution: In addition to having a good spatial resolution it is important to have a good gray-scale resolution. There is always a trade-off between the spatial resolution and gray scale. A combination of range and azimuth averaging of independent samples greatly improves the gray scale of an image. As the separation between different categories is not very great, a difference of at least 55 dB in the value of σ^{o} should be recognizable on the radar image. For a dynamic range of 30 dB that is about 60 different gray tones with a logarithmic receiver. More would be required with a linear receiver.

Frequency of Measurement: To fully utilize the radar images of sea ice from satellite, these should be at least obtained at a faster rate than what is provided by ERTS satellite. The period of coverage should be at least as often as six days. To be able to measure drift and the changing nature of ice it is important that a frequent coverage be provided. To keep shipping lanes open throughout the year a need exists to map the area used by ships as often as possible, so daily coverage is desirable.

6.0 CONCLUSIONS AND RECOMMENDATIONS

As is evident from the above, SLAR appears to be an excellent tool to map sea ice. Before an optimum ice imager of general utility can be designed, more research should be done. A need exists to conduct more experiments so that an optimum frequency or a combination of frequencies can be established. It is important that the utility of cross-polarized signals in discriminating ice types be explored further. The effect of snow cover and the variations in seasons need to be studied more. A need exists to develop automatic analysis or interpretation techniques which can handle large amounts of data. For frequenc radar images to be operationally useful, techniques for rapidly analyzing the data and presenting it in terms of physically justifiable distribution functions are required.

A need also exists to test and improve theory already developed for scatter from sea ice. The testing of a theory can only be achieved by collecting quantitative scattering data, preferably at several frequencies, with good ground truth information.

If a decision had to be made on the basis of present knowledge, a spacecraft imaging radar for sea ice mapping would have the following parameters:

Frequency: Between 8 and 16 GHz
Polarization: VV or HH, with cross-polarized receiving option for experiment
Spatial Resolution: $\leq$100 m

Gray-scale Resolution: ≤ 0.55 dB
Incident Angles: $>20^{\circ}$
Swath Width: Matched to orbit to achieve <6 day repetition
Sensitivity: ≤ -20 dB
Dynamic Range: ≥ 30 dB

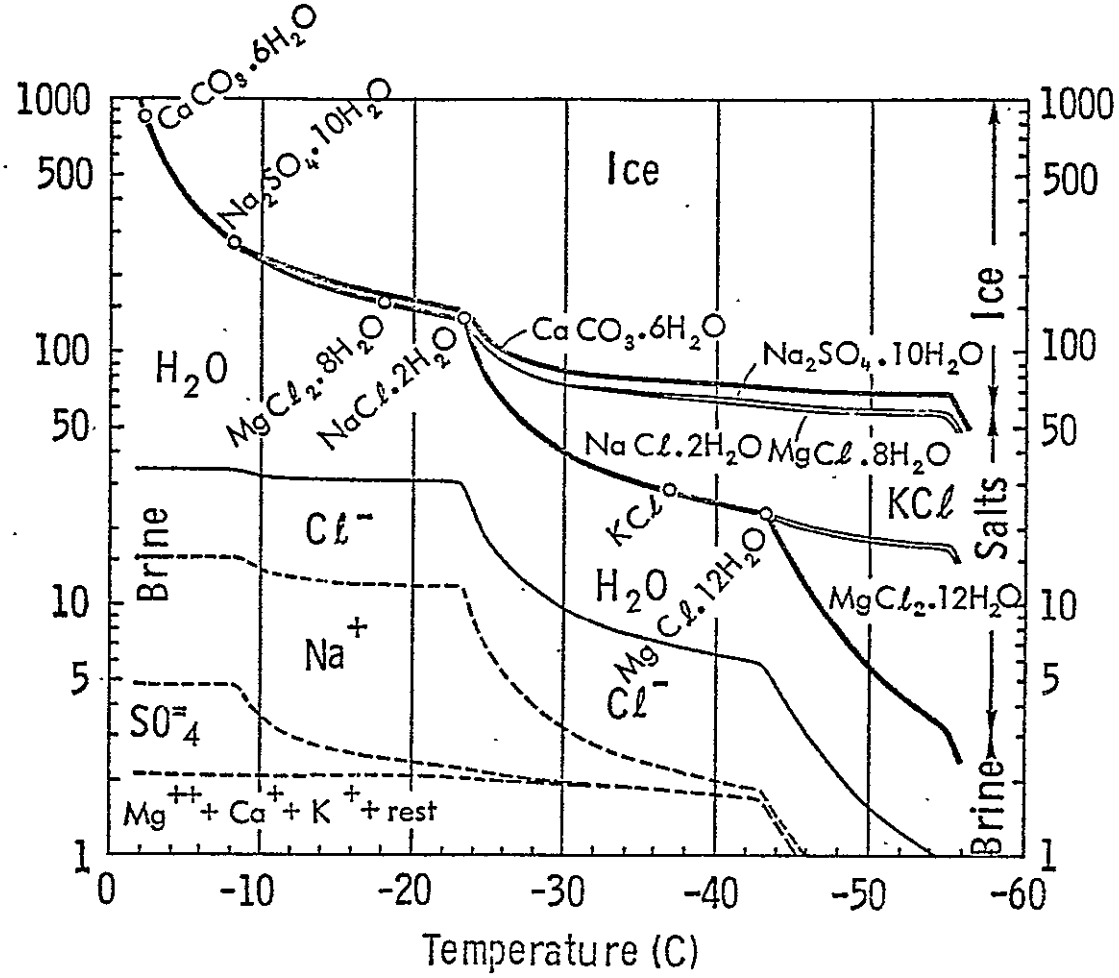

Figure 1. Phase relations for "standard" sea ice. Circles on the brine-salt line indicate temperatures at which solid salts precipitate (Assur, 1958 (31)).

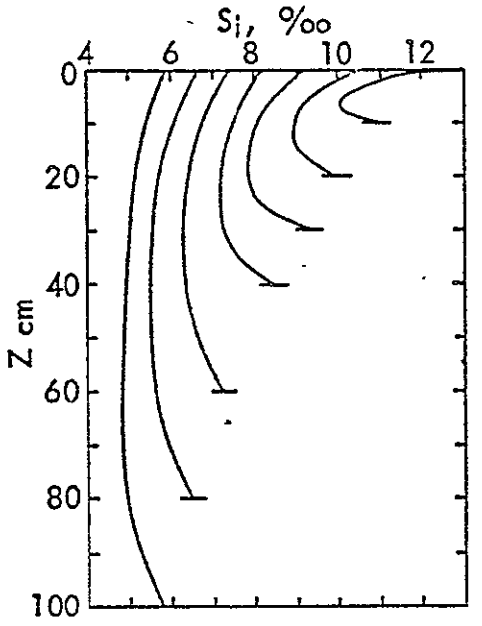

Fig. 2. Schematic salinity profiles for sea ice with a thickness of 100 cm or less (Weeks and Assur (31)).

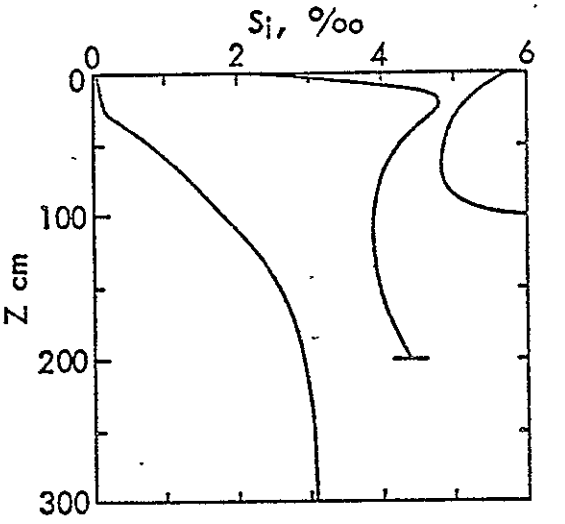

Fig. 3. Schematic salinity profiles for sea ice 100, 200 and 300 cm thick. The low salinity values at the top of the 200-cm profile indicate that this ice has been through a period of summer melt (Weeks and Assur (31)).

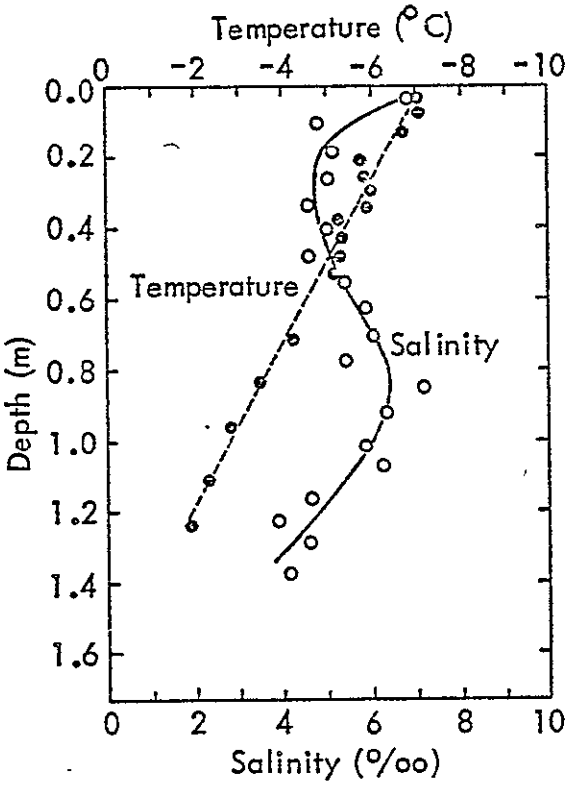

Fig. 4. Temperature and salinity distributions for typical first-year sea ice as a function of depth below the ice surface (McNeill and Hoekstra (22)).

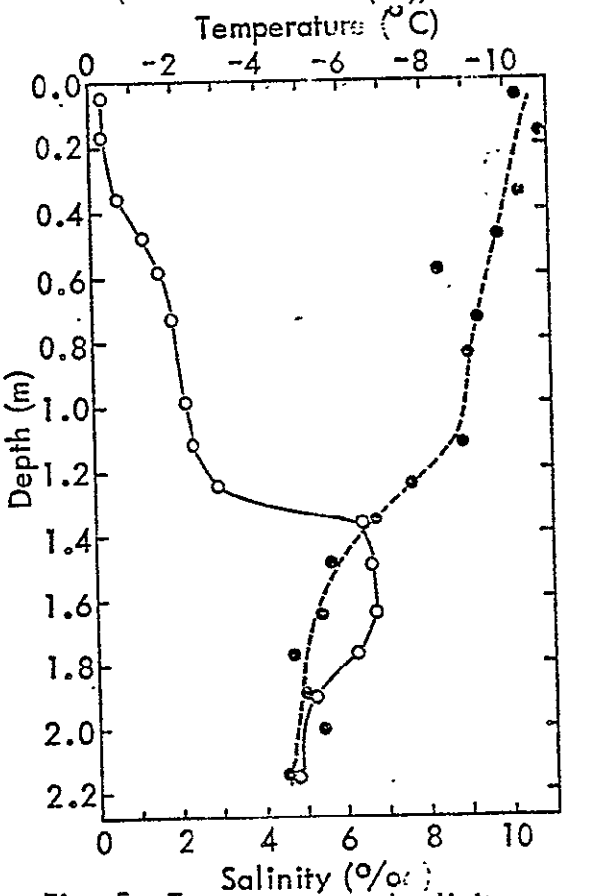

Fig. 5. Temperature and salinity distribution for typical multiyear sea ice as a function of depth below the ice surface (McNeill and Hoekstra (22)).

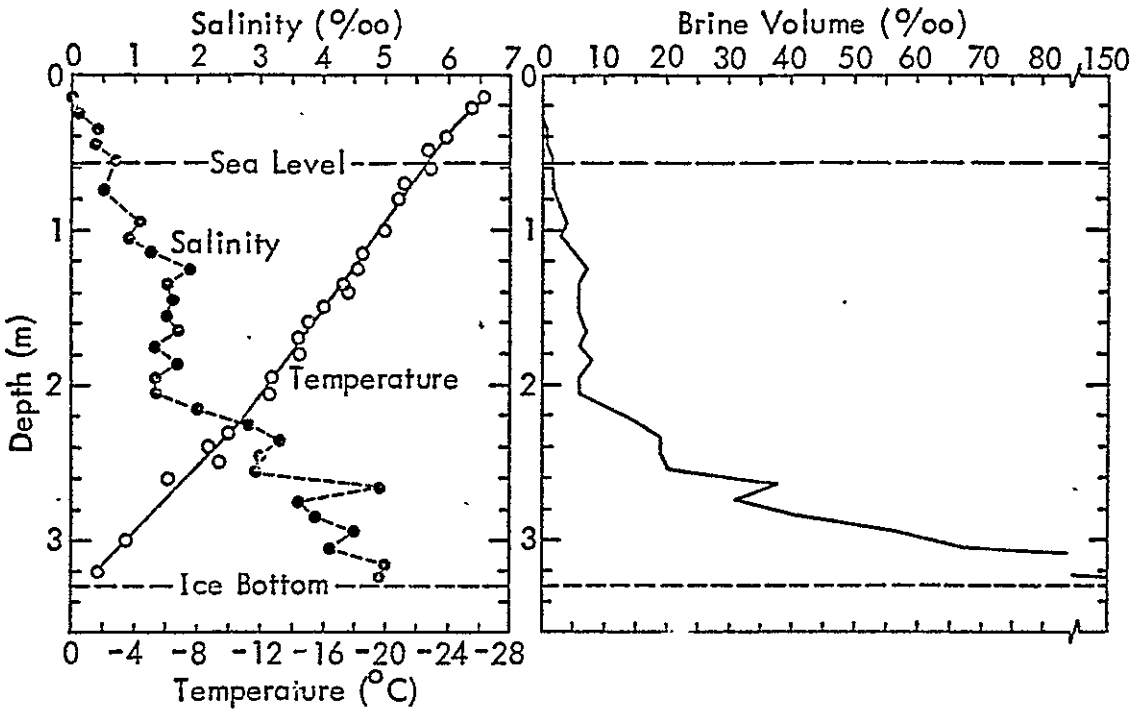

Figure 6. Typical hummock salinity profile with temperature and brine volume profiles (Cox and Weeks (8)).

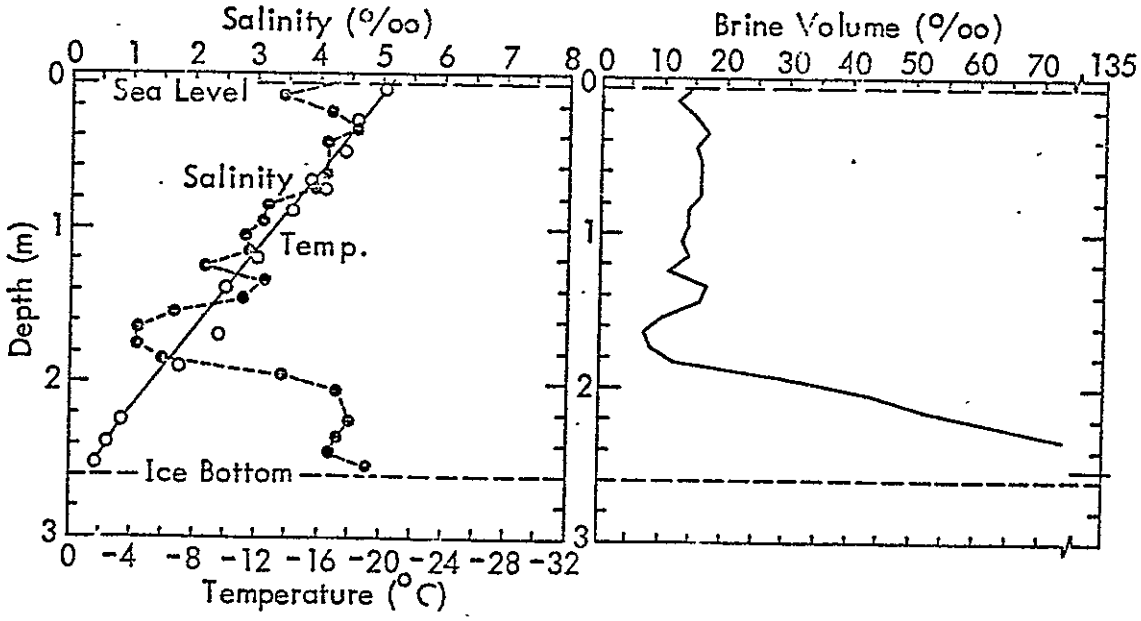

Figure 7. Depression salinity profile with temperature and brine volume profiles (Cox and Weeks (8)).

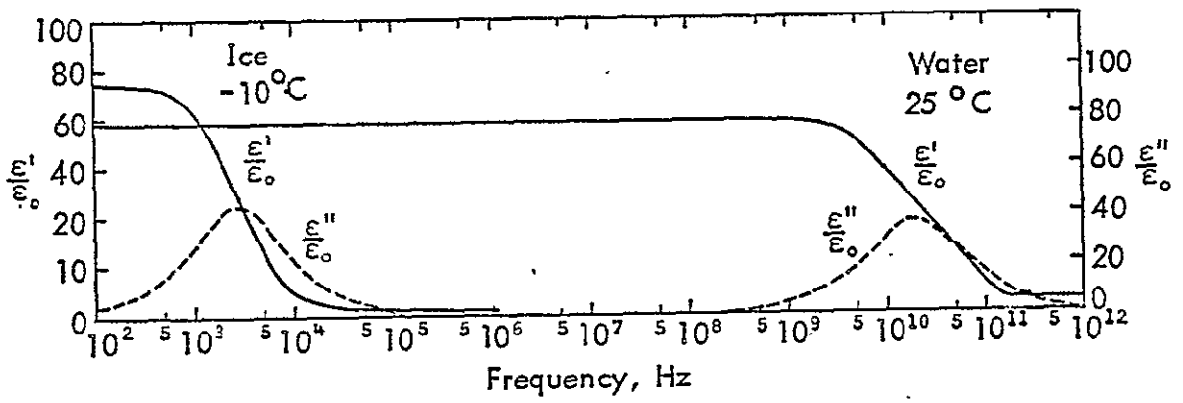

Figure 8. The dielectric behavior of ice and water as a function of frequency (Hoekstra and Cappillino (17)).

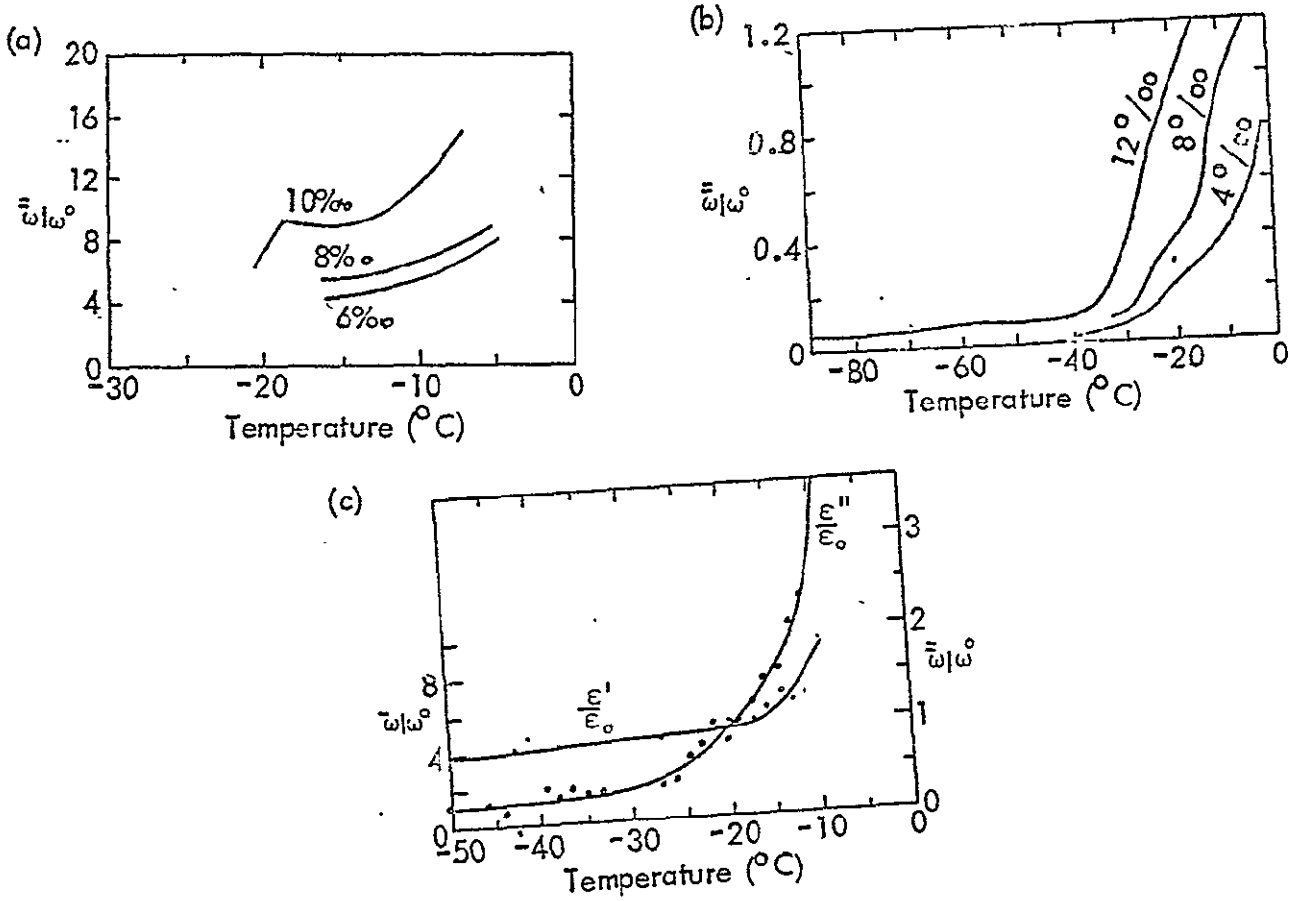

Figure 9. The dielectric loss and constant of sea ice samples as a function of temperature: (a) at a frequency of 4×10^8 Hz; (b) at a frequency of 9.8×10^9 Hz; (c) at a frequency of 2.3×10^{10} Hz (Hoekstra and Cappillino (17)).

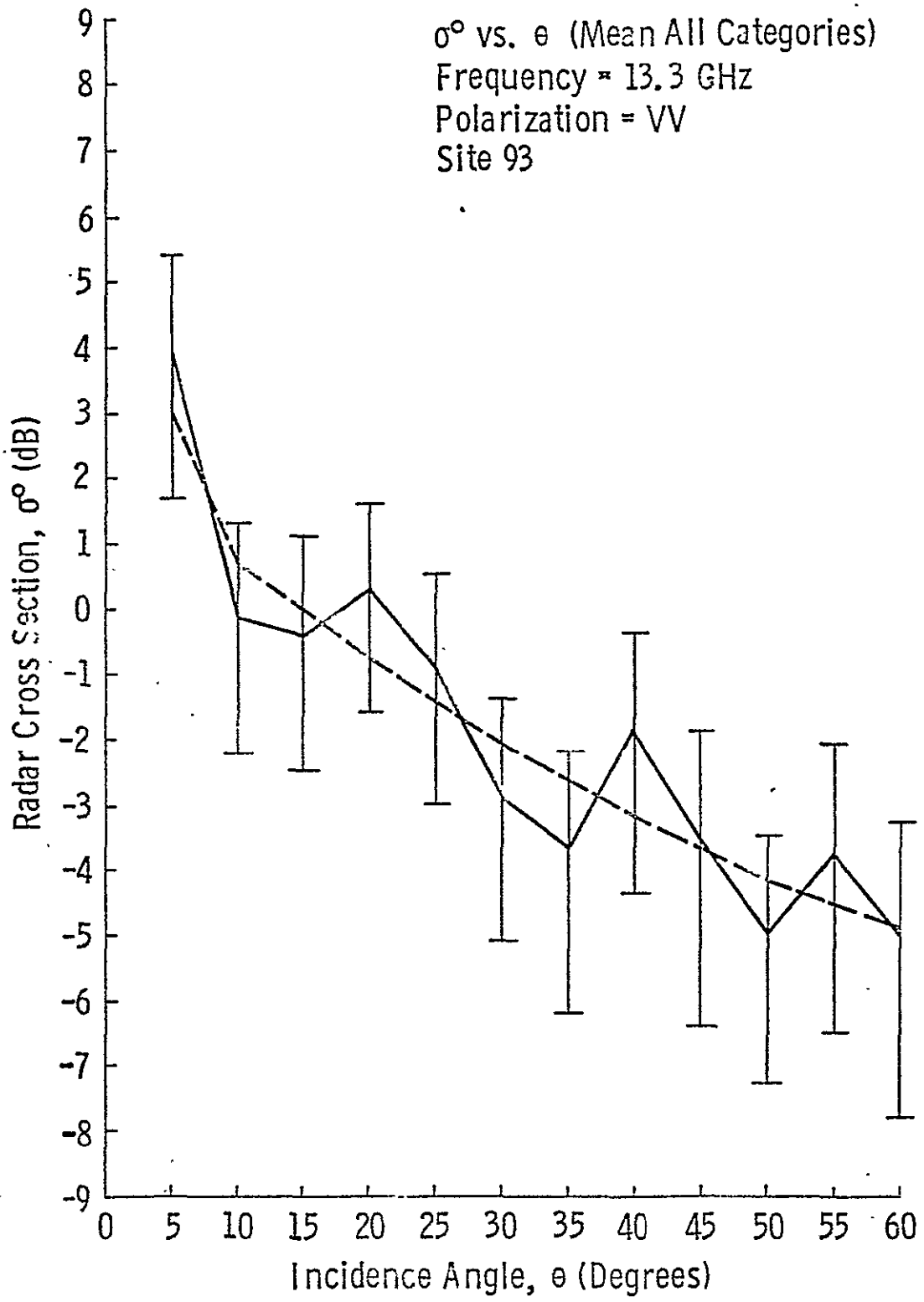

Figure 10. (Parashar (33)).

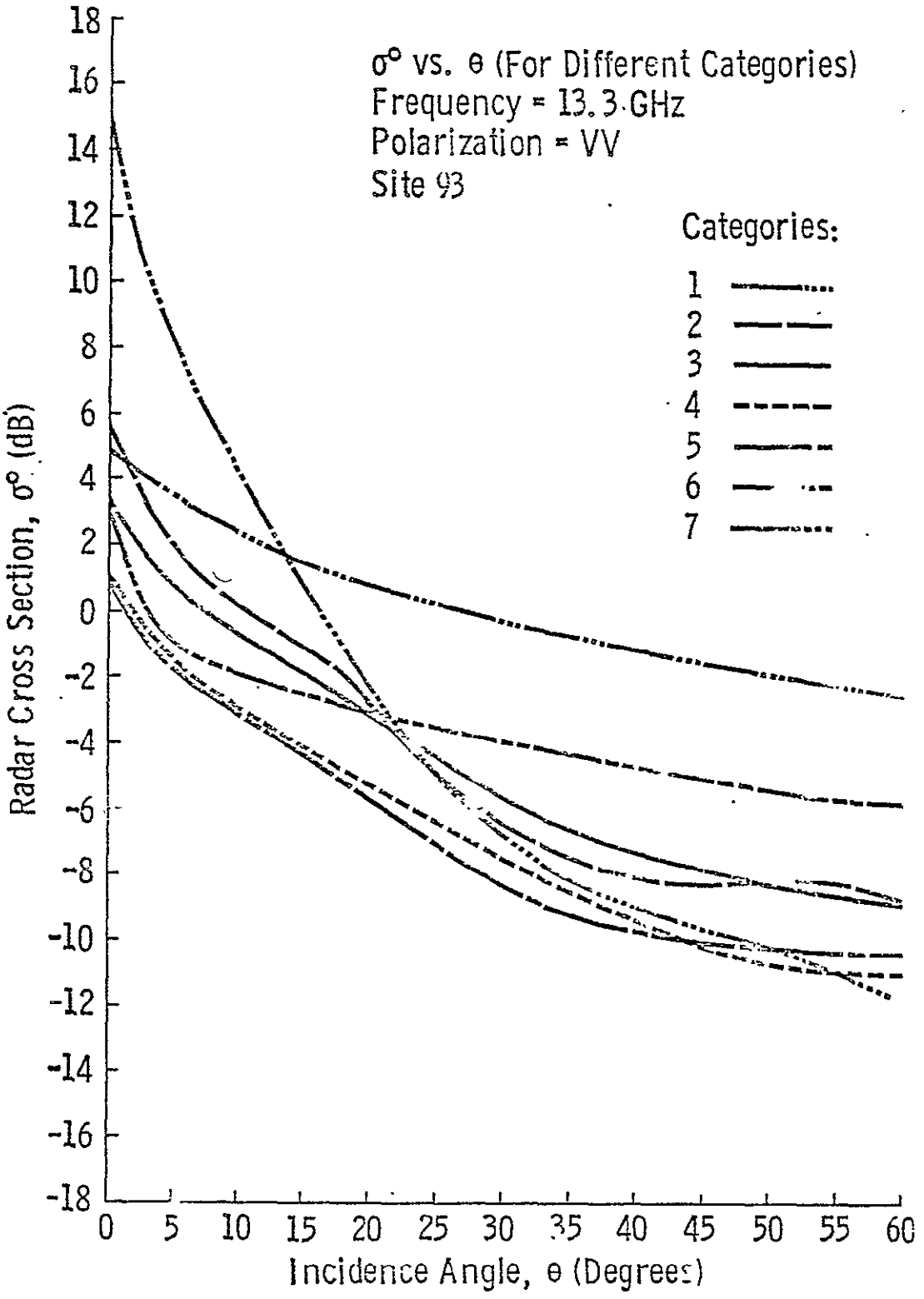

Figure 10a. (Parashar (33)).

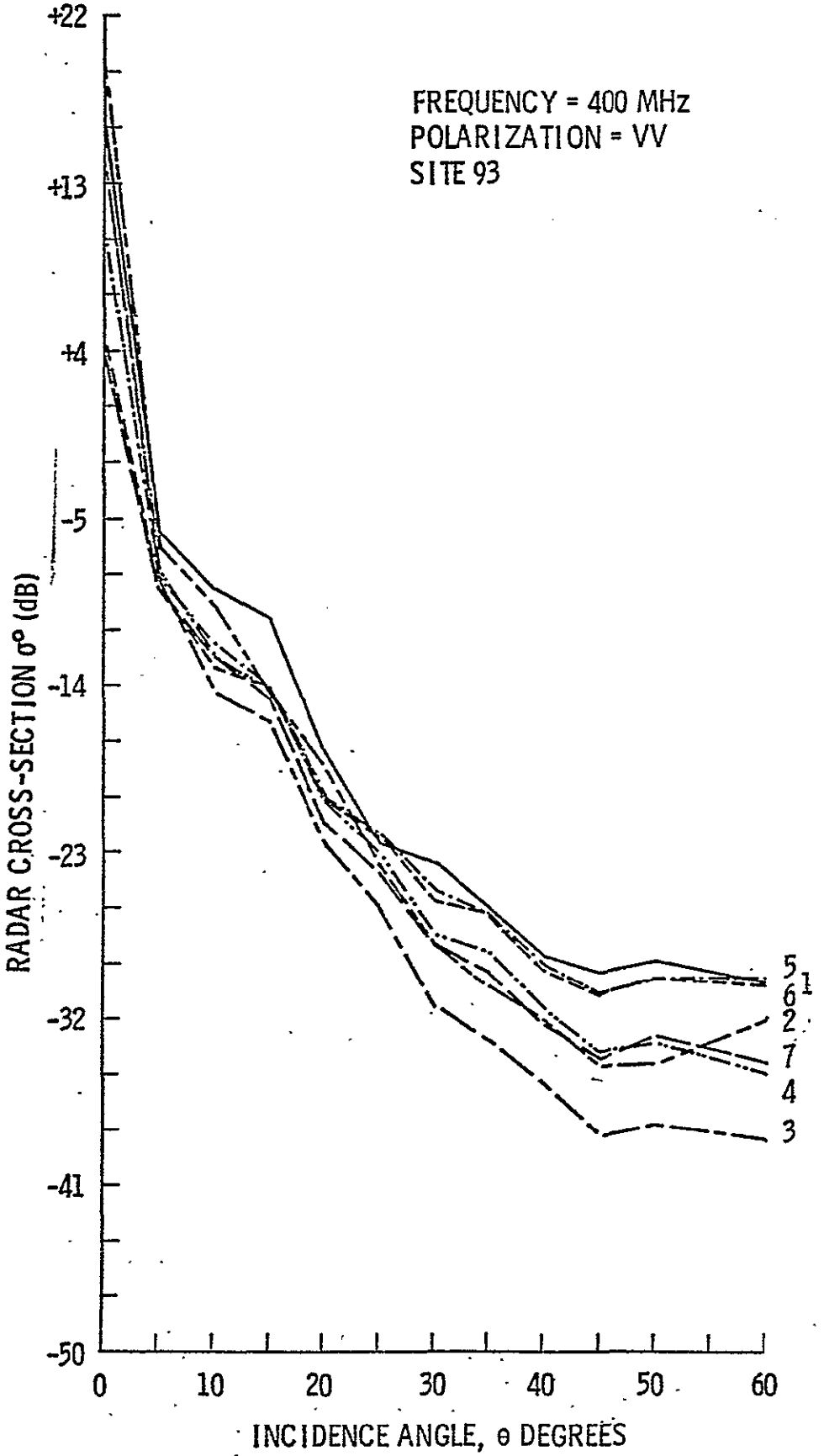

Figure 11. σ° vs. θ for Different Categories of Sea Ice (Parashar (33)).

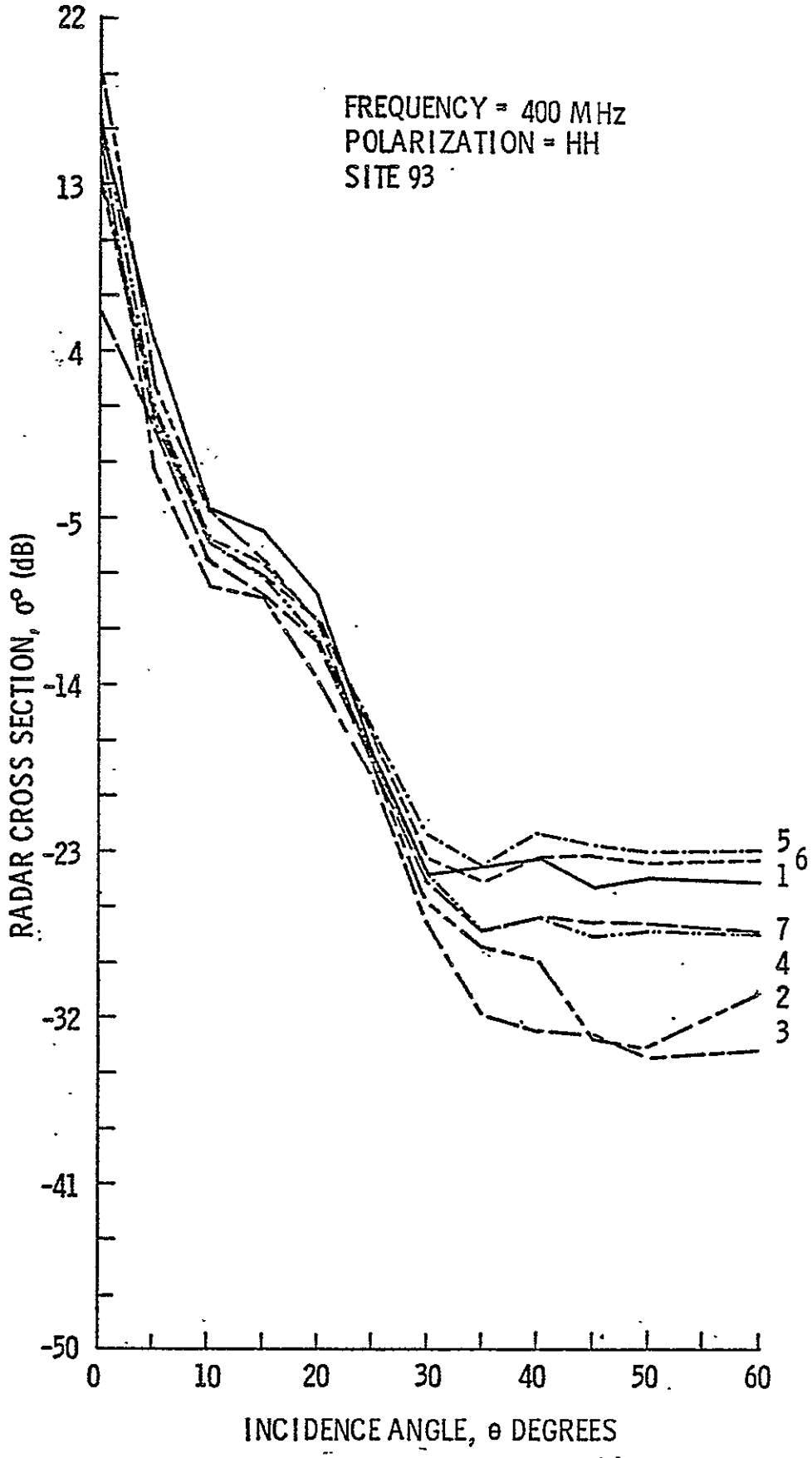

Figure 12. σ° vs. θ for Different Categories of Sea Ice (Parashar (33)).

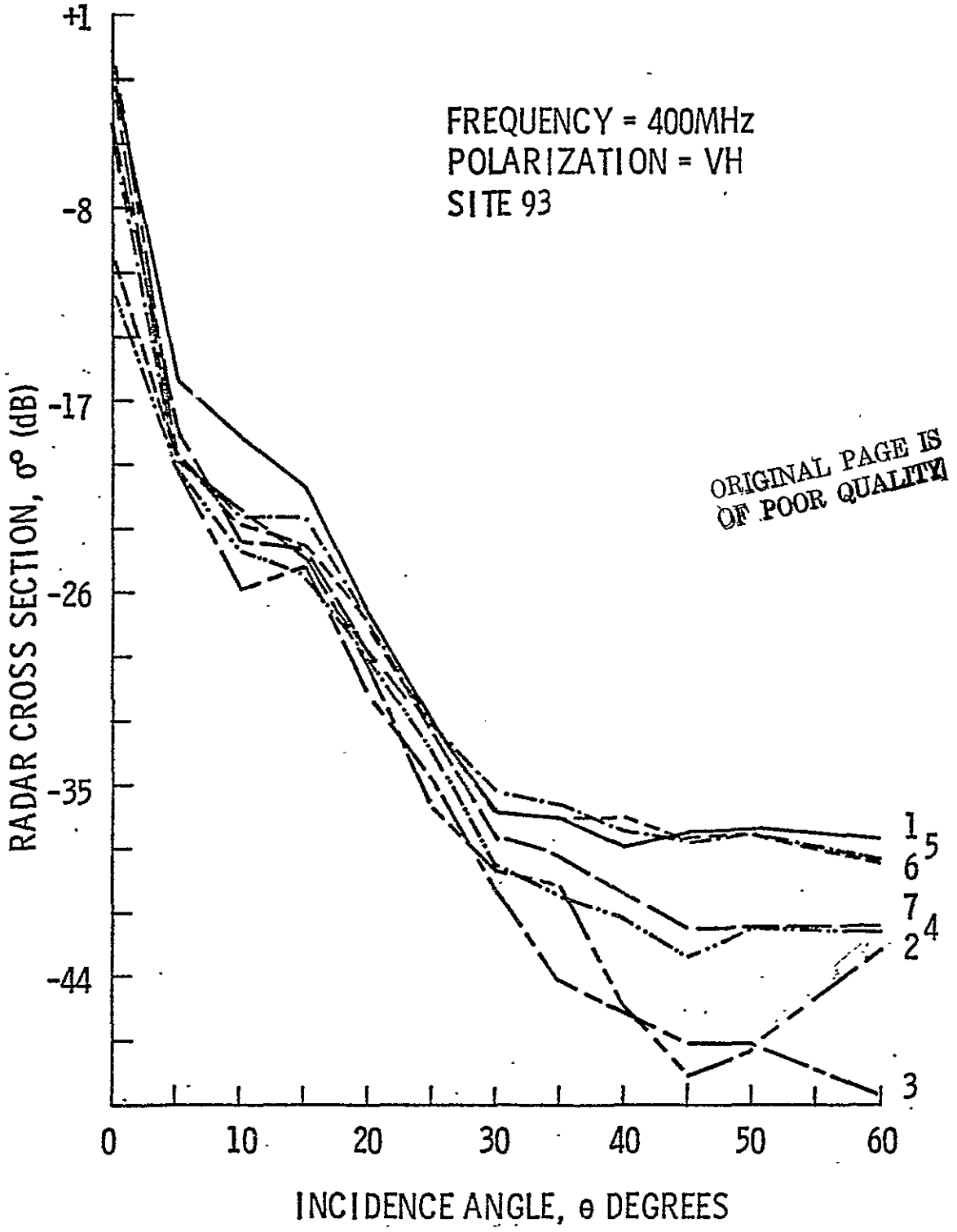

Figure 13. σ° vs. θ for Different Categories of Sea Ice (Parashar (33)).

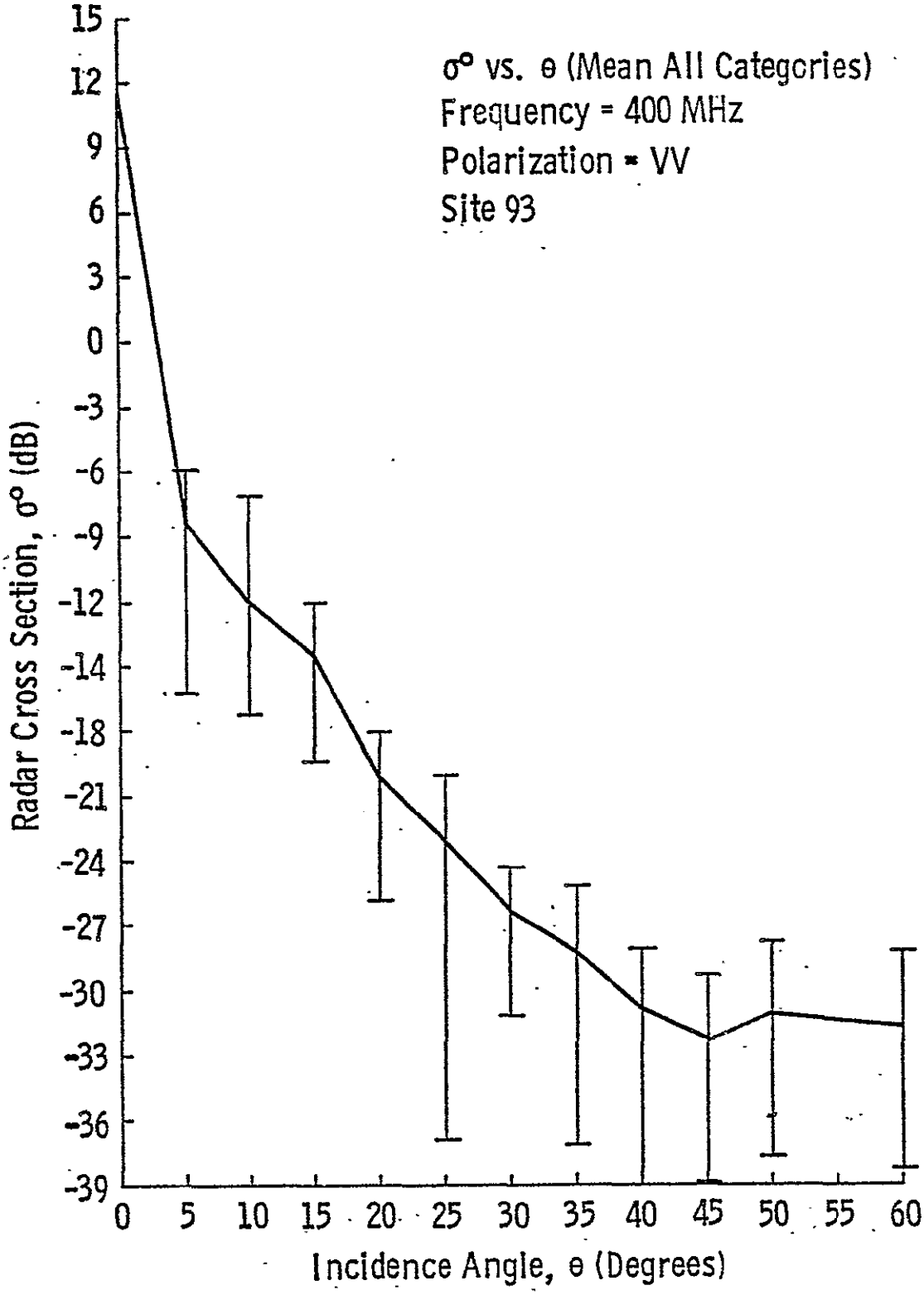

Figure 14. (Parashar (33)).

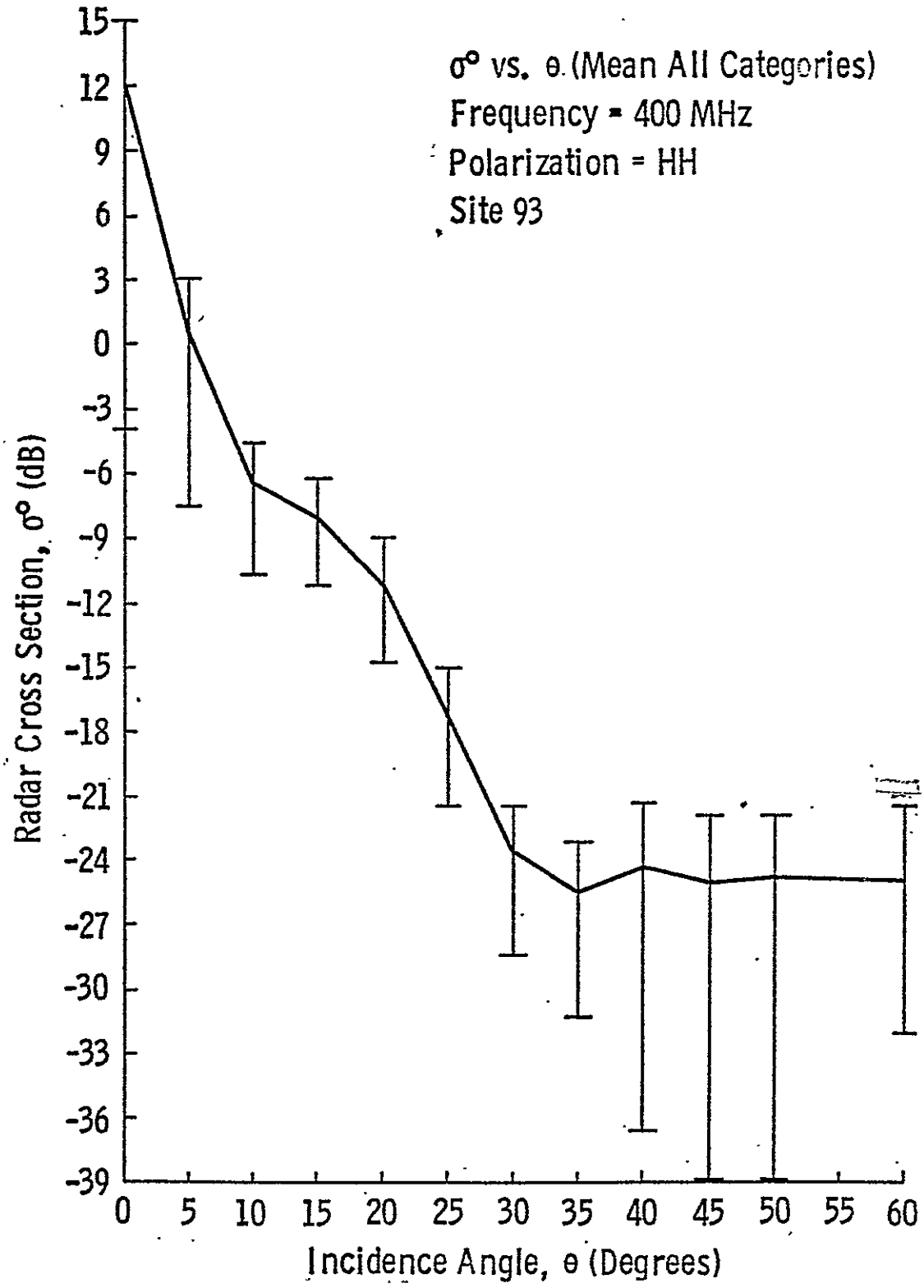

Figure 15. (Parashar (33)).

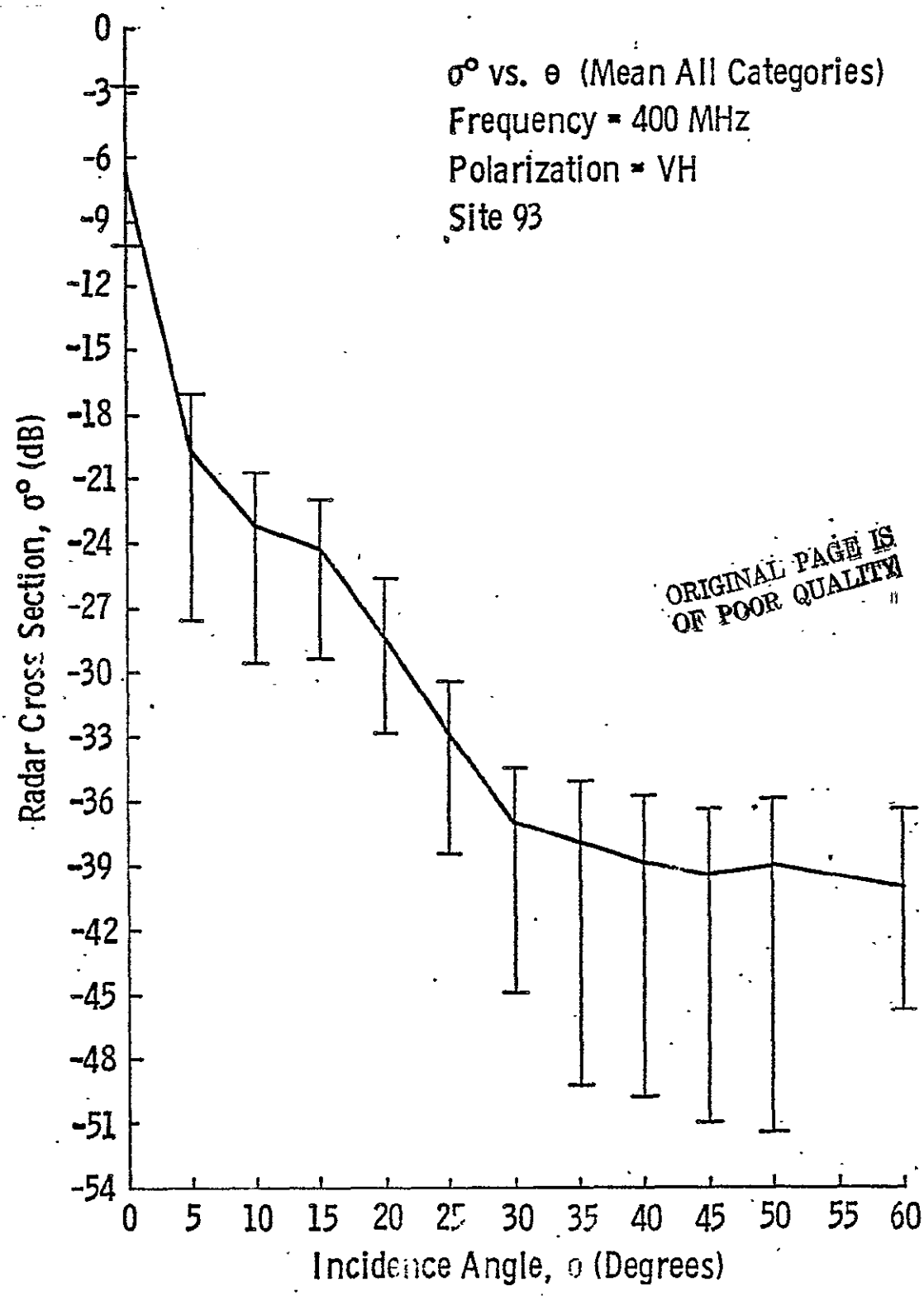

Figure 16. (Parashar (33)).

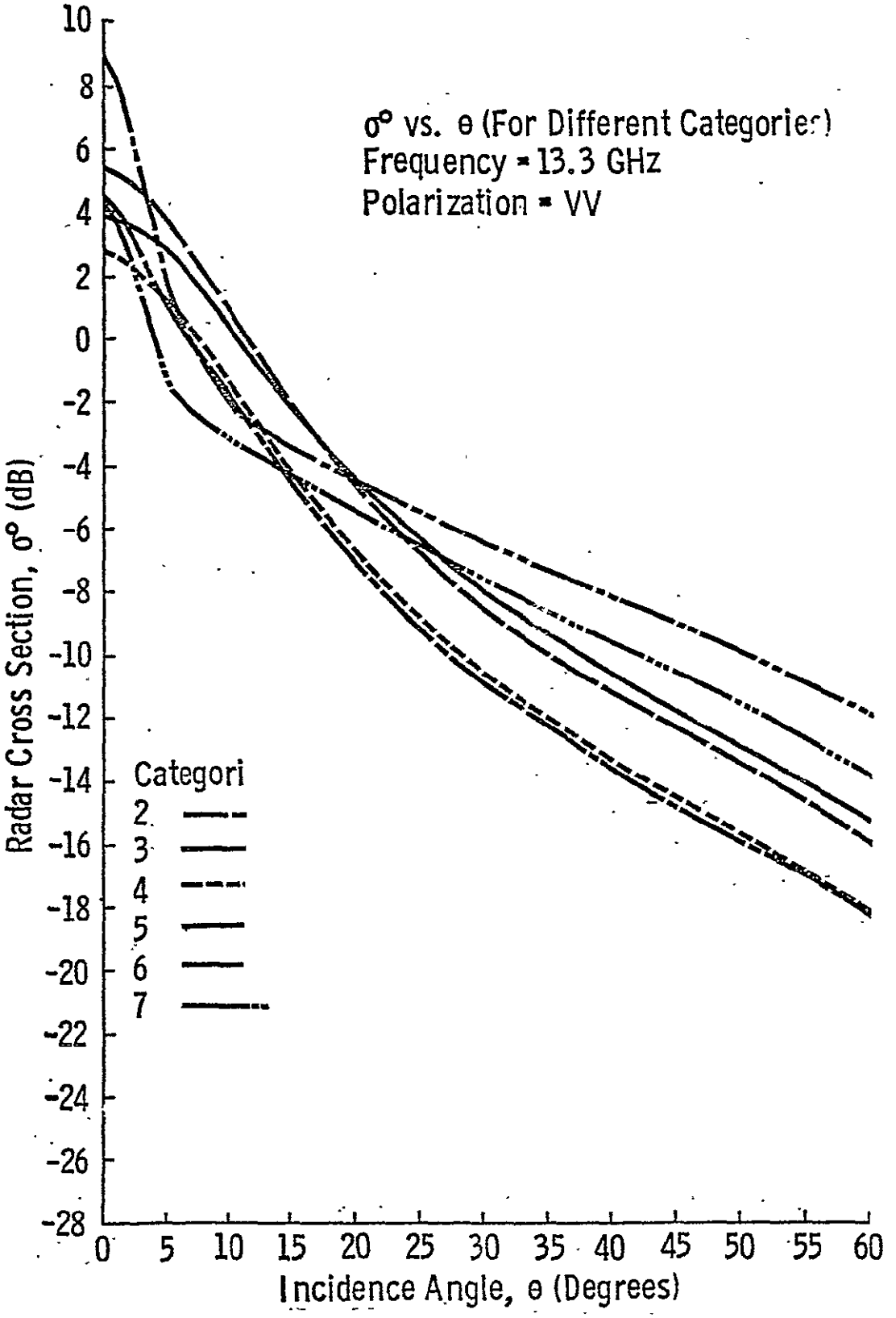

Figure 17 (Parashar (33)).

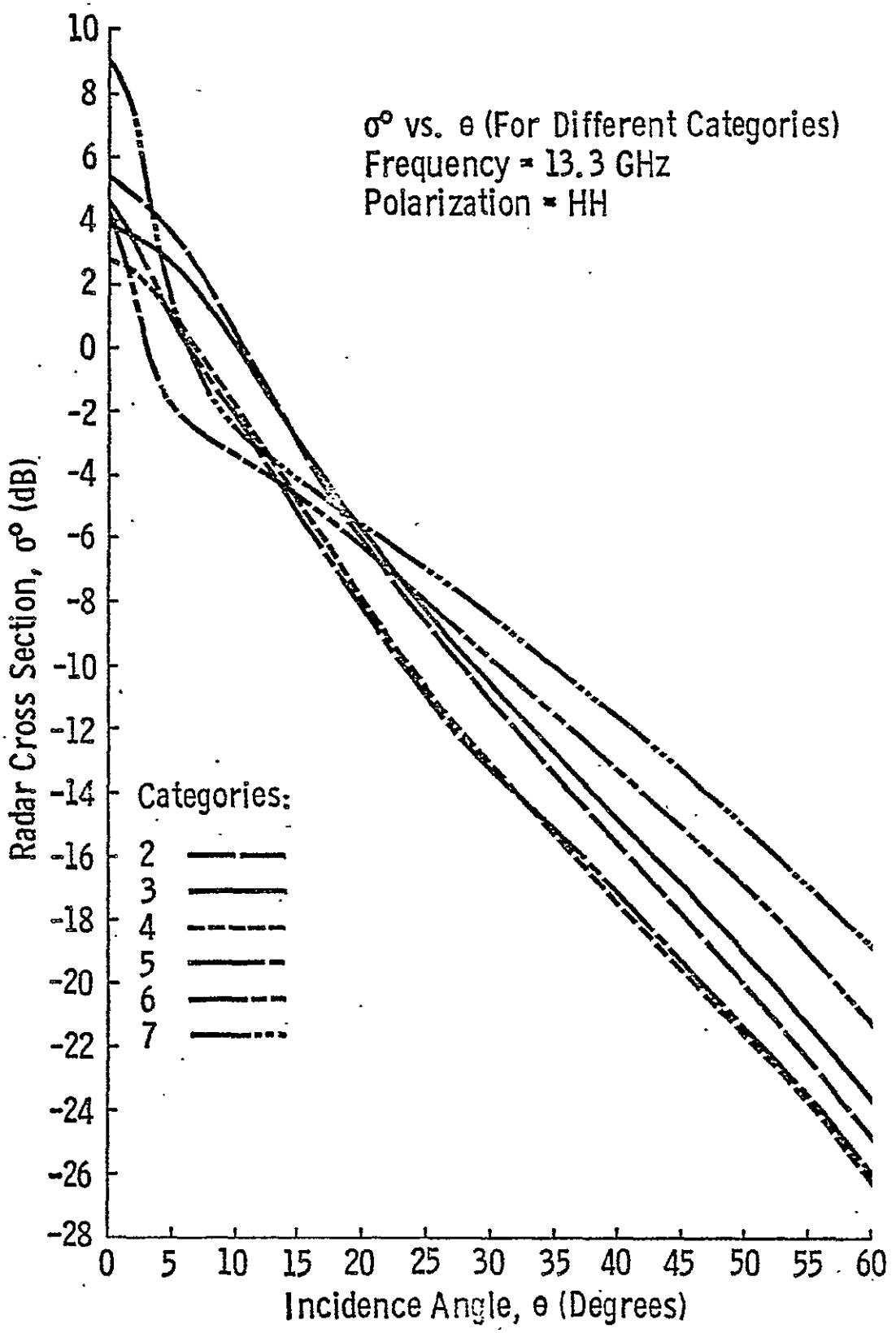

Figure 18. (Parashar (33)).

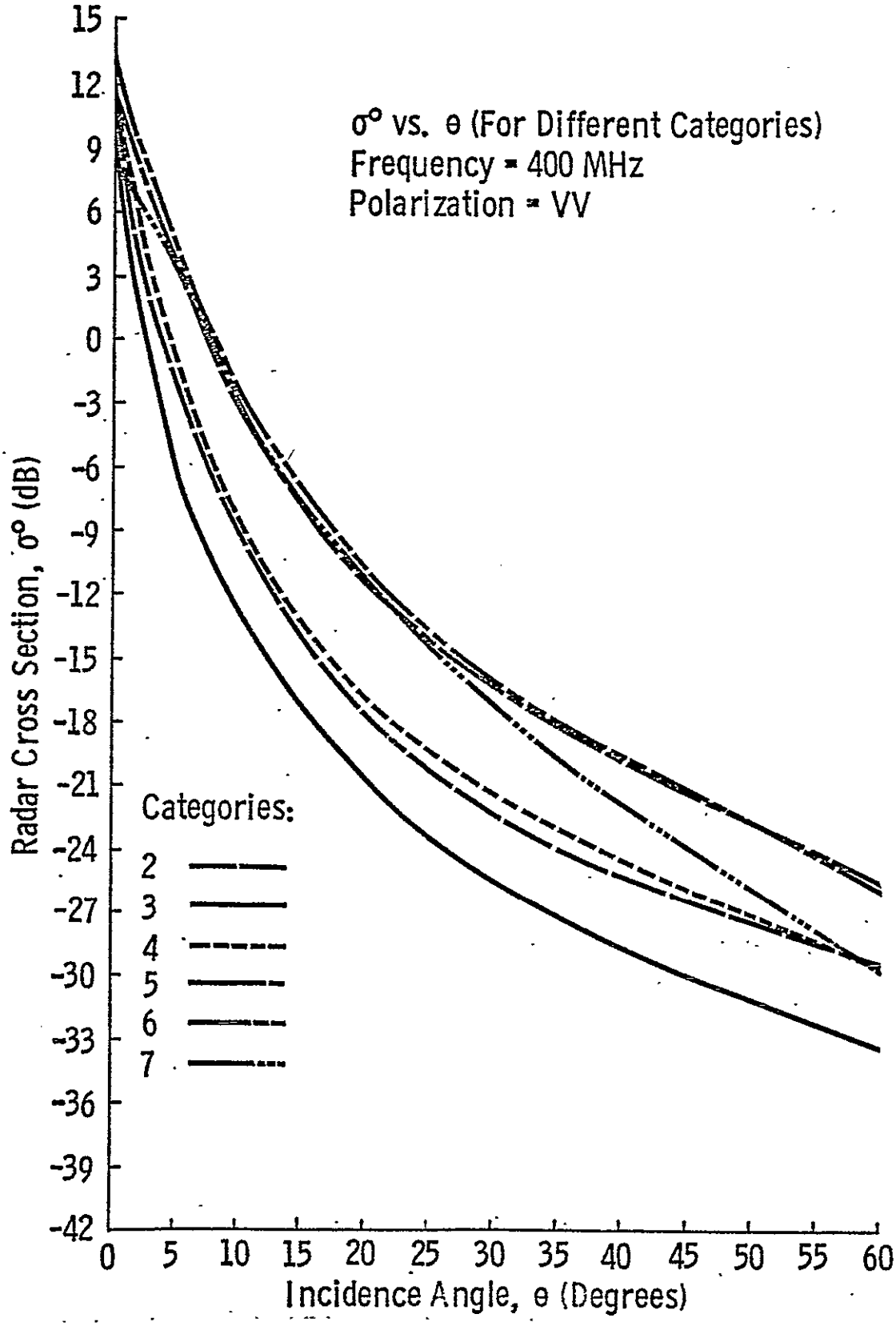

Figure 19. (Parashar (33)).

REFERENCES

1. Addison, J. R., "Electrical Properties of Saline Ice," Journal of Applied Physics, vol. 40, no. 8, pp. 3105-3114, July, 1969.

2. Addison, J. R., "Electrical Relaxation in Saline Ice," Journal of Applied Physics, vol. 41, no. 1, pp. 54-63, January, 1970.

3. Addison, J. R. and E. R. Pounder, " The Electrical Properties of Saline Ice," International Conference on Low Temperature in Science, Sapporo, August 14-19, Proceedings, vol. 1, part 1, 1966.

4. Anderson, V. H., "High Altitude, Side Looking Radar Images of Sea Ice in the Arctic," Proceedings Fourth Symposium on Remote Sensing of Environment, University of Michigan, Ann Arbor, pp. 845-857, June, 1966.

5. Anderson, V. H., "Sea Ice Pressure Ridge Study: An Airphoto Analysis," Photogrammetria, Elsevier Publishing Company, Amsterdam, 1970.

6. Auty, R. P. and R. H. Cole, "Dielectric Properties of Ice and Solid D_2O," Journal of Chemical Physics, vol. 20, no. 8, pp. 1309-1314, 1952.

7. Byrd, R. C., M. Yerkes, W. M. Sackinger, and T. E. Osterkamp, " Millimeter Wave Reflectivity of Sea Ice," Ocean '72, IEEE International Conference on Engineering in the Ocean Environment, IEEE Publication, 1972.

8. Cox, G. F. N. and W. F. Weeks, "Salinity Variations in Sea Ice," AIDJEX Bulletin No. 19, pp. 1-17, March, 1973.

9. Cummings, W. A., "The Dielectric Properties of Ice and Snow at 3.2 cm," Journal of Applied Physics, vol. 23, no. 7, pp. 768-773, 1952.

10. Dorsey, N. E., "Properties of Ordinary Water Substance in All Its Phases: Water Vapour, Water and All the Ices," Reinhold, New York, 1970. (American Chemical Society, Nomograph Series, No. 81).

11. Dunbar, Moira, "A Glossary of Ice Terms (WMO Terminology)," Ice Seminar, Special Volume 10, The Canadian Institute of Mining and Metallurgy, pp. 105-110, 1969.

12. Fletcher, J. O., "Probing Secrets of Arctic Ice," AIDJEX Bulletins.

13. Frankenstein, G. and R. Garner, "Equations for Determining the Brine Volume of Sea Ice from -0.5° to -22.9° C," Journal of Glaciology, vol. 6, no. 48, pp. 943-944, 1967.

14. Fujino, K., "Electrical Properties of Sea Ice," International Conference on Low Temperature Science, Sappro, Proceedings, vol. 1, pt. 1, August 14-19, 1966.

15. Glushkov, V. M. and V. B. Komarov, "Side-Looking Imaging Radar System TOROS and Its Application to the Study of Ice Conditions and Geological Explorations," Proceedings 7th International Symposium on Remote Sensing of Environment, University of Michigan, Ann Arbor, 1971.

16. Groen, P., The Waters of the Sea, D. Van Nostrand Co. Ltd., London, 1967.

17. Hoekstra, P. and P. Cappillino, "Dielectric Properties of Sea Ice and Sodium Chloride Ice at UHF and Micro-Wave Frequencies," Journal of Geophysical Research, vo. 76, no. 20, pp. 4922-4931, July, 1971.

18. Johnson, J. D. and L. D. Farmer, "Use of Side-Looking Airborne Radar for Sea Ice Identification," Journal of Geophysical Research, vo. 76, no. 9, pp. 2138-2155, March, 1971.

19. Johnson, J. D. and L. D. Farmer, "Determination of Sea Ice Drift Using Side-Looking Airborne Radar," Proceedings 7th International Symposium on Remote Sensing of Environment, The University of Michigan, Ann Arbor, 1971.

20. Ketchum, R. D., Jr. and S. J. Tooma, Jr., "Analysis and Interpretation of Airborne Multi-Frequency Side-Looking Radar Sea Ice Imagery," Journal of Geophysical Research, 78C37, pp. 520-538, 1973.

21. Loshchilov, V. S. and V. A. Voyevodin, "Determination of Elements of Ice Cap Drift and Movement of Ice Edges by Means of the Airborne Side-Scan Radar 'TOROS'," Problems in Arctic and Antarctica, vol. 40, pp. 23-30, 1972.

22. McNeill, D. and P. Hoekstra, "In-situ Measurements on the Conductivity and Surface Impedance of Sea Ice at VLF," Radio Science, vol. 8, no. 1, pp. 23-30, January, 1973.

23. Moore, R. K., "Radar Scatterometry — An Active Remote Sensing Tool," University of Kansas Center for Research, Inc., CRES Technical Report 61-11, Remote Sensing Laboratory, Lawrence, Kansas, April, 1966.

24. Murphy, E. J., "The Temperature Dependence of the Relaxation Time of Polarizations in Ice," Transactions of the Electrochemical Society, vol. 65, pp. 133-142, 1934.

24a. Ragle, R. H., R. B. Blair, and L. E. Persson, "Ice Core Studies of Ward Hunt Ice Shelf, 1960," Journal of Glaciology, vol. 5, no. 37, pp. 39-59, 1964.

25. Rouse, J. W., Jr., "Arctic Ice Type Identification by Radar," University of Kansas Center for Research, Inc., CRES Technical Report 121-1, Remote Sensing Laboratory, Lawrence, Kansas, August, 1968.

26. Skolnik, M. I., Radar Handbook, McGraw-Hill Book Company, 1970.

27. United States Coast Guard, "Data Reduction of Airborne Sensor Recrods," Report No. DOT-CT-01-800-A, Department of Transportation, Office of Research and Development, Washington, D. C. 20591, July, 1970.

28. United States Coast Guard, "Interpretation of Winter Ice Conditions from SLAR Imagery," Report No. DOT-CT-14486-1A, Department of Transportation, Office of Research and Development, Washington, D. C. 20591, February, 1972.

29. United States Coast Guard, "Analysis of SLAR Imagery of Arctic and Lake Ice," Report No. DOT-CG-14486-A, Department of Transportation, Office of Research and Development, Washington, D. C. 20591, March, 1972.

30. Weeks, W. F., "Understanding the Variations of the Physical Properties of Sea Ice," Special Report 112, Cold Regions Research and Engineering Laboratory (CRREL), Hanover, New Hampshire, May, 1967.

31. Weeks, W. F. and A. Assur, "Fracture of Lake and Sea Ice," Research Report 269, Cold Regions Research and Engineering Laboratory, Hanover, New Hampshire, September, 1969.

32. Wentworth, F. L. and M Cohn, "Electrical Properties of Sea Ice at 0.1 to 30 M c/s," Radio Science, Journal of Research, NBS/USNC-URSI, vo. 68D, no. 6, pp. 681-691, June, 1964.

33. Parashar, S. K., "Investigation of Radar Discrimination of Sea Ice," (Ph.D. Dissertation), University of Kansas Center for Research, Inc., CRES Technical Report 185-13, 1974.

34. Zagorodnikov, A. A., V. S. Loshchilov, and K. B. Chelyshev, "Two-Dimensional Statistic Analysis of Radar Imagery of Sea Ice," 8th International Proceedings, University of Michigan, Ann Arbor, v.1, 1972.

35. Canadian Department of Atmospheric Environment, "Operation Ice Map II, Side-Looking Radar Trials," 1972.

36. Weeks, W. D., Hibler III, and S. F. Ackley, "Sea Ice: Scales, Problems and Requirements," Interdisciplinary Symposium on Advanced Concepts and Techniques in the Study of Snow and Ice Resources, 2-6 December 1972, Monterey, California.

37. Kazo, Thomas L. and Orest I. Diachok, "Spatial Variability of Topside and Bottomside Ice Roughness and its Relevance to Underside Acoustic Reflection Loss," AIDJEX Bulletin No. 19, March, 1973, Arctic Ice Dynamics Joint Experiment, Division of Marine Resources, University of Washington, Seattle, Washington 98105.

38. Ling, Chi-Hai and Norbert Untersteiner, "On the Calculation of the Roughness Parameter of Sea Ice," AIDJEX Bulletin No. 23, January, 1974.

39. Ackley, S., W. Hibler, III, F. Kugzruk, A. Kovacs and W. Weeks, "Thickness and Roughness Variations of Arctic Multi-year Sea Ice," AIDJEX Bulletin No. 25, July, 1974.

40. Thorndike, A. S. and G. A. Maykut, "On the Thickness Distribution of Sea Ice," AIDJEX Bulletin No. 21, pp. 31-48, Division of Marine Resrouces, University of Washington, 1973.

41. Koerner, R. M., "The Messbalance of the Sea Ice of the Arctic Ocean," Journal of Glaciology, vol. 12, No. 65, pp. 173-185, 1973.

42. Bradie, R. A., "SLAR Imagery for Sea Ice Studies," Photogrammetria Engineering, vol. 33, no. 7, 1967.

43. Biache, A., Jr., C. A. Bay and R. Bradie, "Remote Sensing of the Arctic Ice Environment," 7th International Symposium on Remote Sensing of Environment, Proceedings, University of Michigan, Ann Arbor, vol. 1, 1971.

44. Personal Communication with Dr. L. Gray of Canadian Center for Remote Sensing.

45. Moore, R. K., report on trip to USSR, June, 1973 (unpublished memorandum).

APPENDIX B

RSL TECHNICAL REPORT 291-2

VOLUME III

THE UNIVERSITY OF KANSAS SPACE TECHNOLOGY CENTER
Raymond Nichols Hall
2291 Irving Hill Drive—Campus West Lawrence, Kansas 66045
Telephone:

STATE OF THE ART —
RADAR MEASUREMENT OF ICEBERGS

RSL Technical Memorandum 291-2
Remote Sensing Laboratory

S. K. Parashar

January, 1976

Supported by:

NATIONAL AERONAUTICS AND SPACE ADMINISTRATION
Goddard Space Flight Center
Greenbelt, Maryland 20771

CONTRACT NAS 5-22325

ABSTRACT

Radar can be useful for sensing icebergs, and in fact radar may be the most useful sensor because of its wide coverage under adverse weather conditions. Although several experiments have been conducted in the use of radar for this purpose, these have been performed on a somewhat qualitative basis and with equipment that happened to be available. Consequently, it can be stated that X-band and K-band radars operating at modest angles of incidence are useful for iceberg discrimination and that horizontal polarization with resolutions between 20 and 100 meters could be used successfully. Research is needed, however, to ascertain the best frequency or frequencies, the best incidence angles, and the best resolutions for detecting icebergs and discriminating them both from ships and from water and sea-ice backgrounds.

State of the Art -- Radar Measurement of Icebergs

S. K. Parashar

1.0 INTRODUCTION

Though icebergs can be most dangerous, under some circumstances, to shipping, little effort to sense them remotely other than with ship radars has been reported. Icebergs can be found in a large area and thus cannot be monitored on a continuous basis by any means but wide-coverage remote sensing.

Aerial reconnaissance has been the major source of information on icebergs since shortly after World War II. The problem with the direct visual observations or the conventional photographic method is the inability to provide reliable information in non-ideal weather conditions. Most of the areas where icebergs are found have uncertain weather conditions throughout and there is often lack of light. The ability of radar to perform reliably under uncertain weather conditions and during day or night makes it quite an attractive and useful potential tool for monitoring icebergs. But despite this advantage not much effort has been made in understanding the nature of radar return from icebergs and in collecting radar data which could aid in the design of future systems. Most of the work done and reported to date has been by the U.S. Coast Guard. No dobut other countries' ice patrols have also studied the problem but published reports are hard to find.

This report is intended as a review of the past research efforts in the radar measurement of icebergs. An effort is made to specify design parameters for future operational systems. Also included is a section on the formation and characteristics of icebergs. Recommendation is made to conduct future research and experiments with a view of ascertaining optimum operational parameters of iceberg-mapping radar as it is felt that the current knowledge about the radar return from icebergs is insufficient.

2.0 CHARACTERISTICS OF ICEBERGS

"Land ice" occurs in the sea, as does sea ice. Land ice is all the ice not formed from sea water, hence it is that which in its natural state does not contain sea salt. Although land ice includes ice formed in the rivers, most of the land ice found in the ocean is from glaciers. Glacier ice breaks away into the ocean and

is normally found in the form of icebergs or ice islands. Icebergs are the predominant type of floating ice away from the polar regions.

2.1 Formation of Icebergs

Icebergs are formed by the 'calving' of glaciers on the coast (5). Greenland in the north and Antarctica in the south are the chief producers of icebergs. Some glaciers on some of the smaller islands situated in or around the polar seas are also important in producing icebergs. To understand icebergs it is important to know something about glaciers. The following four types of glaciers occuring in the polar regions and extending down to the coast can be distinguished (4).

a) Inland ice: It is an ice-sheet covering a large area, only allowing pinnacles of rocks to project here and there.

b) Valley glacier: It is a glacier following the course of a valley.

c) Piedmont glacier: Sometimes known as the extended-foot glacier, it is a terrace of ice which spreads out at the foot of one or more valley glaciers at the base of a mountain or mountains.

d) Ice barrier, or shelf-ice: It is a layer of ice which stretches out from the shore (from inland ice) into the sea.

Valley glaciers are also called ice-rivers, for a glacier is not a motionless mass of ice. Even if the foot of the valley glacier remains at approximately the same place, it does not mean there is no movement in the ice. Glacier ice 'flows' because its internal structure is somewhat different from that of freshly formed ice. Freshly formed ice consists of fairly large, coherent crystals, whereas glacier ice is snow-ice of many years standing and is of slightly plastic consistency. Moreover, ice under heavy pressure is liable to begin to melt somewhat at the bottom.

The mass of ice of a valley glacier slowly glides downward under the influence of gravity operating downward along the slopes. The rate of travel of the valley glaciers can be 4 meters to as much as 20 meters a day. This fact can be unnoticeable at the lower end of the glacier because there the ice melts away sometimes as fast as it comes down. Sometimes a huge fragment of the glacier ice suddenly breaks off into the ocean as the tongue of ice at the foot of the glacier slowly slips into the water. This is called 'calving' and the broken piece of ice is known as an iceberg.

2.2 Shapes and Characteristics of Icebergs

Valley glaciers deliver icebergs of comparatively limited horizontal dimensions, whereas the chunks that break away from ice barriers may be some tens of kilometers in length and sometimes in fact as much as one hundred kilometers. These icebergs are called tabular bergs or barrier bergs. The maximum width of the bergs depends on the width of the glacier ending which is related to the width of the fjord. Often, the height of the broken-off ice masses is greater than their width and as a result of this instability the icebergs may capsize and turn over to find a more stable position. Instead of turning over completely they may tip at a certain angle. Later they may either turn in another direction or roll completely over.

Arctic icebergs are usually of irregular shape and may tower 80 - 100 meters high, with a width of several hundred meters. The shape of icebergs varies; most obvious is the difference between the shape of Arctic and Antarctic icebergs (4). The irregular shape of an iceberg is partly due to distortion of the tongues of the valley glaciers by the floor of the valley. Icebergs assume an astounding variety of shapes, from fairly uniform geometrical figures to castles with turrets, domed structure or minarets, and mountains with peaks and gorges. Some of the icebergs may have deep clefts, fissures or cavities.

The depth of immersion of icebergs depends on the difference between specific weight of glacier ice and sea water. As the specific gravity of ice of the berg is from 0.8 to 0.9 (depending on the amount of air enclosed in the ice), the underwater volume of an iceberg is something like approximately seven times that of the projecting part. The submersion of an iceberg does not depend on the vertical height but rather on the volumetric proportions.

The volume of an iceberg gradually declines as it travels farther and farther from its birthplace and becomes older. The decrease of the volume may happen in three ways: by calving, by melting and by erosion. An iceberg is said to calve when it throws off a part of itself. Melting can be due to the rays of the sun or warm water. Erosion is due to scouring action of waves and rain (5).

The electrical properties of ice in the berg are not clearly established. However, the electrical and physical properties of pure ice are fairly well understood. An excellent review of such properties is presented by Evans (6). The unusual features of pure ice are its extremely high static permittivity (on the order of 100) and its long relaxation time (on the order of 10-40 sec). Between a frequency

of 1 MHz and the far infrared region there is no absorption band in the spectrum of ice. The limiting value of the relative permittivity of ice is about 3.2 at high frequencies and varies with temperature. The relaxation spectrum of ice is related to temperature. The glacier ice, and thus an iceberg, exhibits properties similar to pure ice because very few impurities are present.

3.0 STATE OF THE ART IN RADAR MEASUREMENT OF ICEBERGS

The first field experiment using radar to detect icebergs was conducted in 1945 by the Ice Information Group (Task Group 24.7) with the goal to devise a method for the quantitative analysis of shipboard radar as an iceberg detection instrument. During the 1946 season supplemental work was done by the International Ice Patrol (IIP). The National Research Council of Canada performed qualitative tests of shipboard radar for ice navigation between 1953 and 1957. These studies indicated that icebergs are not consistent targets. An in-depth experiment was conducted in 1959 by the U.S. Coast Guard, in which the microwave reflective characteristics of glacial ice were determined by using radar (1). Results of this study indicated that icebergs are poor reflectors of electromagnetic energy. All these experiments were conducted by shipboard radars but now experience has shown that aircraft radars like SLAR tend to detect icebergs more reliably than shipboard radars.

Dempster at the Memorial University of Newfoundland (2) has used an X-band radar on ships and on a cliff 730 m above sea level in Labrador to detect icebergs almost without fail, the only exceptions being a few low-profile domed bergs in heavy swell. His conclusions on the use of this type of radar are more encouraging than those reported by Super and Osmer (3), who stress problems with ship-mounted radars in the Grand Banks area. Perhaps some of the difference may be ascribed to radar characteristics, for the modern radar used by Dempster has a 10.5 m range resolution at the shorter distances.

The U.S. Coast Guard first conducted experiments with Side Looking Airborne Radar (SLAR), for use on the International Ice Patrol mission, as early as 1957. It was apparent then that the high resolution of SLAR imagery would provide a number of clues useful for the discrimination of icebergs from man-made objects like ships. These tests were conducted using the AN/APQ-55 (XA-1) K-band real-aperture radar system. Only a limited amount of data was collected at that

time and most of it was not useful because of the experimental nature of the system. The U.S. Coast Guard did not conduct any further experiments using SLAR until 1969. In 1969, an unfocussed synthetic-aperture SLAR system, AN/DPD-2, operating at Ku-band was utilized to test its capabilities as an iceberg discrimination tool for the IIP. These test flights were repeated in 1970, 1971, and 1973 (3).

Subsequently, in 1975, the AN/APS-94C used by NASA Lewis Research Center was flown experimentally in support of the International Ice Patrol in the Grand Banks and Labrador Coast area. The system was used successfully, including detection of small bergs to 48 km range, but target identification remains a problem (3). This is not surprising in view of the coarse resolution of the system (7.5 m/km in azimuth, 37.5 m in range).

The main problem in the detection of icebergs is that they sometimes give the same return as given by ships. Thus the important thing is to devise methods for interpreting radar imagery by which the icebergs can be identified and discriminated from other objects. The usual basic clues of radar imagery interpretation, such as size, shape, shadow, tone, texture, and pattern, can be used to identify icebergs. There are also some clues which apply to icebergs on SLAR imagery but are not commonly used. These clues are the presence and shape of a wake and the edge sharpness of an image.

The overall size of icebergs and ships may vary considerably in each case. If the length-to-width ratio exceeds 5 to 1, the object is usually a ship. An approximate measurement of the height can be made if sufficient detail in the radar shadow is present. If the radar shadow exceeds 25 meters, then the object is usually an iceberg.

It should be pointed out that the dimensions of the object being measured must be greater than the resolution of the radar at the range to the object if these clues are to be used. The shapes of the iceberg on the radar images often tend to be repetitive. Several basic shapes can be identified. Medium and large icebergs generally have square or rectangular shaped images. Small bergs and growlers tend to have either circular or oval shaped images. The SLAR images of the icebergs are highly irregular and complex within the confines of the above shapes. Ships and fishing boats have uniformly shaped returns on the SLAR imagery and the larger vessels frequently exhibit definitive shape.

Icebergs often exhibit a shadow or a no-return area behind them. When the

iceberg is surrounded by sea ice, it almost always has a shadow, depending on the height of the iceberg and the angle of incidence. Because open water gives a black tone as compared to sea ice, the shadow effect is not as readily apparent when icebergs are in the open water. Man-made features such as ships usually give a brighter tone than the icebergs. Icebergs have texture because they are many-faceted and normally have a very irregular structure. Ships on the other hand, give a more even tone, although ship echoes can also be complicated. The edges of SLAR imagery of icebergs are normally not clearly defined.

Large moving ships generally exhibit a well-defined wake on SLAR imagery with the apex at the target. Icebergs may on occasion exhibit a wake, but there is generally no defined apex and the width is fairly constant with little or no flaring.

In the data presented by Anderson (7) icebergs give brighter return as compared to surrounding sea ice. Their small size, angular shape, and concentration of high signal return help to identify them as icebergs.

As is evident from the above, SLAR can be used to map icebergs. The interpretation techniques to identify icebergs are developed to some extent. A need exists to test different parameters such as frequency, polarization, and angles in mapping icebergs. This will help to see the effect of these parameters on the images of icebergs.

4.0 SPECIFICATION OF PARAMETERS FOR ICEBERG MAPPING RADAR

Little information is available which can be helpful in the design of future iceberg mapping radar. The radar images presented by Farmer (1) and Anderson (7) were taken by systems operating at K band. Icebergs can be identified on both the X-band and K-band images. Thus, either of these two bands or some frequency in between can be suitable for detecting icebergs. There is no indication as to which polarization will be optimum in discriminating icebergs. VV polarization may be suitable for such purpose as the data taken so far corresponded to this polarization, but HH should give better discrimination against water. The range of angles should be definitely near grazing so that the shadow effect of the iceberg can be exploited to the fullest extent. Angles from 40 to 70 degrees from vertical may be appropriate for this. The azimuth resolution of the system originally used by Coast Guard was about 9.5 meters per kilometer of slant range. The range resolution on the ground

varied from 20 to 27 meters. The spatial resolution neede for iceberg-mapping radar essentially depends on the minimum size of the iceberg which needs to be detected. In order to identify an iceberg which is 200 meters in width and length, a resolution of at least 50 meters should be made available. Smaller bergs may be easily detected with poor-resolution systems but identification is difficult unless resolution is less, in one dimension at least, than the berg dimension. It is important that a good gray-scale resolution also be provided so that the texture of the iceberg may be detected and the maximum contrast is achievable between iceberg and other objects. A tentative estimate, unsupported by data, is that a dynamic range of 30 dB should be appropriate. Data should be collected as close to daily intervals as possible so that individual icebergs can be tracked by identifying them on successive images.

5.0 CONCLUSIONS AND RECOMMENDATIONS

A review of the above suggests that radar could indeed be a useful tool in mapping icebergs. The all-weather, day/night, operational capability of a radar system is especially useful for such a purpose. However, as is evident from the above, more research, both experimental and theoretical, needs to be conducted for the purpose of specifying optimum operational parameters such as frequency, polarization and angles. A need exists to find the effect of resolution and seasonal variation on the radar images of icebergs.

REFERENCES

1. Farmer, L. D., "Iceberg Classification Using Side-Looking Airborne Radar," United Coast Guard, Office of Research and Development, Applied Science Division, U. S. Coast Guard Headquarters, Washington, D. C. 20591, May, 1972.

2. Dempster, R. T., Personal communication provided by L. Gray, Canada Centre for Remote Sensing.

3. Super, A. D., and S. R. Osmer, "Remote Sensing As It Applies to the International Ice Patrol," Proc. 10th Symposium on Remote Sensing of Environment, University of Michigan, Ann Arbor, 1975.

4. Groen, P., The Waters of the Sea, D. Van Nostrand Co., Ltd., London, 1967.

5. Neuman, G. and W. J. Pierson, Jr., Principles of Physical Oceanography, Prentice-Hall, Inc., New Jersey, 1966.

6. Evans, S., "Dielectric Properties of Ice and Snow - A Review," Journal of Glaciology, vol. 5, pp. 773-792, 1965.

7. Anderson, V. H., "High Altitude, Side-Looking Radar Images of Sea Ice in the Arctic," Proceedings Fourth Symposium on Remote Sensing of Environment, University of Michigan, Ann Arbor, pp. 845-857, June, 1966.

THE UNIVERSITY OF KANSAS SPACE TECHNOLOGY CENTER
Raymond Nichols Hall
2291 Irving Hill Drive—Campus West Lawrence, Kansas 66045

Telephone:

GLACIER STUDIES USING SLAR -- A REVIEW

Remote Sensing Laboratory
RSL Technical Memorandum 291-6

James R. McCauley

March, 1976

Supported by:

NATIONAL AERONAUTICS AND SPACE ADMINISTRATION
Goddard Space Flight Center
Greenbelt, Maryland 20771

CONTRACT NAS 5-22325

TABLE OF CONTENTS

		Page
ABSTRACT		ii
1.0	INTRODUCTION	1
	1.1 Types of Glaciers	1
2.0	DISTRIBUTION OF GLACIERS	2
	2.1 Formation of Glacial Ice	3
3.0	REMOTE SENSING OF GLACIAL ICE WITH ORBITAL SLAR ..	6
	3.1 Electrical Properties of Glacial Ice	7
4.0	SLAR STUDIES OF GLACIAL ICE	9
REFERENCES		16

LIST OF FIGURES

Figure	1	Relative permittivity of snow (ordinates) versus density (abscissae). (From Evans, 1965).	10
	2	Permittivity of wet snow at high frequencies (ordinates) versus volume percentage of liquid water (abscissae). (From Evans, 1965).	10

ABSTRACT

Glaciers cover 11 percent of the earth's surface and contain over three-fourths of the world's fresh water. They are dynamic systems fed by accumulating snow which is slowly metamorphosed into dense crystalline glacier ice. This ice flows from areas of accumulation to areas of ablation where the ice is eventually wasted. Although most common in polar regions, glaciers exist throughout the world. Their accurrance in remote and inhospitable environments make their study on the ground difficult. Orbital remote sensors can overcome these problems and also provide the repetitive coverage necessary for the study of a dynamic system. SLAR has the capability of overcoming the additional problems of cloud-cover, snow storms, poor illumination, and darkness which are common to most glacial environments. Studies of the electrical properties of snow and ice have shown that relative permittivity is a function of snow density and that the presence of small amounts of liquid water in snow greatly increases permittivities, thus indicating that possibility that the various stages of the metamorphism of snow into glacial ice may be interpreted by the relative strength of their radar returns. Studies of SLAR imagery of glaciers have demonstrated SLAR's ability to penetrate recent snow cover. In most cases, the limits of glaciers can be delineated and in at least one study, firm or old snow was found to have a very distinctive radar return. Surface features such as crevasses which are important in the structural and dynamic interpretation of glaciers can be seen in some cases. Areas of meltwater, an important index of a glacier's mass budget, give characteristic low returns on glacier imagery. However, more work needs to be done to determine the snow-penetrating ability of SLAR; the effect water content, crystal size and other glacier variables have on radar return; and the optimum SLAR parameters for obtaining the greatest amount of information from SLAR imagery of glaciers.

GLACIER STUDIES USING SLAR -- A REVIEW

Jim McCauley

1.0 INTRODUCTION

This is a review of the current state of the art of glacial studies using imaging radars. To provide a background for this review, the hydrologic significance and geographic occurence of glaciers are briefly discussed together with the physical and electrical properties of glaciers which are pertinent to their study by radar. Finally, recommendations are made for future studies in order to determine the optimum parameters for use in an operational orbital radar for the study and/or monitoring of glaciers.

Glaciers are moving bodies of ice that are characterized by a zone of perennial snow accumulation, the slow metamorphism of this snow into glacial ice, the movement of this ice as a total mass in response to loading and gravity, and the eventual destruction of this mass as a result of melting, sublimation, or mass wasting. Glacial ice covers 11 percent of the earth's land surface (Shumskii, 1964) and it has been estimated that glacial ice constitutes 77 percent of the world's fresh water (U.S.G.S., 1968). Some parts of the world, especially mountainous areas, are highly dependant upon the reliable sources of water that glaciers provide. Glaciers play an important role in determining the heat budget of the earth's atmosphere and oceans. Those glaciers that flow into the sea are the sources of icebergs, a continuous hazard to the world's shipping lanes. Glaciers are also recorders of variations in the world's climate with their mass budgets changing in response to these variations.

1.1 Types of Glaciers

Glaciers can be classified into three types based on their morphology: 1) alpine or valley glaciers, 2) piedmont glaciers and 3) glacial ice-caps. Included with the valley glaciers are the smallest type of glacier, the niche glaciers which form on steep valley walls. The more characteristic form of valley glaciers exists in mountainous areas receiving accumulations of snow in amphitheater-shaped

basins at the heads of valleys. These basins are called cirques and have been carved out of the mountain walls by the erosive forces of moving ice. Some glaciers, cirque glaciers, fail to flow out of these basins, however if the snow-line (lower limit of perpetual snow) is low enough, glacial ice can flow out of the cirques and down the valley forming a valley glacier. Smaller valley glaciers heading in separate cirques can unite to form one large valley glacier in the same way that tributaries join to form larger streams. When valley glaciers exit from the mountains into level lowlands they tend to spread out into large flat lobes of glacial ice called piedmont glaciers. Ice-caps are the largest types of glaciers and include mountain ice-caps, lowland ice-caps, and continental ice-sheets. Mountain ice-caps forming in the high parts of mountain ranges and plateaus cover much of the higher elevations and send valley-like glaciers down to lower levels. Lowland ice-caps develop at low elevations in relatively flat terrain and are found only in high arctic areas. Continental ice-sheets, by far the largest glacial form, are capable of covering continent-size areas (Embleton and King, 1968).

2.0 DISTRIBUTION OF GLACIERS

Glaciers, although generally associated with polar regions, can and do occur in high mountains at virtually any latitude including the equator. Mount Kilamanjaro and Mount Kenya in Kenya both support glaciers. Small glaciers are also present in the high mountains of New Guinea. The Alps of Southern Europe and the Southern Alps of New Zealand are both noted for their many well-developed valley glaciers, and owe their rugged landscapes to the effects of glacial erosion. Valley glaciers are also found in the Himalayas, the Andes, and the Caucasus, as well as in the high mountains of the western United States and Canada. In general, as one approaches the poles, the lowest elevation at which glaciers can occur decreases until at very high latitudes, glaciers exist at sea level and in fact are capable of flowing out over the sea forming ice-shelves.

Of course, it is in the high latitudes that most glacial ice occurs and where the various glacial forms are more widespread. Alaska, Canada, Iceland, and Scandinavia all contain large areas covered by various forms of glacial ice. However, the largest glacial form, the continental ice-sheets, are found only in Greenland and Antarctica. These two ice-sheets contain 11 percent and 85 per-

cent respectively of the world's ice. The Antarctic ice-sheet covers an area of 11.5 million km^2, one and a half times the area of the United States, and has a mean thickness of between 2000 and 2500 pr. (Embleton and King, 1968).

2.1 Formation of Glacial Ice

Glacial ice is formed almost exclusively from precipitation falling as snow and accumulating year after year. This snow undergoes extensive physical changes and nourishes the glacier, while being gradually transformed into glacial ice. Fresh dry snow has a very low density because of its loose packing and many air spaces, generally in the neighborhood of 0.05 grams $/cm^3$. With time, the weight of additional accumulations of snow, sublimation, and periods of partial melting and refreezing all act to increase the density of new snow and change its texture. The first stage of this transformation is called granular snow and is reached when a density of 0.2 grams $/cm^3$ is attained. The pressure responsible for the increase in density also acts to increase the crystal size of the snow, forming large crystals at the expense of smaller ones. The next stage of metamorphism occurs when a density of about 0.4 to 0.55 grams$/cm^3$ is reached. Snow in this stage is called firn and is characterized by a further increase in crystal size. At a density of 0.8 to 0.9 grams$/cm^3$, glacial ice is formed. At such densities, most of the trapped air has been removed and the texture becomes homogeneous, composed of equidimensional interlocking grains on the order of 1.5 cm in size (Ragle et al., 1964). Such high densities nearly approach the density of pure ice, which is 0.9168 grams$/cm^3$. Glacial ice is usually blue in color as opposed to snow and firn which are white.

The metamorphism of fresh snow into glacial ice is generally a slow process, the length of time depending upon the climate. In areas with a pronounced warm season, transformation of snow into glacial ice may proceed much more quickly than in areas that are perennially cold where the process may require hundreds of years. Since temperature plays such an important role in glacier formation and, subsequently glacial activity, an alternative scheme of glacier classification has been suggested by Ahlmann (1948). In this classification, there are two fundamental types: temperate and cold (or polar) glaciers. Temperate glaciers are at the pressure melting point throughout their thickness all year except in the winter when the upper

levels may become colder. Such glaciers have also been termed permelting glaciers because they are permeated by melt water. In such glaciers, the metamorphism of new snow to firn and subsequently to glacial ice is quite rapid. As a result, the accumulation of firn is thinner than it would be on colder glaciers. The presence of melt water at the base of the temperate glacier facilitates its movement over the land surface, making it more active and capable of greater erosive work than other types. The glaciers of the Alps, New Zealand, and southern Scandinavia are considered temperate glaciers as are those in the Rockies of the United States and Canada.

Cold or polar glaciers differ greatly from temperate glaciers in their temperature characteristics and consequently in their internal and surface characteristics as well. Ahlmann has separated this type into sub-polar and high-polar types. In the sub-polar glacier the temperature is below freezing throughout the year except during the summer when some surface melting may occur and water may be present. Because of the colder conditions and fewer freeze-thaw cycles, the metamorphism of snow into glacial ice proceeds at a slower rate than in temperate glaciers. As a result, sub-polar glaciers have thicker accumulations of firn on their surfaces extending downward 10 to 20 meters. Sub-polar glaciers also tend to be less active than temperate glaciers. The high polar type glacier never experiences melting throughout its thickness in its accumulation area. It thus lacks interstitial melt water. In such glaciers, snow metamorphism is slowest. Snowfall in high polar areas is very low in density and since it never melts even intermittently, it must accumulate to great depths before pressures are sufficient to cause the formation of firn, generally more than 75 meters. Thus glacial ice in high polar glaciers is deeply buried beneath a thick layer of firn which is in turn buried beneath thick accumulations of old and new snow. Most cold glaciers are frozen to the earth's surface by the extremely low internal temperatures. At such low temperatures ice is much stronger than it is when near the melting point. As a result, cold glaciers flow at much slower rates than temperate glaciers. Some high polar glaciers appear not to move at all or, if so, at imperceptable rates.

It should be noted that various parts of a glacier may belong to more than one thermal type depending upon local conditions. For instance, some cold glaciers are classified as such because of their surface characteristics even though they may be at the pressure melting-point at their bases.

Mass budget studies are concerned with the loss and gain of snow in a glacier and are of primary interest to many glaciologists. The mass budget of a glacier is highly dependent on climate and reflects climatic fluctuations. World-wide changes in the amount of water locked up in the form of glacier ice can in turn affect the relative position of sea level. Mass budget studies can also provide important hydrologic data for areas downstream from glacier ice.

The opposing forces of accumulation on the plus side of the ledger and ablation on the negative side determine a glacier's mass budget. A glacier's mass budget may be defined as its gross annual accumulation less its net ablation during the budget year. The size of a glacier's budget in relation to its area determines its activity as do the absolute rates of accumulation and ablation. Glaciers having high rates of accumulation and ablation such as those in New Zealand and elsewhere must flow very fast whereas those having low rates such as those of Antarctica move very slowly. Very active glaciers are capable of more erosion and deposition and have more effects on the landscape. The net budget of a glacier determines its thickness and the location of its snout. A glacier in equilibrium has a stationary snout which may be buried beneath debris being carried down by the glacier and deposited by the ablating ice. This debris tends to accumulate in linear ridges called moraines. A terminal moraine forms at the snout of a glacier and lateral moraines form along the sides. A glacier with a positive budget has an advancing snout which may override older terminal moraines. Some glaciers have surged at rates of up to 100 m/day in response to large, climatically induced, budget increases. Conversely, a glacier with a negative balance has a retreating snout which may leave terminal moraines in its wake.

One criterion useful for estimating the mass budget of a glacier is the location of the firn line. The firn line is the uppermost line on a glacier to which the snowfall and firn of the winter season melts during the summer ablation season. On most glaciers, this is a clearly defined line separating white snow and firn above from hard blue glacial ice below. This line is most apparent and meaningful when observed in late summer at the end of the ablation season. The movement of the firn line from year to year is a gauge of the mass budget, moving downhill in response to a positive budget and uphill in response to a negative budget.

It should be noted that a balanced mass budget is rarely achieved by a

glacier for a long period of time. Mass budgets are constantly fluctuating and rates of glacial activity are constantly changing in response.

3.0 REMOTE SENSING OF GLACIAL ICE WITH ORBITAL SLAR

Numerous factors contribute to make the study of the world's glaciers difficult and in some cases dangerous. Glaciers, by their very nature, are restricted to areas of severe climate, either polar regions or the highest portions of mountain ranges. These regions are the most remote and inaccessible areas on earth, and offer the most inhospitable climate to be faced by man anywhere. Field studies in such areas are severely hampered by terrain, weather, and isolation from sources of supply. Glaciers are also widely spread throughout the world, occurring on six of the seven continents and at virtually every latitude. Attempts at their study should therefore be on a global scale. They range in size from very small niche glaciers to ice sheets which reach continental proportions. Continual field study of larger glaciers such as the various ice caps and piedmont glaciers would be in regions covering hundreds and thousands of square kilometers. Even valley glaciers, one of the smaller forms, can attain lengths of 120 km. Finally, glaciers are dynamic systems having mass inputs in the form of snow accumulation and mass losses due to ablation. The relative rates of these two factors determines the activity of a glacier, the speed at which it moves, and the location of its terminous. Because of this dynamic return, glacial studies must be repetitive, thus compounding necessary field work.

Remote sensors especially those operating at orbital altitudes are capable of overcoming the many obstacles to the study of glaciers, and hold the promise of providing information that might not otherwise be obtained. Of the various sensors available, side-looking radar appears to be the best suited to coping with the unique geographic and climatic problems inherent in the study of glaciers. By providing its own illumination, radar could operate independently of the darkness and low sun angles which prevail throughout the year in polar regions. Satellite-borne radar could also operate independently of the severe winter weather common to glaciated areas, being unaffected by falling and blowing snow. Long term cloud cover often occurs in polar and high mountain areas, thus posing a problem to those sensors operating in the visible and infrared portions of the spectrum. Such

is not the case with radar which is capable of penetrating cloud cover. Visible and infrared imagery acquired from space over partly cloudy snow-covered terrain present a potential problem to the interpreter. It is often difficult to separate clouds from snow and ice, and old snow and ice from snow-dusted outcrops (Wobber, 1969). Since clouds are invisible to radar, they would not appear on imagery. In addition, radar appears to be capable of penetrating recent snow cover, thus reducing the possibility of confusing ice and firn with snow-covered terrain. Radar is also highly sensitive to surface roughness and may provide otherwise unattainable information on the surface configuration of glaciers.

3.1 Electrical Properties of Glacial Ice

Much interest has been expressed in the possibility of sounding the depths of snow and ice by electromagnetic means. As a result, many experiments have been performed to determine the dielectric properties of snow and ice. However, many of these experiments have used energy with frequencies that are much lower than those generated by most imaging radar systems. In addition, many of these studies used solid ice or compressed snow prepared in the laboratory instead of actual glacial ice. Such artificial samples lack the impurities, and internal structure and texture of naturally occurring glacial ice. These studies are also concerned only with the electrical properties of ice and snow and do not touch on the surface and internal configurations these materials possess in their natural state, which play such an important role in determining the reflection of radar energy back to an imaging system. For these reasons, electrical studies of ice and snow can provide only partial answers to questions concerning the manner of appearance of glacial ice on radar imagery and the applicability of radar imagery to glacial studies. A few of those electrical studies considered pertinent to the study of glaciers by radar are reviewed below.

Cumming (1952) determined the permittivity and the loss tangent of snow and ice samples at a frequency of 9.375 GHz (λ = 3.2 cm). Snow samples were prepared in the laboratory with densities that ranged from 2.3 to 9.1 grams/cm^3. Permittivities increased with density, ranging from approximately 1.35 for the least dense sample to 3.15 for solid ice. This data appears in Figure 1. Permittivities were also found to be constant for a given sample throughout the

temperature range of 0° to -20° C. The loss tangent was found to decrease with decreasing density and with lower temperature over a range of 0° to -20° C. The presence of small amounts of free water in snow samples was found to drastically increase the loss tangent. The presence of only 0.8 percent free water by weight was sufficient to increase the loss tangent by a factor of ten.

Cumming also experimented with two antennas mounted over a test plot to determine the reflectivity over a complete range of grazing angles from a smooth sandy soil and a metal plate when each was covered by various types of snowfall. The apparent lack of multiple reflections from the snow-covered sandy soil led Cumming to conclude that radar reflection was predominantly at the air-snow interface. However these measurements were made when the air temperature was at or within 1° F of freezing and the snow cover was moist, and probably contained small amounts of interstitial water. When the metal plate was covered with moist snow, the predominant reflection was again from the air-snow interface. However, when the metal plate was covered by cold, dry snow at temperatures well below the freezing point, multiple reflections were quite apparent indicating penetration of the snow but not without a reduced coefficient of reflection.

Cumming concludes that a smooth snow cover over a terrain would reduce its reflection back to a monostatic radar system at low grazing angles due to specular reflection. Cumming also concludes that, except for a thin covering of dry snow over a good refelctor, at near normal incidence, snow cover usually increases specular reflection.

Watt and Maxwell (1960) working in the field with low frequency radio waves (20 Hz - 200 kHz) found appreciable differences between snow and pure ice and between glacial ice and pure ice. A paper by Ragle et al. (1964) contains a table of dielectric measurements made by Westphal on core samples of glacial ice and sea ice collected from the Ward Hunt Ice Shelf off Ellesmere Island. These measurements cover a frequency range of 150 - 1000 MHz and a temperature range of -1° C to -60° C. Dielectric constants and loss tangents for all frequencies decreased with decreasing temperature. In addition, sea ice was found to have a consistently larger dielectric constant and loss tangent (about twenty times larger) than that of glacial ice, the higher density of glacial ice and the larger loss tangent resulting from a higher concentration of conducting ions. The dielectric constant of glacial ice ranged from 2.90 to 2.95 and that of sea ice

ranged from 2.95 to 3.18. The difference in dielectric constant led the authors to suggest the possibility of detecting the glacier ice - sea ice boundary using reflections of electromagnetic waves.

Evans (1965) reviewed previous work concerning the dielectric properties of ice and snow and compared the results obtained by various investigators. In Figure 1, Cumming's data is incorporated to show the relation of relative permittivity to density for high frequency radio waves. Also shown are theoretical curves showing the same relation for various Formzahl values (u) as defined by Weiner and determined by snow structures as shown below the graph. The various stages in the metamorphism of snow to glacial ice would have Formzahl values of 2 to 25 and their relative permittivities should increase with progressive metamorphism thus having differing reflective properties with respect to radar and offering the possibility of being discriminated by an imaging radar.

In Figure 2, Evans shows the effect of liquid water content on the relative permittivity of snow at high frequencies. The snow sample used in producing this data would have a specific gravity of about 0.5 grams/cm^3 and thus is actually firn. At a water content of approximately 10 percent, the relative permittivity surpasses that of solid ice as shown in Figure 1. The contrastingly high values of the permittivity of wet snow or firn make its mapping by imaging radars a possibility. If so, it may enable the thermal classification of glaciers as temperate, sub polar, or high polar glaciers based on the presence of liquid water. Another potential result is mapping of old snow or firn at the end of the ablation season which will survive into the next budget year. Such information would be useful in estimating the mass budget of a glacier.

4.0 SLAR STUDIES OF GLACIAL ICE

Studies of glacial ice using side-looking airborne radar (SLAR) are limited in both scope and number. The greatest effort to apply imaging radars to glaciology has been expended in the study of sea ice. Various types and ages of sea ice can be inferred from their distinctive appearances on SLAR images. In addition, areas of open water can usually be distinguished from areas of ice-cover. These capabilities have made SLAR a useful navigational aid for those government agencies responsible for the maintenance of shipping lanes in polar environments. However, sea ice differs markedly from glacial ice in composition, internal and external

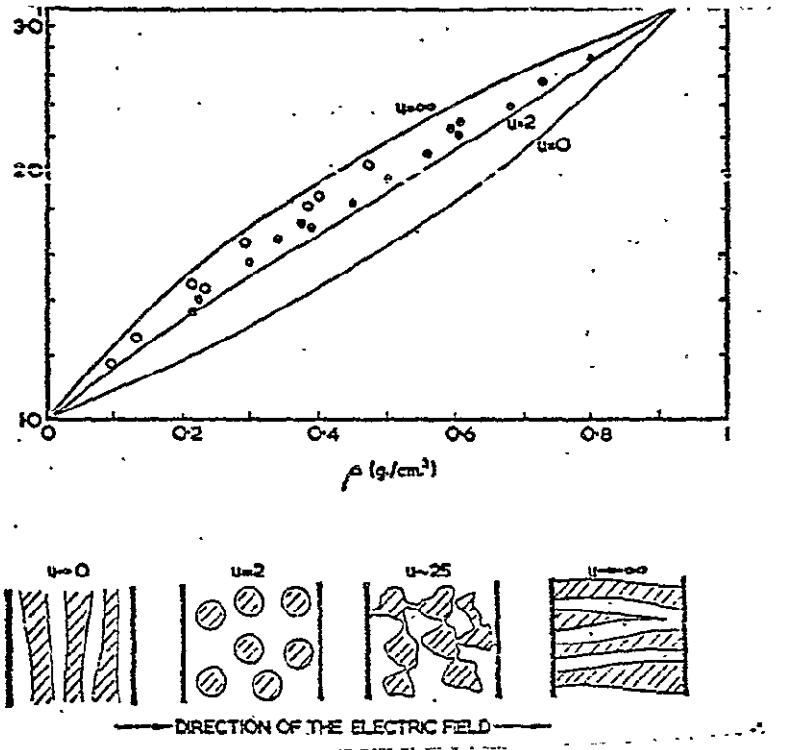

Figure 1. Relative permittivity of snow (ordinates) versus density (abscissae). (From Evans, 1965).

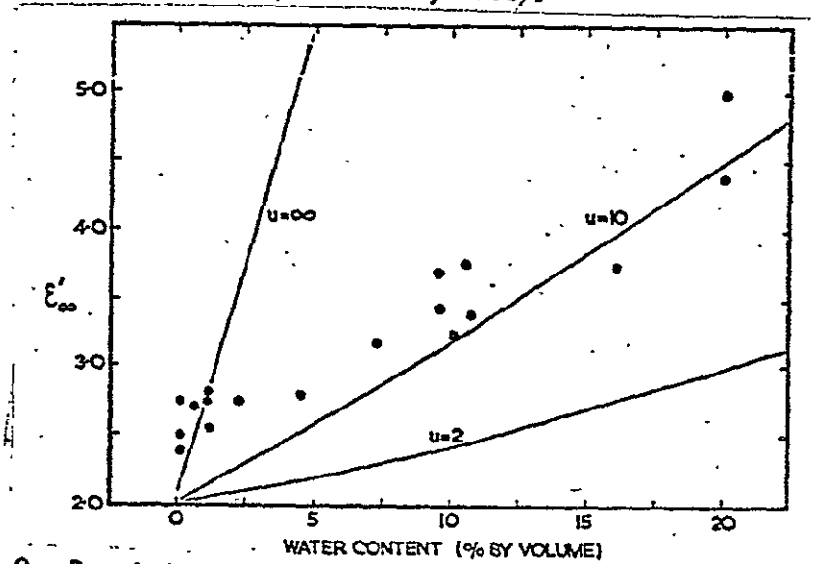

Figure 2. Permittivity of wet snow at high frequencies (ordinates) versus volume percentage of liquid water (abscissae). (From Evans, 1965).

structure, and as a result in its electrical and scattering properties as well. Thus, SLAR studies of sea ice are only marginally applicable to studies of glacial ice. Despite their small number, those SLAR studies of glaciers that have been conducted have demonstrated SLAR's ability to provide useful information to the glaciologist.

Meier et al.(1966) evaluated the glaciological data content of several sensors in tests carried out at South Cascade Glacier, Washington. Among the sensors evaluated was the AN/APQ-97 Ka-band side-looking airborne radar and the imagery it produced. The investigators found that morphological features associated with glaciers such as moraines, crevasses, and textural patterns show up clearly. They were also able to distinguish between snow and ice and found that gross textural differences between glaciers and land were apparent even when both had a thin covering of snow. The high relief and steep slopes in the area caused some shadowing problems, however, judicious choice of depression angles can overcome this problem (MacDonald and Waite, 1971). Because of radar's ability to distinguish glaciers from surrounding terrain and icebergs from the sea independently of weather conditions and even through a thin snow cover, the authors conclude that it is possible to inventory the world's glaciers. The authors also point out that while multispectral and color photography from satellites may provide useful glaciological information, their use would be limited by the paucity of colors and tonal contrasts in snow and the operating restrictions imposed by darkness and cloud cover.

Leighty (1966) described the terrain information contained in AN/APQ-56 Ka-band radar imagery acquired over northwestern Greenland. Four general terrain types were covered by the imagery: the Greenland ice cap interior, the ice cap margin, land, and sea and ice. The ice-cap interior, lying beyond the firn line, was found to be snow-covered and monotonous, having very small-scale relief due to wind erosion and deposition. Radar imagery acquired over the ice-cap interior was uniform and without detail except along transportation routes where compacted snow gave lower returns. In addition, these transportation routes were discernable on imagery even when they were covered by at least a foot of uncompacted snow.

On imagery acquired over the ice-cap margin, crevasses were very apparent and based upon their arrangement, Leighty was able to make structural interpretations and estimations of relative rates of ice movement in various parts of the glacier. Moraines, snow drifts, and standing water were also observable, and Leighty was able to differentiate different types of glacial ice based on image tone. Leighty

found the ice-cap - land contact difficult to determine where no great change in slope existed or where the area was covered by snow. Elsewhere, margin identification was relatively easy. Leighty rates the relative signal return from terrain materials in the following decreasing order: snow, glacial ice, soils and rocks, lake ice and sea ice, and open water. Leighty also concludes that different look directions are important for maximum information retrieval.

Waite and MacDonald (1970) investigated the feasibility of mapping perennial snowfields with imaging radars by studying AN/APQ-97, Ka-band imagery acquired in alpine environments of the western United States and comparing this imagery with field data and simultaneously acquired oblique photography. They found snowfields to have anomalously high radar returns, appearing as bright radar images. These high returns occurred independently of slope and look directions and registered with better contrast on the cross-polarized imagery. Field work found these anomalous snowfields to be composed of firn. In one area of investigation, comparison with oblique photography revealed radars ability to penetrate a covering of new fallen snow. Small glaciers in the Three Sisters Region of Oregon were found to have dominantly low returns with some areas of high return.

The authors theorize on the causes of the anomalously high returns from the old snowfields and conclude that it is due to some factor in addition to moisture content. The authors suggest that the high returns may result from volume scattering from randomly distributed spheres with the behaviour of moisture possibly playing an important role, such as forming a wet coating on grains. These wet coatings could then be considered a continuous water film with a roughness in the sensing wavelength due to the size of the snow granules.

Page (1975) reviewed the applications of various radar techniques to studies of ice and snow. His discussion of imaging radar is largely concerned with mapping and monitoring sea ice using NA/APS-940 X-band SLAR imagery acquired along the northeastern coast of Ellesmire Island. Some of this imagery however, covers a portion of the Grant Ice Cap and Page mentions the typical "milky appearance" of the glacial ice. This glacier has a fine-grained texture and brighter tones than those produced by glaciers on most of the Ka-band imagery analyzed in the other studies. Page also mentions that there is some evidence to indicate that radar is capable of detecting subsurface structures in glacier ice. He also points out that use of radar with a wavelength longer than the 3 cm of X-band results in decreased gray tones in images of ice.

In 1973, Moore (1973) was shown radar images of glaciers obtained during the USSR monitoring of sea ice. These 16 GHz real-aperture images showed the flow lines on glaciers very clearly. No attempt was made to analyze the images, and any Soviet analyses of them were not provided.

Radar imagery produced by the Jet Propulsion Laboratories' L-band ($\lambda = 25$ cm) SLAR over southeastern Alaska was described by Elachi and Brown (1975). This imagery covered areas in southeastern Alaska that include several large valley glaciers and part of the Malaspina piedmont glacier. The glaciers could be identified by a combination of shape and tonal contrasts. Medial moraines in the glaciers which are characterized by concentrations of erosional debris and surface roughness differences were visible on the imagery. Deformation of these medial moraines together with other patterns visible on the glaciers indicated stresses present in the ice and relative rates of movement. Numerous tonal variations within the glaciers were apparent on the imagery and were most likely caused by physical difference in the glacial ice. The authors maintain that since SLAR resolution is independent of range, similar imagery could be obtained from an orbital spacecraft.

It is worth noting that the above studies of SLAR's applicability to the study of glacial ice have been carried out in different environments, at various times of the year, and used radars with important system parameter differences. In addition, few of the investigations included the simultaneous collection of ground truth. As a result, the ice and system parameters that are important in determining the reflection of radar from glacial ice are poorly understood, and conclusions drawn from the study of glacier imagery are often sketchy and, in some cases, seemingly contradictory.

It is obvious that more work needs to be done before the full applicability of SLAR to glacial studies is understood. However, some of the results presented in the publications reviewed above are encouraging. In most of these studies, it was discovered that radar had the ability to penetrate snow to some degree. This is an important ability since it could make possible the delineation of glaciers from snow-covered terrain at all times of the year. It could also allow the identification of sub-snow terrain features in areas where snow cover is present during much of the year.

The very high radar returns from old snow or firn as described by Waite and MacDonald (1970) indicates the possibility of mapping firn fields using SLAR. Such

mapping ability could provide information necessary to make fairly accurate estimates of a glacier's mass balance. One method of achieving this estimate is by noting the position of the firn line which separates firn above and glacial ice below on a glacier at the end of the ablation season. The yearly movement of this line either up or down the glacier could tell whether the mass balance is negative or positive respectively (LaChappelle , 1962). Another method of mass balance estimation which is also described by LaChappelle is the use of the accumulation area ratio as defined by Meier (1962). This ratio is equal to the area of snow cover at the end of the ablation season (= firn) within a given locality divided by the total area of glacial ice present. Changes in this ratio can signify changes in glacier mass balance and also weather conditions.

The amount of melt water present on, near and downstream from a glacier is also an important indicator of its mass balance, especially the negative portion. Water has a very distinctive low return on SLAR imagery that allows it to be easily mapped in most situations.

The appearance of glacial ice on SLAR as described in the publications reviewed varied considerably from fairly bright, fine textured tones on the X-band imagery studied by Page to widely varying tones on the Ka-band imagery of Leighty to generally dark tones on imagery analyzed by Waite and MacDonald, also Ka-band. The ability to recognize glacial ice is essential to its study with SLAR since the mapping of glaciers on a world-wide basis would be an important objective with an orbital system. The location of the margins of glaciers and the movement of those margins with time are important indicators of glacial activity and possibly climatic changes as well. The shape of the glacial margin is also important, La-Chappelle (1962) has shown that an advancing glacier usually has a steep or vertical front, a retreating glacier has a gently sloping front and a glacier in equilibrium has a front with a moderate slope. The identification and monitoring of crevasses in glaciers can provide information on structural glaciology and relative rates of flow in glacial ice as extracted by Leighty in Greenland. This information can in turn allow the inference of subglacial topography due to the deformation it induces in overflowing glacial ice.

Ideally, SLAR should be able to penetrate ephemeral snow; distinguish between firn, glacial ice, water, and land; and provide information on the surface features of glaciers. To some extent, SLAR can do all of these things right now; however, studies should be conducted to determine how well it does them, what surface

conditions influence radar performance, and what system parameters could give optimum results. A year long study of both a temperate and polar type glacier by multifrequency and possibly multipolarized imaging radars assisted by simultaneous ground truth collection, could provide answers to these questions. Ground truth should include air and snow and ice temperatuers, snow depth, the density, size, and water contents of snow, firn, and glacial ice, and depth to glacial ice. Experiments should be performed several times in the course of a year to determine the effects that increasing snow depth, physical changes in snow and ice, and the onset and progression of ablation have on radar imagery of glacial environments.

REFERENCES

Ahlmann, H. W., 1948, "Glaciological Research on the North Atlantic Coasts," Royal Geographical Society, serial 1, 80 pp.

Cumming, W. A., 1952, "The Dielectric Properties of Ice and Snow at 3.2 Centimeters," Journal of Applied Physics, Vol. 23, No. 7, pp. 768-783.

Elachi, C. and W. E. Brown, Jr., 1975, "Imaging and Sounding of Ice Fields with Airborne Coherent Radar," Journal of Geophysical Research, Vol. 80, No. 8, pp. 1113-1119.

Embleton, C., and C.A.M. King, 1968, "Glacial and Periglacial Geomorphology," St. Martin's Press, New York, NY, 608 pp.

Evans, S., 1965, "Dielectric Properties of Ice and Snow - A Review," Journal of Glaciology, Vol. 5, pp. 773-782.

LaChappelle, E., 1962, "Assessing Glacier Mass Balance By Reconnaissance Aerial Photography," Journal of Glaciology, Vol. 4, No. 33, pp. 290-291.

Leighty, R. D., 1966, "Terrain Information From High Altitude Side-Looking Radar Imagery on an Arctic Area," in Fourth Symposium on Remote Sensing of Environment Proceedings, Univ. Michigan, Ann Arbor, pp. 575-597.

MacDonald, H. C. and W. P. Waite, 1971, "Optimum Radar Depression Angles for Geological Analysis," Modern Geology, Vol. 2, No. 3, pp. 179-193.

Meier, M. F., 1962, "Proposed Definitives for Glacier Mass Budget Terms," Journal of Glaciology, Vol. 4, No. 33, pp. 252-265.

Meier, M. F., W. J. Campbell, and R. H. Alexander, 1966, "Multispectral Sensing Tests at South Cascade Glacier, Washington," in Fourth Symposium on Remote Sensing of Environment, Proceedings, Univ. Michigan, Ann Arbor, pp. 145-160.

Moore, R. K., 1973, Private report on visit to USSR, University of Kansas.

Page, D. F., 1975, "Application of Radar Techniques to Ice and Snow Studies," Journal of Glaciology, Vol. 15, No. 73, in Symposium on Remote Sensing in Glaciology, Proc., Cambridge, England, pp. 171-192.

Ragle, R. H., R. G. Blair, and L. E. Persson, 1964, "Ice Core Studies of Ward Hunt Ice Shelf," Journal of Glaciology, Vol. 5, No. 37, pp. 39-59.

Shumskii, P. A., 1964, "Principles of Structural Glaciology," Dover Publications, New York, NY.

United States Geological Survey, 1968, "News Release - Water of the World," prepared July 1968.

Waite, W. P. and H. C. MacDonald, 1970, "Snowfield Mapping with K-band Radar," Remote Sensing of Environment, Vol. 1, pp. 143-150.

Watt, A. D. and E. L. Maxwell, 1960, "Measured Electrical Properties of Snow and Glacial Ice," Journal of Research of the National Bureau of Standards (Washington, D. C.), Sect. D., Vol. 64, No. 4, pp. 357-363.

Weiner, O., 1910, "Zur Thoerie Oer Refranktion Konstanten," Berichte Uber Die Verhandlungen Der Koniglich Sachsischen Gesellschaft der Wissenschafter Zu Leipzig, Mathematisch-Physikalische Klasse, Band 63, Ht. 5, pp. 256-260.

Wobber, F. T., 1969, "Environmental Studies Using Earth Orbital Photography," Photogrammetrics, Vol. 24, No. 3/4, pp. 107-165.

APPENDIX D

RSL TECHNICAL REPORT 291-2

VOLUME III

THE UNIVERSITY OF KANSAS SPACE TECHNOLOGY CENTER
Raymond Nichols Hall
2291 Irving Hill Drive—Campus West Lawrence, Kansas 66045
Telephone:

SOME COVERAGE CONSIDERATIONS FOR A SCANNING SYNTHETIC APERTURE SPACEBORNE RADAR

Remote Sensing Laboratory
RSL Technical Memorandum 291-11

Richard K. Moore

January, 1977

Supported by:
NATIONAL AERONAUTICS AND SPACE ADMINISTRATION
Goddard Space Flight Center
Greenbelt, Maryland 20771

CONTRACT NAS 5-22325

SOME COVERAGE CONSIDERATIONS FOR A SCANNING SYNTHETIC APERTURE SPACEBORNE RADAR

ABSTRACT

Calculations of swath width for a scanning synthetic-aperture space radar are considerably more complicated when the spherical nature of the earth must be taken into account than when a plane-earth approximation can be made. The methods for calculating the swath width and other relevant parameters are outlined here.

Calculated examples show that the swath width can be improved significantly if smaller pointing and incidence angles can be tolerated, but that the effect of altitude is small over the range from 400 to 1000 km for outer pointing angles exceeding 30°. Beamwidths required at higher altitudes and larger pointing angles are quite narrow, resulting in rather large required vertical apertures. Thus, the vertical aperture ranges from 260 wavelengths at 55° outer pointing angle and 1000 km down to only 10 wavelengths at 30° and 400 km for a system with a 10 m long antenna and 5 scan cells.

SOME COVERAGE CONSIDERATIONS FOR A SCANNING SYNTHETIC APERTURE SPACEBORNE RADAR

1.0 INTRODUCTION

Most of the calculations in reports dealing with the SCANSAR [1 - 6] have been based on plane-earth geometry. For angles of incidence near vertical, such as those used in soil moisture measurement and in the Seasat imaging radar, results obtained with the use of planar rather than spherical geometry are not far from the more correct values obtained using spherical geometry. On the other hand, for angles of incidence exceeding about 30° such as those of most importance in ice sensing, spherical geometry must be used, and the results obtained differ appreciably from those based on plane geometry. This memorandum illustrates the conditions placed upon SCANSAR when spherical geometry is used.

2.0 GEOMETRIC CONSIDERATIONS

The basic geometry of the spherical-earth situation is shown in Figure 1. For spherical geometry the angle of incidence θ and the nadir-reference pointing angle δ are different. θ is the relevant angle for considering the strength of the backscatter and δ is the relevant angle for antenna pointing. Ground coverage is given in terms of the arc length ρ. For the purpose of this report, the earth is considered a true sphere of 40,000 km circumference; oblateness is not considered, but would be a minor effect.

The horizontal distance from nadir ρ is given in terms of the central angle γ by

$$\rho = a\,\gamma \tag{1}$$

Applying the Law of Sines to the triangle in Figure 1,

$$\sin(180 - \theta) = \sin\theta = \frac{a + H}{a}\sin\delta \tag{2}$$

Hence,

$$\gamma = \theta - \delta \tag{3}$$

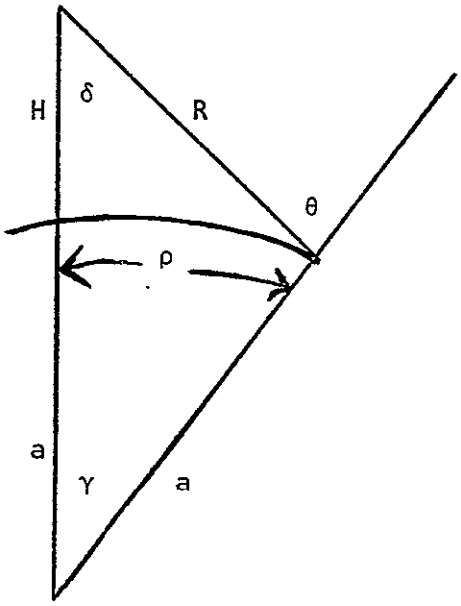

FIGURE 1 . Geometry of Spherical-Earth Calculations.

If both γ and δ are known, R can be found from

$$R = a \frac{\sin \gamma}{\sin \delta} \tag{4}$$

The maximum possible number of scan cells is the ratio of the maximum available length of synthetic aperture to the amount of aperture required by each cell to obtain the desired resolution and number of independent samples. Thus, if N independent looks are to be obtained for each cell,

$$M = \min \left[L_T / NL_1 \right] \tag{5}$$

where L_T is the total synthetic aperture length available (the distance occupied on the ground by the real along-track beamwidth), L_1 is the length of a single synthetic aperture, and min [ ] is to be read as "least integer in []." Substituting the usual approximate expressions for L_T and L_1, we find for azimuth resolution r_a and along-track aperture D,

$$M = \min \left[\left(\frac{\lambda R}{D}\right) \Big/ N \left(\frac{\lambda R}{2r_a}\right) \right]$$

which simplifies to

$$M = \min \left[2r_a / ND \right] \tag{6}$$

As an example of the application of this result, consider the number of independent looks N to be 3, the desired along-track resolution r_a to be 50 m, and an effective antenna aperture of 10 m. Then

$$M = \min [100/30] = [3.33] = 3$$

Thus, with these conditions only 3 scan positions (scan cells) are possible. With a shorter aperture, the beam would spread out more on the ground, and more scan positions would be possible; on the other hand, a shorter aperture requires more beam positions because of ambiguity considerations.

The ambiguity conditions limit the swath width possible for each cell. The prf must be at least equal the Doppler bandwidth, so that

$$prf = \frac{2u\lambda}{\lambda D} fa$$

where u is the horizontal speed and f_a is the factor of safety in the anong-track direction used to account for the fact that the gain does not go to zero as soon as the nominal beamwidth is reached. The pulse repetition period is the reciprocal of the prf, and the swath per scan cell cannot be greater than the spatial separation of successive pulses; thus this place a limit

$$\Delta R f_R = \frac{.c}{2prf}$$

where ΔR is the slant-range swath per cell, and f_R is the factor of safety that accounts for the finite range of angles for the vertical gain pattern to drop off to negligible value. Combining these two criteria gives

$$\Delta R_{max} = \frac{cD}{4uf_R f_a} \tag{7}$$

The procedure for calculating the coverage is best understood by reference to Figure 2, a flow chart for this calculation. Since the beamwidth in elevation must be minimum (for a given ΔR) at the maximum pointing angle, the parameters for the outermost scan cell must be calculated before those for the other cells. Once the vertical beamwidth has been calculated for this cell, it may be multiplied by the number

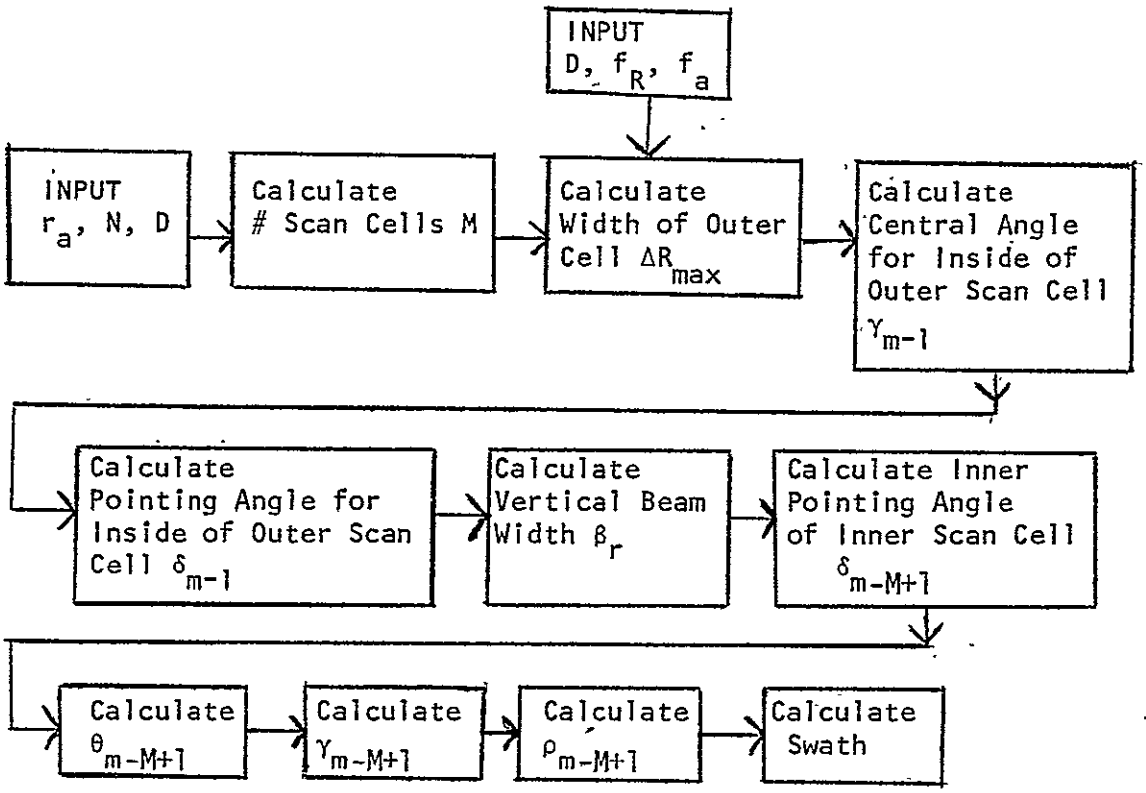

FIGURE 2. Procedure for Determining Swath Width - Constant Vertical Beamwidth.

of permitted scan cells and the result subtracted from the outermost pointing angle to determine the pointing angle to the inside of the innermost cell. From this the swath may be calculated.

To obtain the central angle of the inner edge of the outer cell, the Law of Cosines may be applied to the triangle of Figure 1, obtaining

$$\cos \gamma_{m-1} \cong \frac{a^2 + (a + H)^2 - (R_{max} - \Delta R)^2}{2a\ (a - H)} \tag{8}$$

This value and the slant range $(R_{max} - \Delta R)$ may be substituted in (4) to obtain the pointing angle at the inside of the outer cell δ_{m-1}, and the elevation beamwidth β_v determined from

$$\beta_v = \delta_m - \delta_{m-1} \tag{9}$$

In theory one could perform these calculations in turn for each cell, obtaining in each case a larger permitted β_v than for cells farther out. In practice, changing the beamwidth in this way as one goes from cell to cell would make the antenna design too complex. If the antenna were a scanned planar array with its normal pointed at the outer cell, the effective aperture would decrease as the beam scanned off normal and the swath for inner cells would therefore be slightly larger than for the outer cell. Test calculations indicate that, at least for the cases considered here, this effect is so small that it may be neglected. This is true because the total angular range of scan in all cases under consideration is small enough that the value of the cosine in the expression for effective aperture does not change appreciably from unity. Hence, these calculations were reported on the assumption that the vertical beamwidth is the same for each scan cell.

With this assumption the total swath may be obtained from determining the inner pointing angle δ_i by

$$\delta_i = \delta_m - M\beta_r \tag{10}$$

From this we use (2) to get θ, (3) to get γ and (1) to get ρ_i. Hence the total swath is

$$\text{Swath} = \rho_m - \rho_i \tag{11}$$

3.0 POSSIBLE SWATH WIDTHS

The procedure outlined above was followed to compute the swath width for several examples of spaceborne SCANSAR systems. In the first example, let the aperture by 10 m long and the number of scan cells be 5. From (6) this can be seen to be valid if N = 2 and r_a = 50 m.

Figure 3 illustrates the effect of the outer pointing angle chosen on the swath obtained at different orbital heights. Two sets of curves are shown based on assuming safety factors of 2 and 1.5 in both dimensions. With $f_R = f_a = 2$, the slant swath of the outer cell is 25 km; and with $f_R = f_a = 1.5$, it is 44.44 km. For the larger incidence angles the ground swath is not much larger than the slant swath, but for the smaller incidence angles it is much larger. This shows clearly in the curves of the figure, where the strong sensitivity of of the swath to maximum pointing angle is clear. Thus, if the application calls for a wide swath, the minimum incidence angle consistent with the known ability to discriminate at different incidence angles should be used. This point is discussed further in Section 4.

The sensitivity of the swath to the safety factors used for the antenna is also apparent from Figure 3. This means that effort to reduce the antenna response outside the main lobe by suppressing sidelobes and steepening the sides of the main lobe can pay off handsomely in improved swath width.

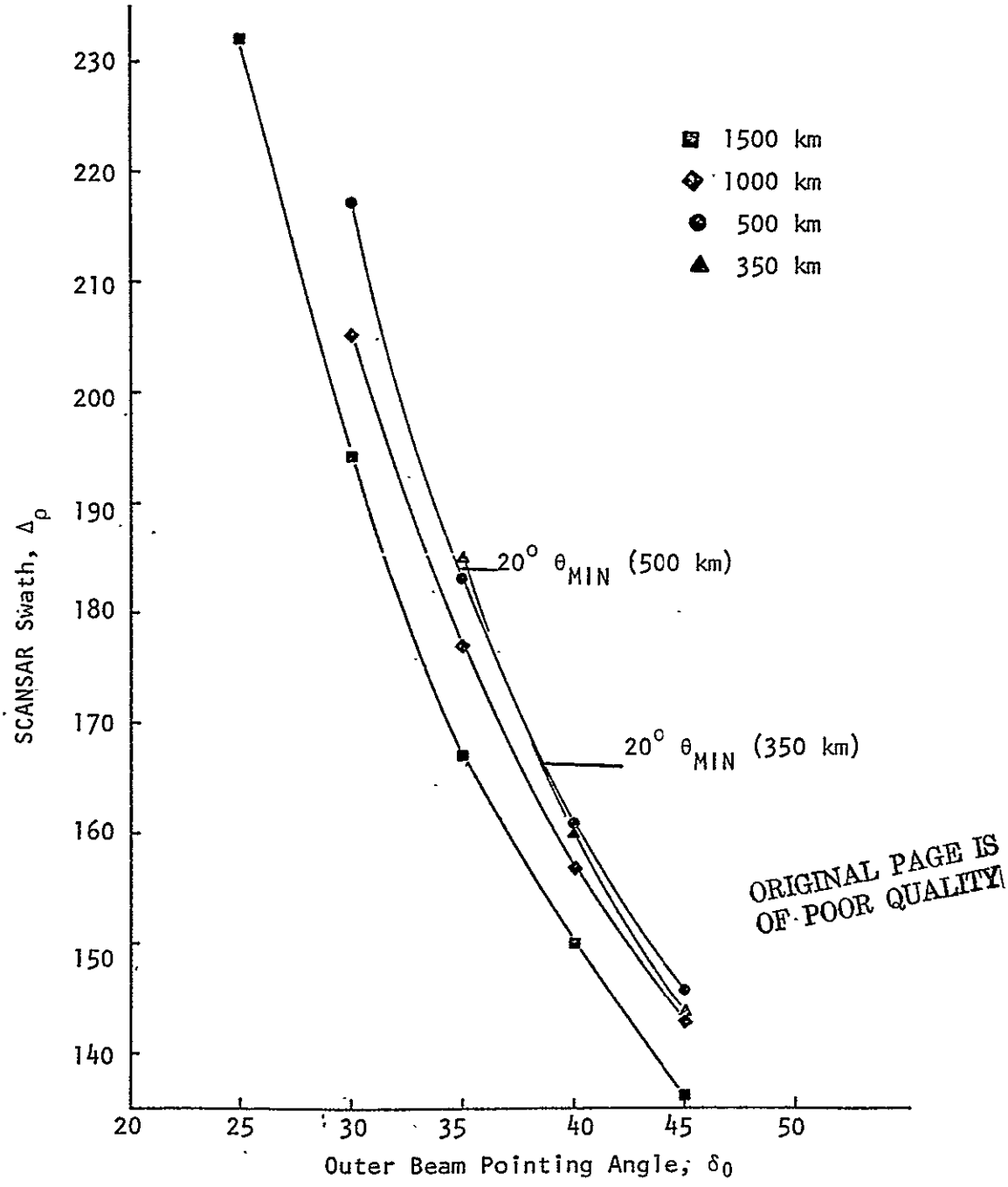

FIGURE 3a. Effect of Outer Beam Pointing Angle on SCANSAR Swath - 10 m Antenna, 5 Scan Cells, Safety Factor of 2 on Range and Azimuth.

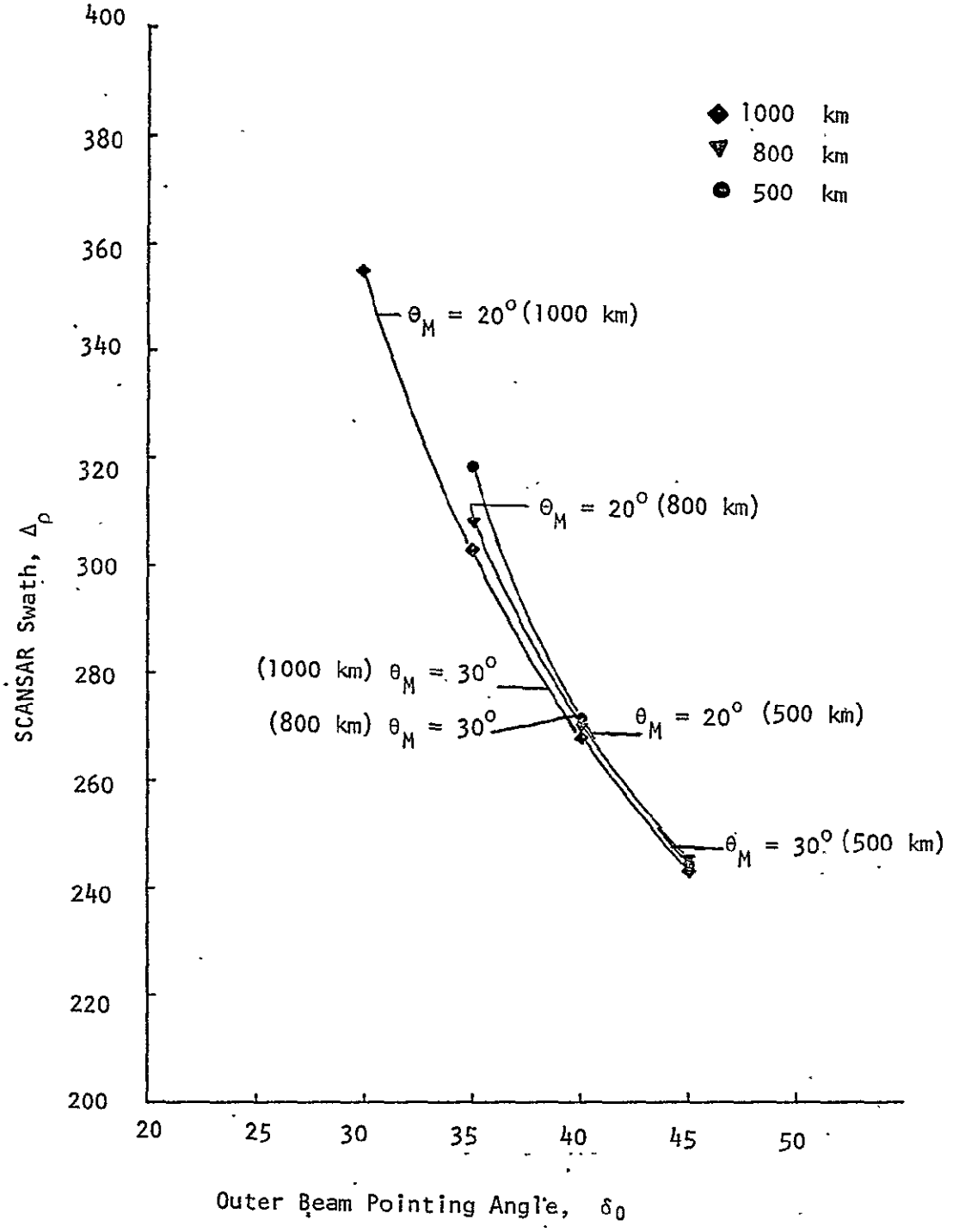

FIGURE 3b. Effect of Outer Beam Pointing Angle on SCANSAR Swath - 10 m Antenna, 5 Scan Cells, Safety Factor of 1.5 on Range and Azimuth.

The results for use of 10 scan cells instead of 5 are shown in Figure 4. This increases the swath, but at a price of poorer resolution in space or gray level. With 50 m spatial resolution, only 1 independent sample can be observed for each cell; however, it has been shown [7] that a more interpretible image is obtained if the spatial resolution is allowed to double to 100 m in the along-track direction and the two samples remain to be averaged. Although the results are shown for this example only at 500 km height, the conclusions would be the same for any height.

The effect of height was shown parametrically in Figures 3 and 4, but it can be seen more graphically in Figure 5. Although the widest swath is obtained at around 600 km height for the larger pointing angles, the swath is almost independent of height from 400 km to 1000 km at these angles. At 30° pointing angle, the swath is more sensitive to height, with the lower heights better, but the inner angles of incidence in this case may be too small to satisfy the need for angles large enough to permit adequate discrimination of different targets.

4.0 ANGLES OF INCIDENCE

The effect of the spherical earth is to make the angle of incidence greater than the nadir-referenced pointing angle. Figure 6 illustrates this. At typical heights for free-flying spacecraft the difference between incidence and pointing angles is quite large when the pointing angle is large. Since the incidence angle determines the ability to discriminate ground targets, not the pointing angle, a system designer should always consult curves such as those of Figure 6 before deciding on an appropriate outer pointing angle.

The inner and outer incidence angles for the 5-scan-cell example are shown in Figure 7 for a factor of safety of 2, and in Figure 8 for a factor of safety of 1.5. Since an angle of incidence below 20° is seldom useful, the wide swath apparently achievable for 30° pointing angle and lower altitudes (see Figures 3 and 4) frequently turns out to be useful only if the smaller incidence angles can be permitted. For this reason, 20° inner incidence angles are indicated

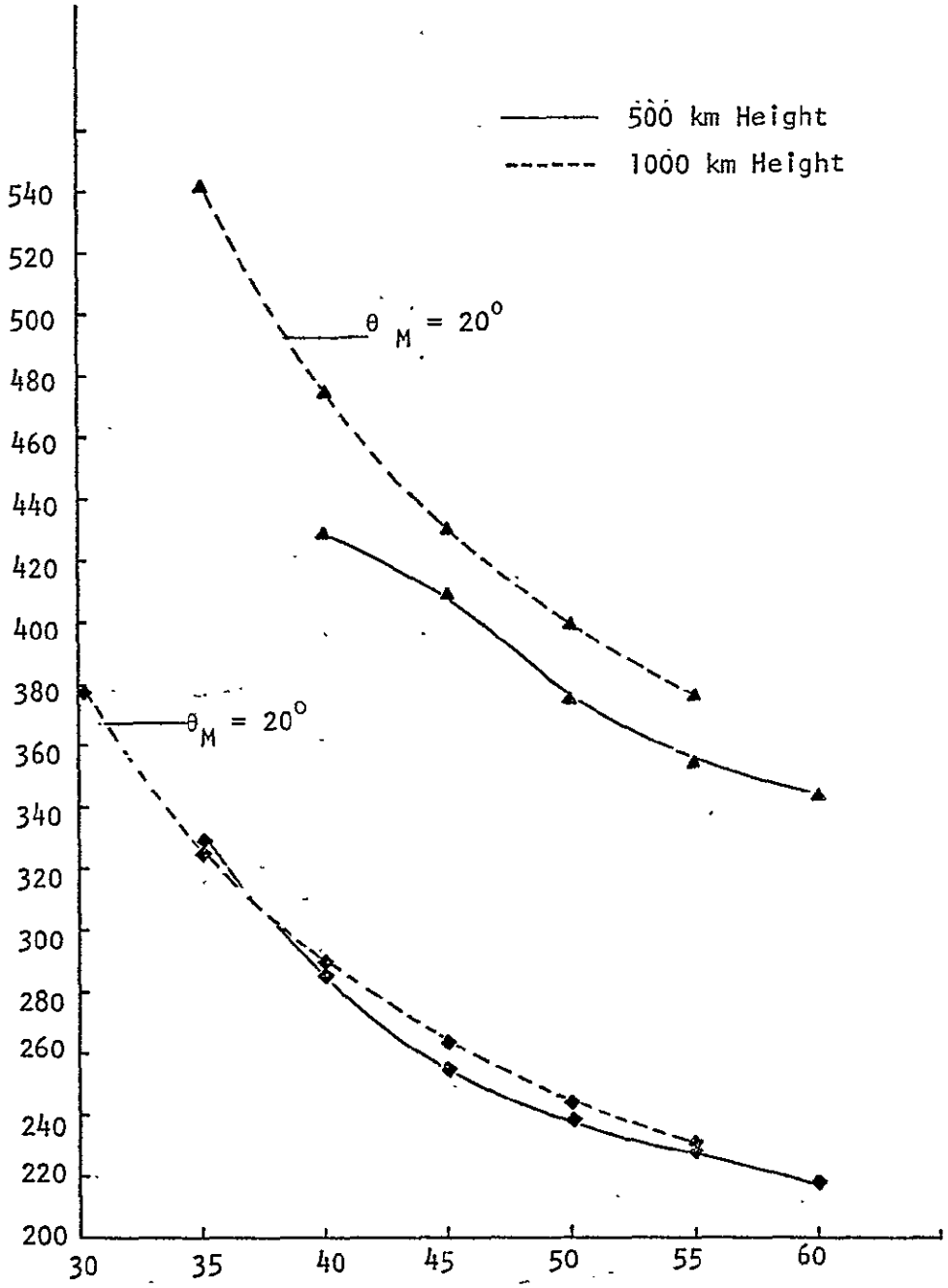

FIGURE 4 .. Effect of Outer Beam Pointing Angle on SCANSAR Swath - 10 m Antenna, 10 Scan Cells, Safety Factor 2◆, Safety Factor 1.5▲ .

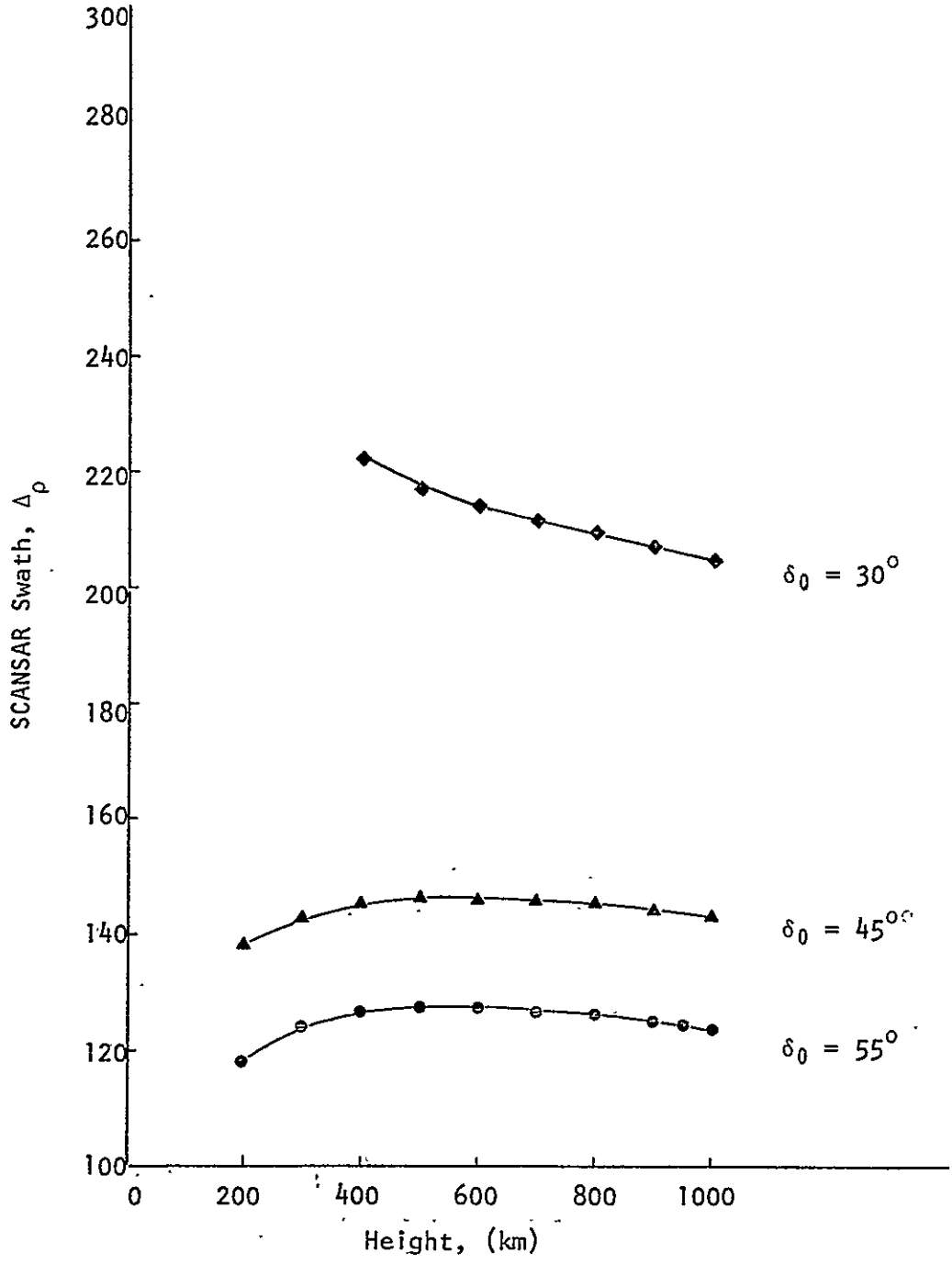

FIGURE 5. Effect of Height on SCANSAR Swath - 10 m Antenna, 5 Scan Cells

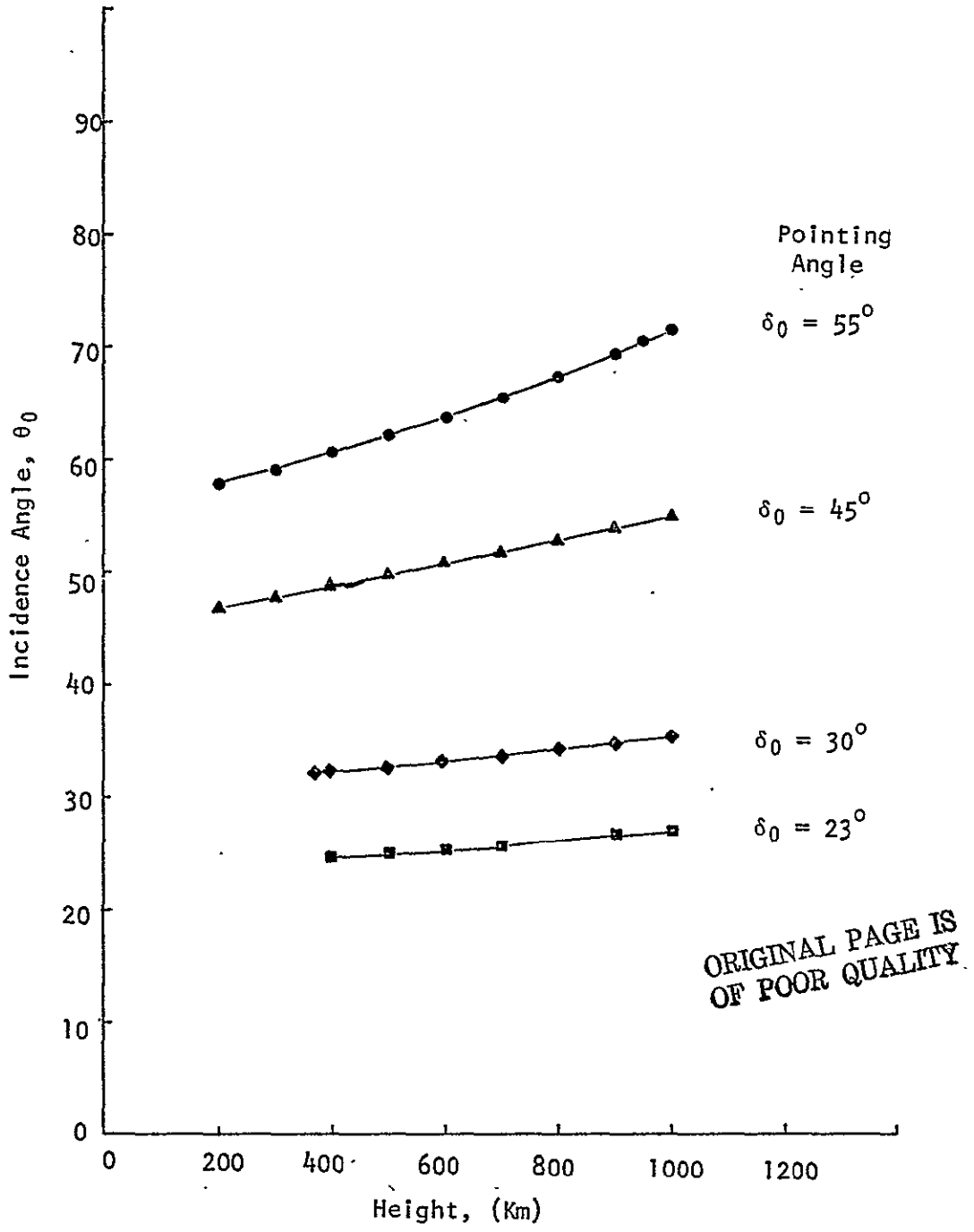

FIGURE 6 . Effect of Height on Incidence Angle

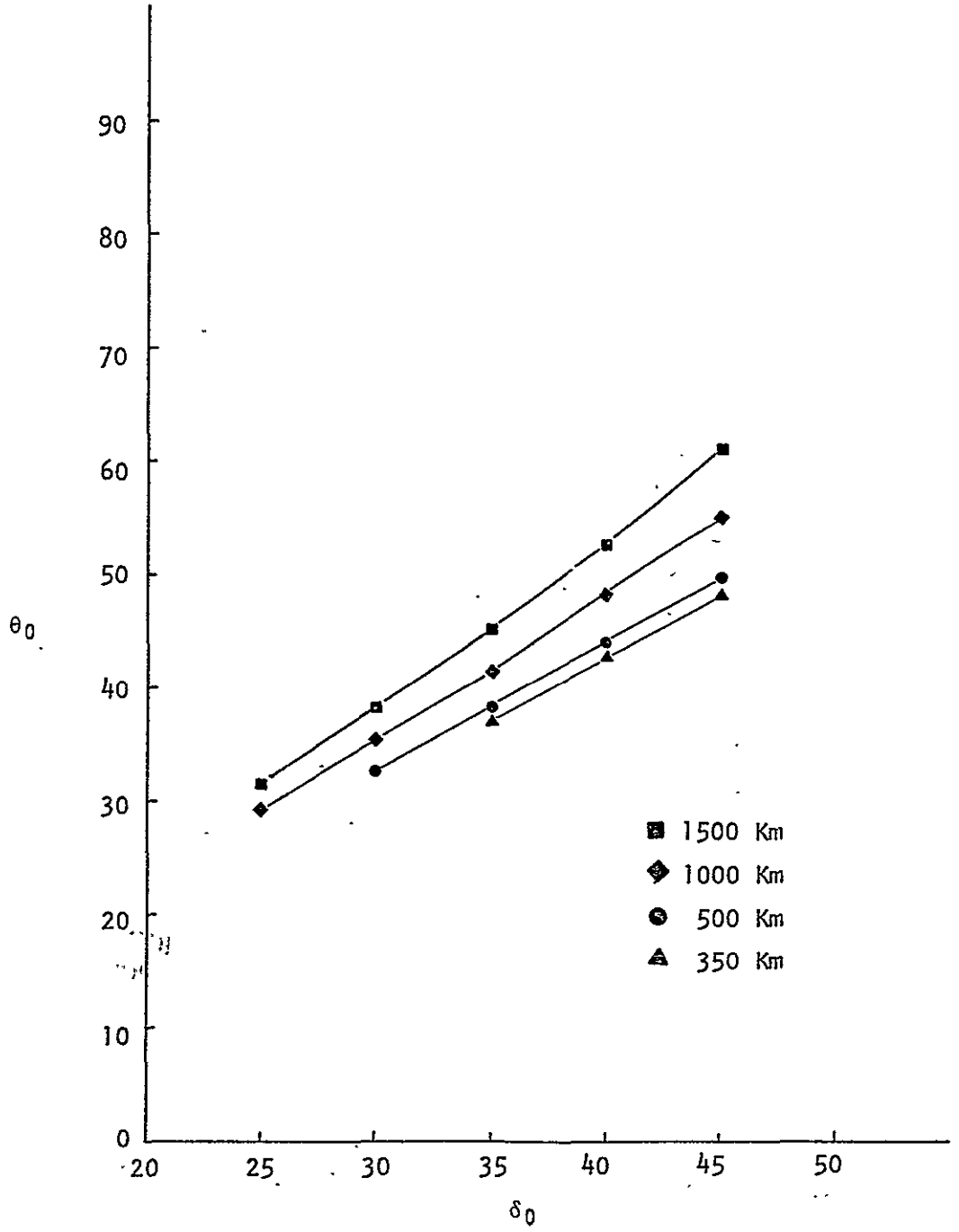

FIGURE 7a. Outer Incidence Angles vs. Outer Beam Pointing Angle for SCANSAR - 10 m Antenna, 5 Scan Cells, Safety Factor of 2 on Range and Azimuth.

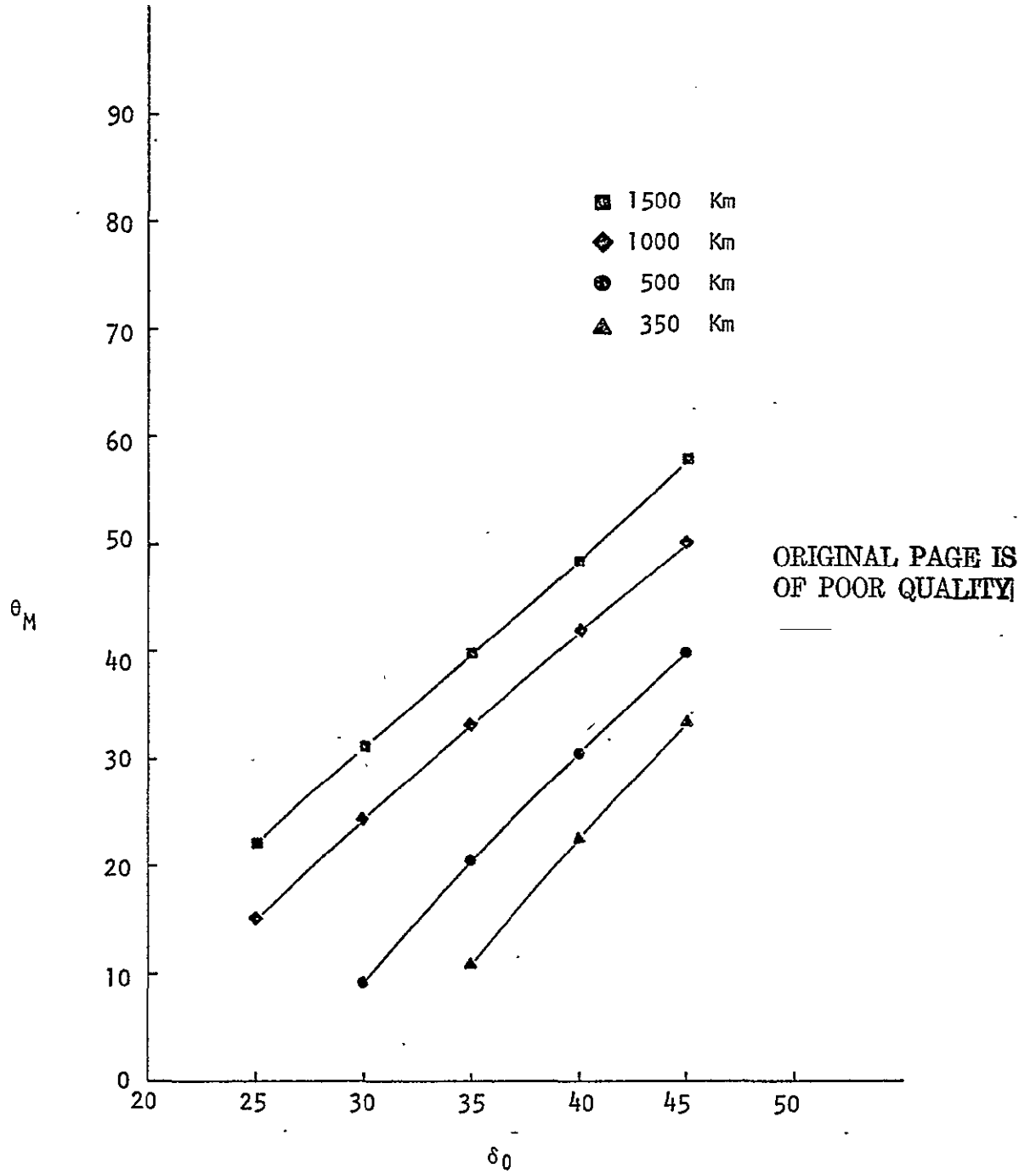

ORIGINAL PAGE IS
OF POOR QUALITY

FIGURE 7b. Inner Incidence Angles vs. Outer Beam Pointing Angle for SCANSAR - 10 m Antenna, 5 Scan Cells, Safety Factor of 2 on Range and Azimuth.

C-2

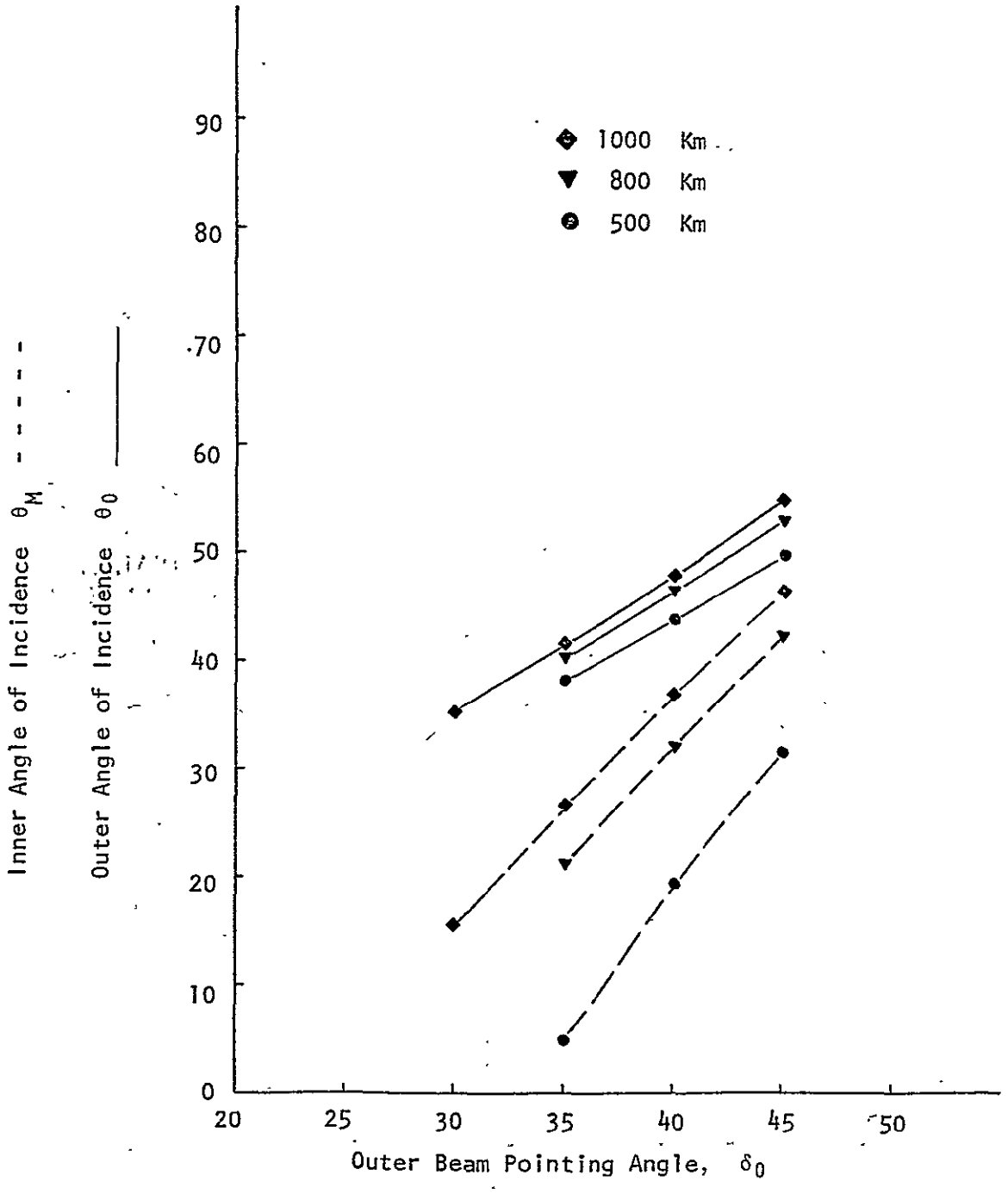

FIGURE 8. Outer and Inner Incidence Angles vs. Outer Beam Pointing Angle for SCANSAR - 10 m Antenna, 5 Scan Cells, Safety Factor of 1.5 on Range and Azimuth.

on Figures 3 and 4. Figures 9 and 10 show the same quantities for the 10-scan-cell example.

5.0 VERTICAL BEAM WIDTH

The vertical beam width of the antenna limits the extent of a single scan cell to that corresponding to the required ΔR. Since the scan cell itself is wider at smaller incidence (and pointing angles) the beam width may be wider at smaller pointing angles. This is illustrated in Figure 11. The figure also shows that the beamwidth is smaller at higher altitudes, as would be expected because the fixed ground distance subtends a smaller angle at longer ranges.

Since smaller beam widths require larger apertures, the largest vertical apertures are required for high-altitude systems pointed far off vertical. For the examples shown in the figure the required aperture ranges from 260 wavelengths for 55° pointing at 1000 km to only 10 wavelengths for 30° pointing angle at 400 km. Therefore, in the interest of keeping the antenna dimensions and complexity down, one would hope to use a relatively small outer pointing angle and low altitude. Of course this advantage must be traded against the problems associated with smaller incidence angles and other constraints that may force the spacecraft to higher altitudes.

6.0 CONCLUSIONS

The effect of altitude and outer pointing angle on incidence angle, swath width, and beam width for a scanning synthetic-aperture space radar has been shown. The method for calculating these quantities has been outlined, and a series of examples illustrates the effects of varying the system and spacecraft parameters.

In particular, we find that for larger outer pointing angles altitude variations make little difference in the resulting swath width. The pointing angles themselves, however, have a major influence; and wider swaths are possible if the smaller incidence angles associated with smaller pointing angles can be tolerated. The factor of safety used to account for realistic antenna patterns in both elevation and azimuth also has a major effect on swath width; if the antenna pattern can be shaped to permit smaller safety factors to be used, the swath width can be significantly increased.

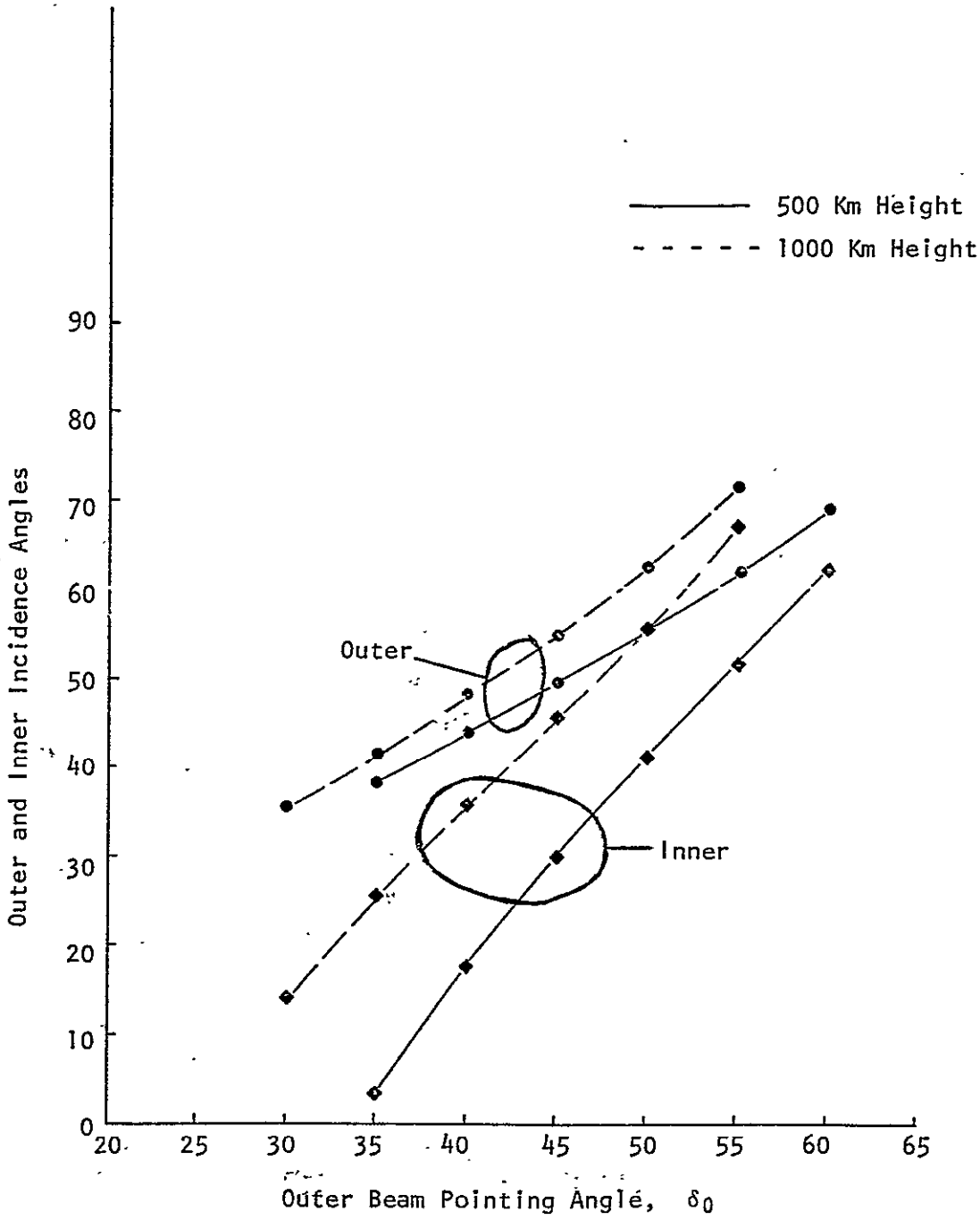

FIGURE 9 . Outer and Inner Incidence Angles vs. Outer Beam Pointing Angle for SCANSAR - 10 m.Antenna, 10 Scan Cells, 500 Km and 1000 Km Height, Safety Factor of 2 in Range and Azimuth.

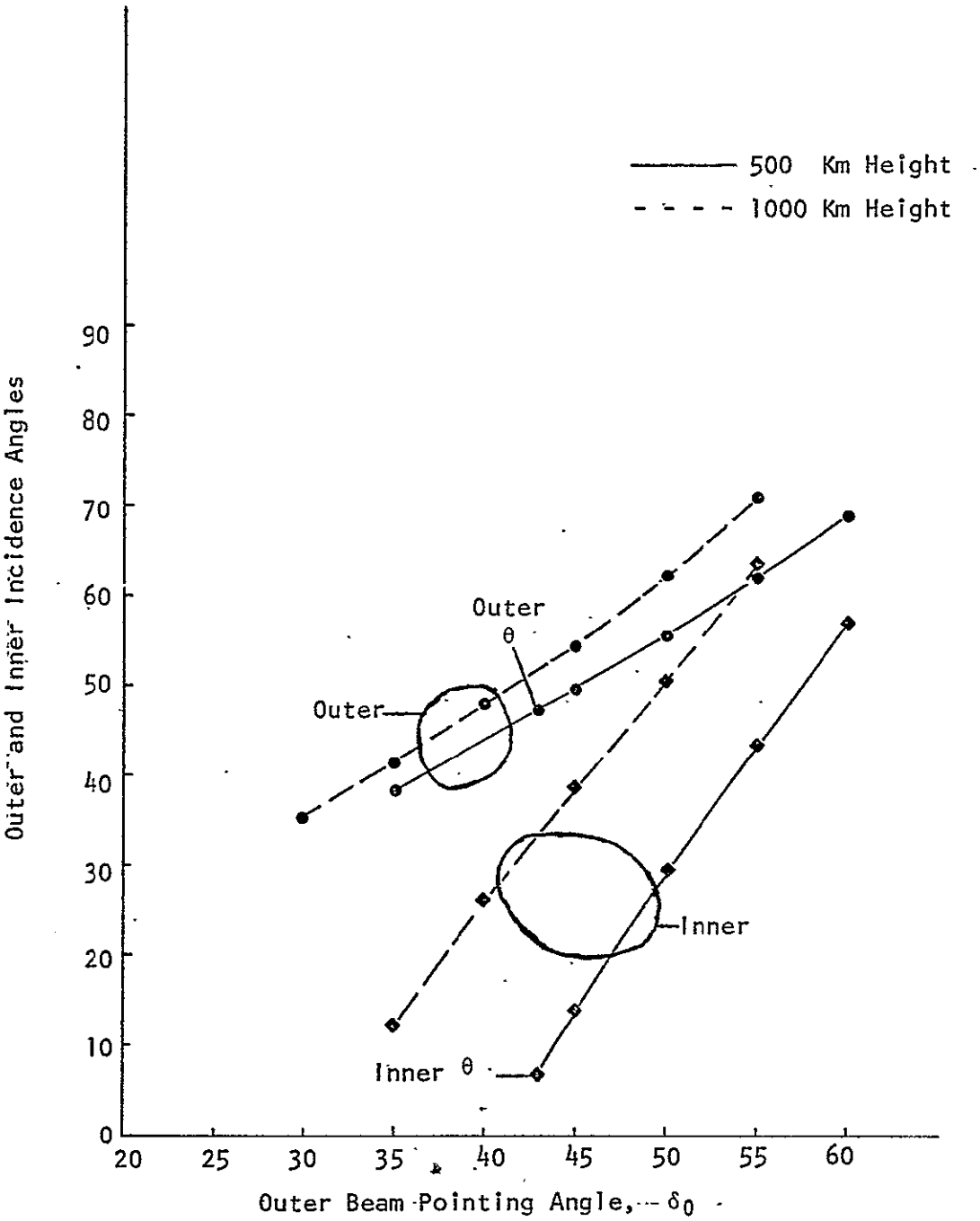

FIGURE 10. Outer and Inner Incidence Angles vs. Outer Beam Pointing Angle for SCANSAR - 10 m Antenna, 10 Scan Cells, 500 Km and 1000 Km Height, Safety Factor of 1.5 in Range and Azimuth.

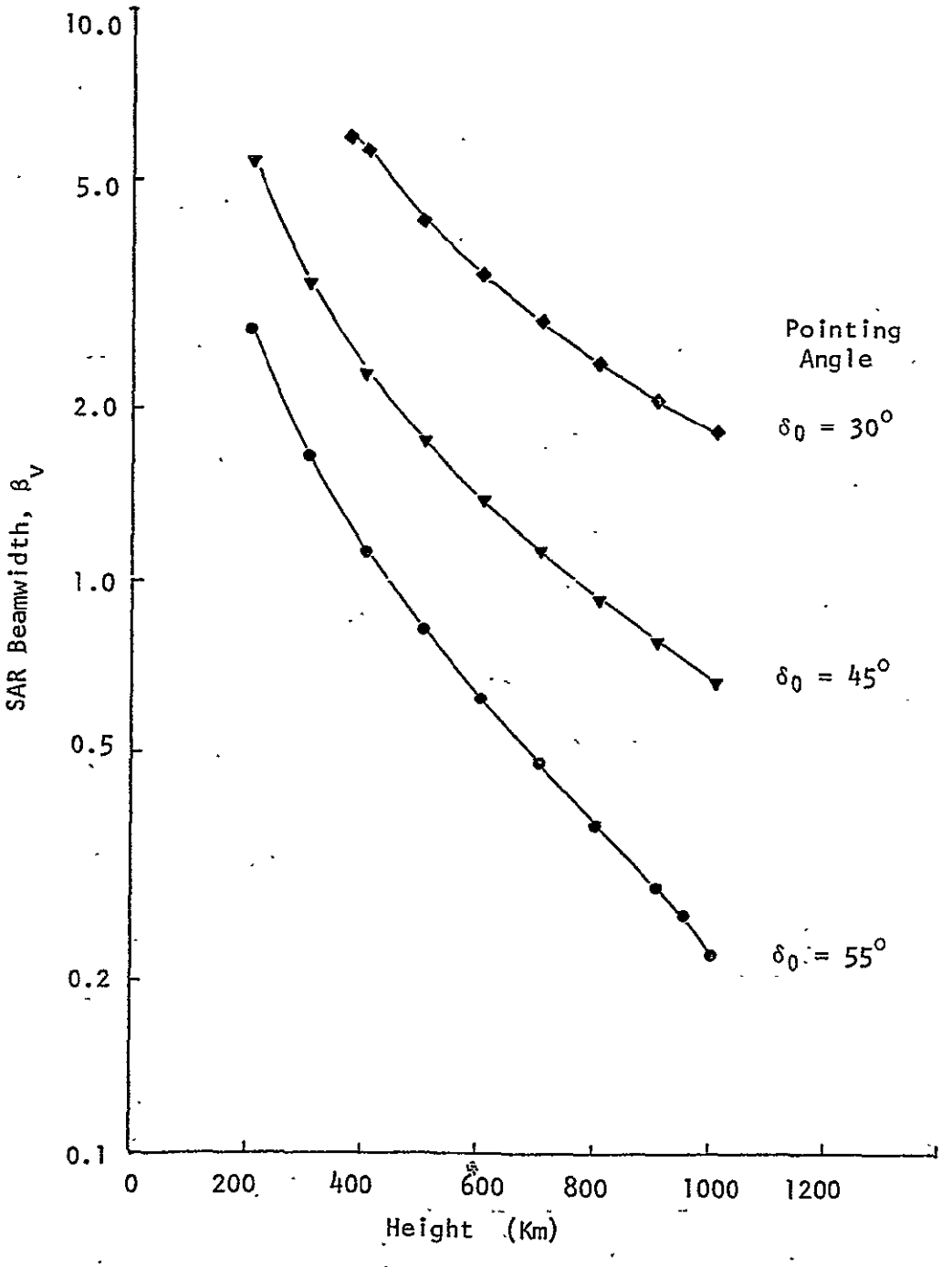

FIGURE 11. Effect of Height on SAR Beamwidth - 10 m Antenna, 5 Scan Cells.

REFERENCES

1. Claassen, John, University of Kansas RSL Report TR 295-1, "A Short Study of a Scanning SAR for Hydrological Monitoring on a Global Basis," September, 1975, (App. E, KU RSL TR 295-3).

2. McMillan, Stan, University of Kansas RSL Memorandum TM 295-3, "Synthetic Aperture Radar and Digital Processing," September, 1975, (App. I, KU RSL TR 295-3).

3. McMillan, Stan, University of Kansas RSL Memorandum TM 295-2, "A Review of Swath-Widening Techniques," January, 1976, (App. H, KU RSL TR 295-3).

4. Fong, Richard K.T., University of Kansas RSL Memorandum TM 294-4, "Methods to Vary Elevation Look Angle and Antenna Beam Pointing Requirements for Spacecraft SAR," January, 1976, (App. J, KU RSL TR 295-3).

5. Komen, Mark, University of Kansas RSL Report TR 295-2, "Detailed System Design for the Scanning Synthetic-Aperture Radar (SCANSAR) Using Comb-Filter Range-Offset Processing," July, 1976, (App. G, KU RSL TR 295-3).

6. Fong, Richard K.T., University of Kansas RSL Memorandum TM 295-8, "Effects of Different Scan Sngles on Ambiguity-Versus-Beamwidth Limitations for SCANSAR," January, 1976, (App. K, KU RSL TR 295-3).

7. Moore, R.K., University of Kansas RSL Report TR 287-2, "SLAR Image Interpretability - Trade-Offs Between Pictures Element Dimensions and Non-Coherent Averaging," January, 1976.

Basic Reference:

Moore, R.K., J.P. Claassen, R.L. Erickson, R.K.T. Fong, B.C. Hanson, M.J. Komen, S.B. McMillan, S.K. Parashar, University of Kansas RSL Report TR 295-3, "Radar Systems for the Water Resources Mission - Final Report," June, 1976, (Volumes III and IV).

THE UNIVERSITY OF KANSAS SPACE TECHNOLOGY CENTER
Raymond Nichols Hall
2291 Irving Hill Drive—Campus West Lawrence, Kansas 66045

Telephone: 913-864-4836

DECREASING SIDELOBE LEVELS IN THE FRESNEL ZONE-PLATE SYNTHETIC APERTURE RADAR PROCESSOR

RSL Technical Memorandum 291-9

Rodney Erickson

September 1976

Supported by:

NATIONAL AERONAUTICS AND SPACE ADMINISTRATION
Goddard Space Flight Center
Greenbelt, Maryland 20771

CONTRACT NAS5-22325

ABSTRACT

This report examines one further method to decrease the sidelobe levels of the Fresnel zone-plate processor (FZPP). This consists of ignoring contributions when the reference function, $\cos kt^2$, is near its zero crossing points. This method, combined with a tapering function developed previously, produces some further decrease in the sidelobe levels, but not enough to justify using this processor type for processing only a small number of zones.

Decreasing Sidelobe Levels in the Fresnel Zone-Plate Synthetic Aperture Radar Processor

by

Rodney Erickson

1.0 INTRODUCTION

In a previous report[1] the theory of the Fresnel zone-plate processor (FZPP) was developed for use in synthetic aperture radar (SAR) processing. Although conceptually simple, it was found that its use for processing only a few zones was precluded by its high sidelobes, usually less than 12 db below the main lobe.

In order to reduce the high sidelobes a tapering function was developed as shown in Figure 1. This is the opposite of the tapering function that was expected. Notwithstanding this, this taper did decrease the sidelobes but in most cases by only a db or less. A rather disappointing result! This report examines one other method of reducing the sidelobes of the FZPP. Although a further decrease in sidelobe levels was achieved, they still remain too high to make the FZPP a desirable SAR processor.

2.0 EXPLANATION OF SIDELOBE SUPPRESSION TECHNIQUE

The ordinary cos kt^2 reference function is shown in Figure 2. Figure 3 shows the inversion of the negative parts of this function. The Fresnel zone reference function required to do this is shown in Figure 4. Even with the use of the type of tapering function shown in Figure 1, the sidelobe levels of the processed signal are unacceptable. See Erickson.[1]

An additional method of sidelobe suppression was suggested.[2] This consists of ignoring contributions near the zero crossing points of the reference function. The result would be as pictured in Figure 5. The corresponding reference function is given in Figure 6.

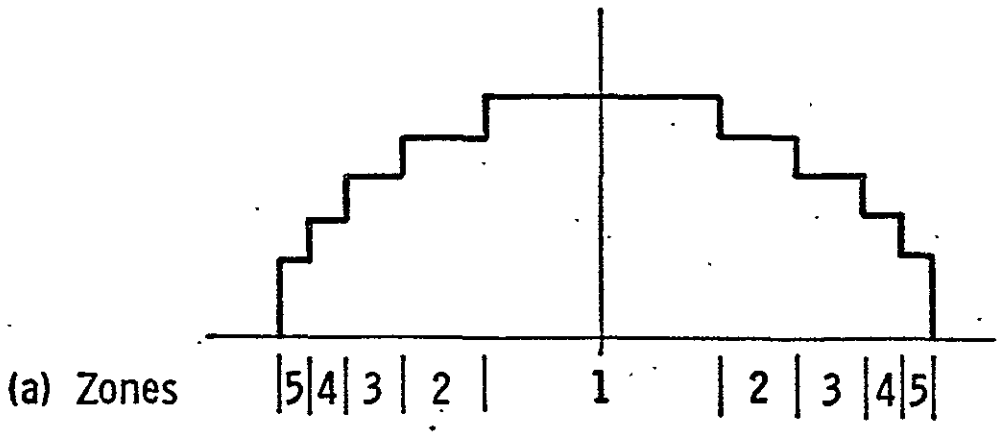

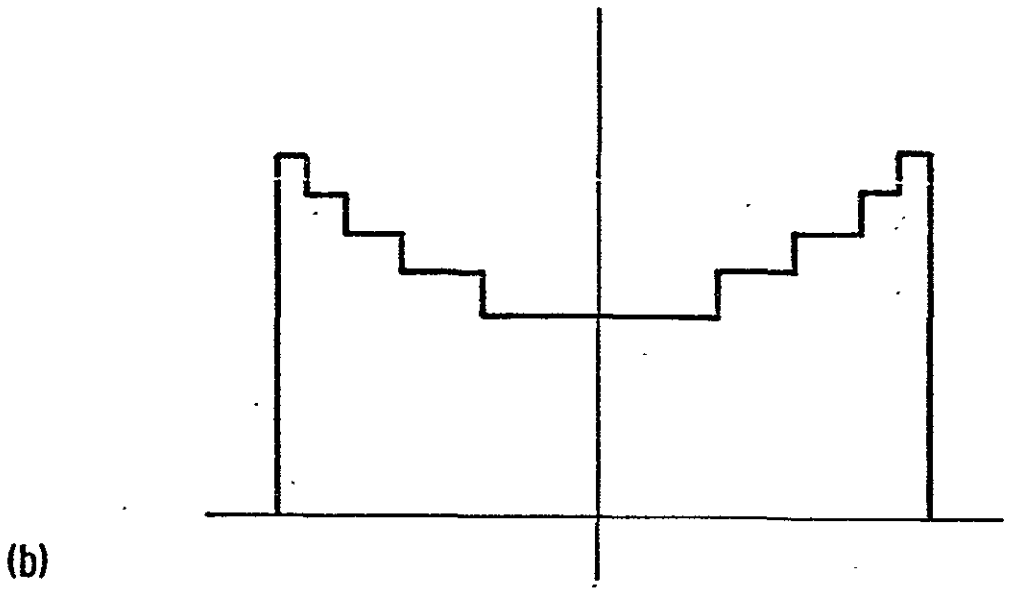

a. Normal Tapering to Reduce Side Lobes
b. Tapering Used with Fresnel Zone-Plate Processor to Reduce Side Lobes

Figure 1.

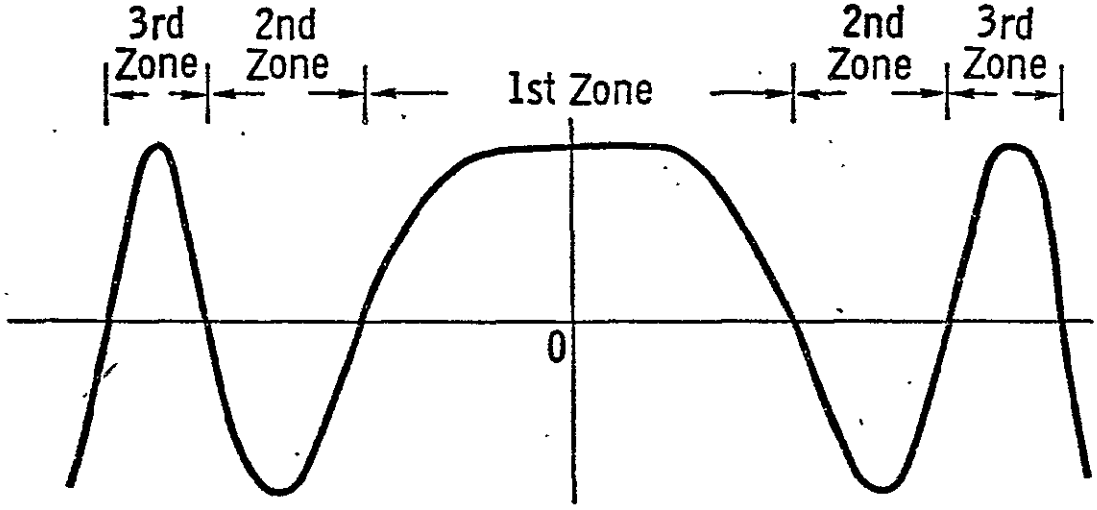

Figure 2. cos kt^2 Function.

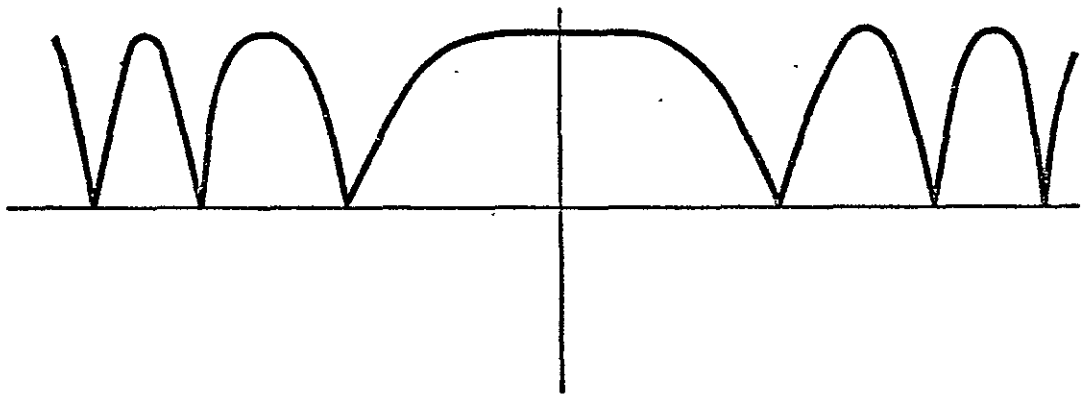

Figure 3.

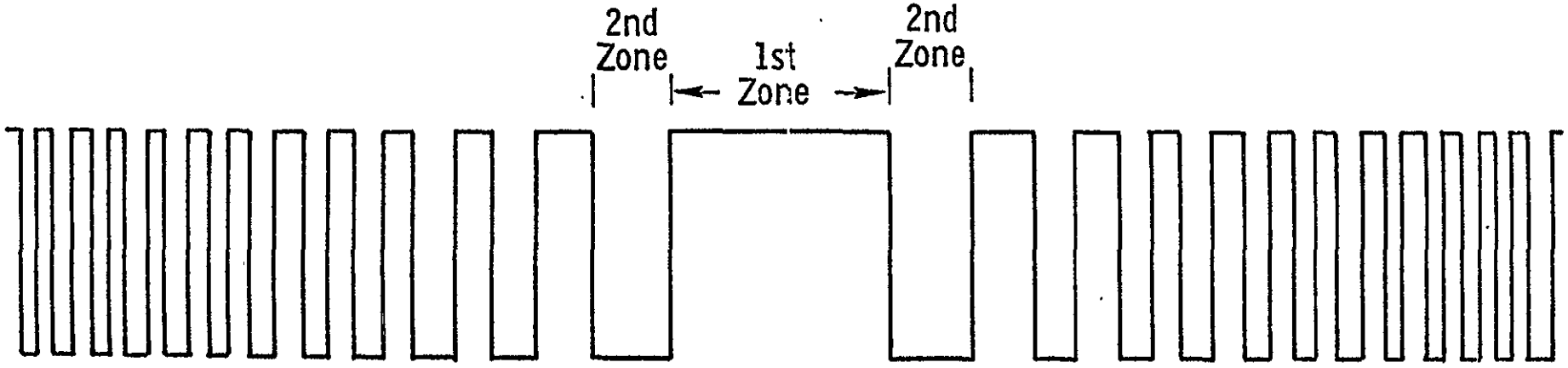

Figure 4. $\frac{\cos kt^2}{|\cos kt^2|}$ - Fresnel Zone Reference Function.

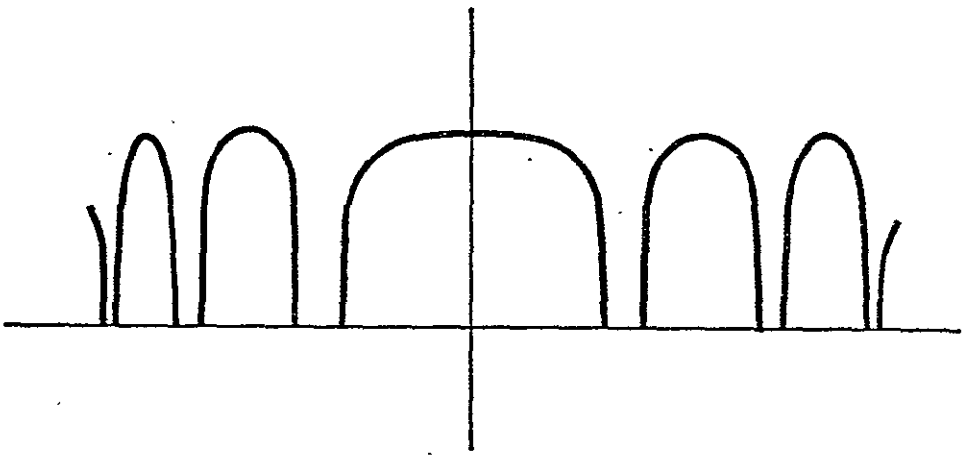

Figure 5.

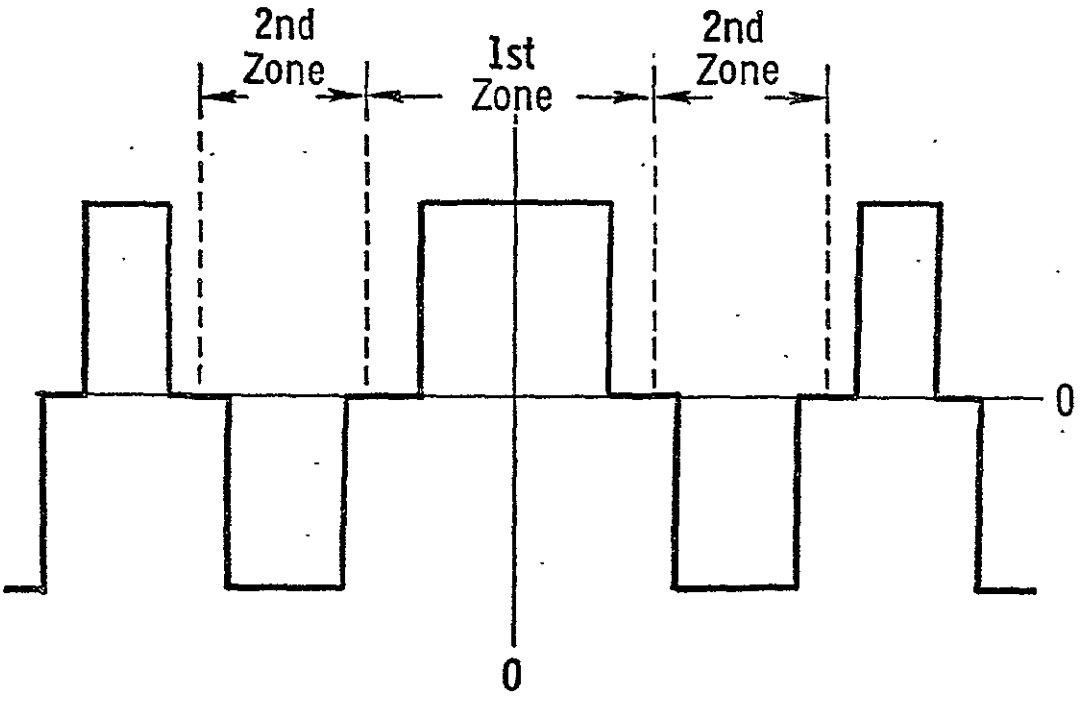

Figure 6.

3.0 RESULTS

The computer program developed previously[1] for calculation of the sidelobe levels of the FZPP was modified to include the zero crossing elimination technique. Two variants of the program were developed and these are given in Appendix A.

The results were once again disappointing. Some slight improvement in sidelobe levels were found, but overall they remained at unacceptable levels. The best results for processing four zones, were found by cutting off 9% from each zone with a taper of 110. For the SCANSAR parameters of Erickson's report the highest sidelobe level was at -12.8 db as compared to -11.3 db with the taper alone. In addition, processing four zones gives better results than processing either 5 or 6 zones. The best results found for processing several numbers of zones are given in Appendix B. The 4-zone case is plotted to illustrate the results of the two methods of sidelobe reduction. Note that -12.8 dB would be acceptable if fully focussed uniform (untapered) distribution were acceptable, but in this case no more improvement is possible by further tapering, whereas in more common processing schemes tapering leads to much lower sidelobes.

4.0 OTHER METHODS

One other method was tried to see if it would reduce the sidelobe levels of the FZPP. This consisted of only adding together the contributions from the odd zones, 1, 3, 5, ..., which are initially positive. The results were sidelobes which were higher by approximately 2 db. This method, analogous with the use of an optical Fresnel-zone plate, was abandoned.

5.0 CONCLUSION

A new method was tried to reduce the sidelobe levels of the FZPP. Some improvement was found but not enough to be of great significance. The FZPP remains undesirable for processing small numbers of Fresnel zones but may be useful in cases where a higher resolution is desirable and more zones may be processed.

ABSTRACT

This program computes power response for the FZPP. Both tapering and zero crossing contributions may be specified.

```
LIST CROSSING

10PRINT"THIS PROGRAM COMPUTES RELATIVE POWER GAIN RESPONSE FOR A FRESNEL"
20PRINT"ZONE-PLATE RADAR PROCESSOR."
30REM*****************************************************************
40REM  INPUT ALL NECESSARY PARAMETERS AND MODIFY AS NEEDED
50REM*****************************************************************
60PRINT"HEIGHT OF RADAR PLATFORM(KM)";
70INPUTH
80LETH=H*1000
90PRINT"VELOCITY OF PLATFORM(KM/S)";
100INPUTU
110LETU=U*1000
120PRINT"LENGTH OF ANTENNA(M)";
130INPUTD
140PRINT"DEPRESSION ANGLE IN DEGREES";
150INPUTT1
160LETT1=SIN((3.14159*T1)/180)
170PRINT"CARRIER WAVELENGTH(CM)";
180INPUTL
190LETL=.01*L
200PRINT"DISTANCE BETWEEN DATA POINTS(M)";
210INPUTX1
220PRINT"WHAT IS THE MAXIMUM DISTANCE VALUE YOU WANT CALCULATED(M)";
230INPUTX2
240LETM=(((L*H/T1)/(D*D))+1)/2
250PRINT"THE MAXIMUM NUMBER OF FRESNEL ZONES IS";M
260 PRINT"HOW MANY ZONES DO YOU WANT TO PROCESS";
270 INPUTM
280 LETM1=M
290 PRINT"WHAT FRACTION OF A ZONE SHALL BE ZERO NEAR A ZERO"
300 PRINT"CROSSING POINT OF THE FUNCTION";
310 INPUT T6
320REM*****************************************************************
330REM  IF ONE ZONE IS TO BE PROCESSED THEN NO TAPER IS POSSIBLE
340REM*****************************************************************
350 IF M=1 THEN 440
360 PRINT"WHAT TAPER AT HIGHEST ZONE";
370 INPUT T
380REM*****************************************************************
390REM  A LINEAR TAPER FROM ZONE TO ZONE IS USED IN THIS PROGRAM
400REM  THE TAPER INCREMENT BETWEEN ZONES IS NOW CALCULATED
410REM*****************************************************************
420 LET T2=(1-T)/(M1-1)
430 GOTO 460
440 LET T=1
450 LET T2=0
460LETC=2*SQR(T1/(H*L))
470LETX=0
480REM*****************************************************************
490REM  PRINT TABLE HEADINGS
500REM*****************************************************************
510PRINT
520PRINT
530PRINTM1;"FRESNEL ZONES"
540PRINT
550PRINT"      X          VOLTAGE        DB."
```

```
560REM*****************************************************************
570REM  INITIALIZE AND EVALUATE FRESNEL INTEGRALS FOR UNFOCUSSED CASE
580REM*****************************************************************
590LETR=0
600LETC1=C*X
610 LET A = 1-T6 + C1
620GOSUB1270
630LETR=P+S
640 LET A = 1-T6-C1
650GOSUB1270
660LETP=P+S
670LETP1=P
680IFM<=1THEN980
690REM*****************************************************************
700REM  IF UNFOCUSSED CASE THEN GO AND PRINT THE RESULTS
710REM  IF NOT, THEN COMPUTE LIMITS OF FRESNEL INTEGRALS
720REM  AND EVALUATE
730REM*****************************************************************
740LETP=0
750LETS1=SQR(2*M-1)
760LETS3=SQR(2*M-3)
770 LET Z2=(S1-S3)*T6
780 LET A = S1+C1+Z2
790GOSUB1270
800LETR=P+S
810 LET A = S3+C1-Z2
820 GOSUB 1270
830LETR=R-S
840 LET A = S1-C1+Z2
850GOSUB1270
860LETR=R+S
870 LET A = S3-C1-Z2
880GOSUB1270
890LETR=P-S
900LETN=1
910FORE=1TOM-1
920LETN=-N
930NEXTE
940LETP1=R1+N*R
950IFM<=2THEN980
960LETM=M-1
970GOTO740
980LETP=R1*P1
990LETV=R1
1000IFX<>0THEN1050
1010REM*****************************************************************
1020REM  SAVE VALUE AT ZERO SO DB. CAN BE CALCULATED
1030REM*****************************************************************
1040LETZ=R
1050LETR1=R/Z
1060LETD1=4.342945*LOG(P1)
1070REM*****************************************************************
1080REM  PRINT RESULTS FOR ONE DISTANCE VALUE
1090REM*****************************************************************
1100PRINTX,V,D1
1110REM*****************************************************************
1120REM  INCREMENT DISTANCE VALUE
1130REM*****************************************************************
1140LETX=X+M1
1150REM*****************************************************************
1160REM  IF THE SPECIFIED DISTANCE HAS BEEN REACHED THEN STOP
1170REM*****************************************************************
1180IFX>X2THEN1210
1190LETM=M1
1200GOTO590
1210STOP
1220REM*****************************************************************
1230REM*****************************************************************
1240REM  THIS IS THE SUBROUTINE WHICH COMPUTES THE VALUE OF THE
1250REM  FRESNEL INTEGRAL
```

```
1260REM**********************************************************
1270LETY=1
1280IFA)=0THEN1300
1290LETY=-1
1300LETA=ABS(A)
1310REM**********************************************************
1320REM  THIS IS THE APPROXIMATION. S IS THE RESULT
1330REM**********************************************************
1340LETF=(1.570796*A*A)
1350LETA1=(1+.926*A)*SIN(F)/(2+1.792*A+3.104*A*A)
1360LETA2=COS(F)/(3+4.142*A+3.492*A*A+6.67*A*A*A)
1370LETS=(T+(M1-M)*T2)*(.5+A1-A2)*Y
1380RETURN
1390END

READY
```

This program is the same as the previous one except that only the relative minimum and maximum values are output.

```
LIST PEAK

10PRINT"THIS PROGRAM COMPUTES RELATIVE POWER GAIN RESPONSE FOR A FRESNEL"
20PRINT"ZONE-PLATE RADAR PROCESSOR."
30REM**********************************************************
40REM  INPUT ALL NECESSARY PARAMETERS AND MODIFY AS NEEDED
50REM**********************************************************
60PRINT"HEIGHT OF RADAR PLATFORM(KM)";
70INPUTH
80LETH=H*1000
90PRINT"VELOCITY OF PLATFORM(KM/S)";
100INPUTU
110LETU=U*1000
120PRINT"LENGTH OF ANTENNA(M)";
130INPUTD
140PRINT"DEPRESSION ANGLE IN DEGREES";
150INPUTT1
160LETT1=SIN((3.14159*T1)/180)
170PRINT"CARRIER WAVELENGTH(CM)";
180INPUTL
190LETL=.01*L
200PRINT"DISTANCE BETWEEN DATA POINTS(M)";
210INPUTX1
220PRINT"WHAT IS THE MAXIMUM DISTANCE VALUE YOU WANT CALCULATED(M)";
230INPUTX2
240LETM=(((L*H/T1)/(D*D))+1)/2
250PRINT"THE MAXIMUM NUMBER OF FRESNEL ZONES IS";M
260 PRINT"HOW MANY ZONES DO YOU WANT TO PROCESS";
270 INPUTM
280 LETM1=M
290 PRINT"WHAT FRACTION OF A ZONE SHALL BE ZERO NEAR A ZERO"
300 PRINT"CROSSING POINT OF THE FUNCTION";
310 INPUT T6
320REM**********************************************************
330REM  IF ONE ZONE IS TO BE PROCESSED THEN NO TAPER IS POSSIBLE
340REM**********************************************************
350 IF M=1 THEN 440
360 PRINT"WHAT TAPER AT HIGHEST ZONE";
370 INPUT T
```

```
380REM**********************************************************
390REM  A LINEAR TAPER FROM ZONE TO ZONE IS USED IN THIS PROGRAM
400REM  THE TAPER INCREMENT BETWEEN ZONES IS NOW CALCULATED
410REM**********************************************************
420 LET T2=(1-T)/(M1-1)
430 GOTO 460
440 LET T=1
450 LET T2=0
460LETC=2*SQR(T1/(H+L))
470LETX=0
480 LET J1 = 0
490 LET J2 = 0
500REM**********************************************************
510REM  PRINT TABLE HEADINGS
520REM**********************************************************
530PRINT
540PRINT
550 PRINT M1;"FRESNEL ZONES, MINIMA AND MAXIMA ONLY"
560PRINT
570PRINT"       X             VOLTAGE          DB."
580REM**********************************************************
590REM  INITIALIZE AND EVALUATE FRESNEL INTEGRALS FOR UNFOCUSSED CASE
600REM**********************************************************
610LETC1=C*X
620 LET A = 1-T6 + C1
630GOSUB1400
640 LET R = S
650 LET A = 1-T6-C1
660GOSUB1400
670LETP=P+S
680LETP1=R
690IFM<=1THEN1010
700REM**********************************************************
710REM  IF UNFOCUSSED CASE THEN GO AND PRINT THE RESULTS
720REM  IF NOT, THEN COMPUTE LIMITS OF FRESNEL INTEGRALS
730REM  AND EVALUATE
740REM**********************************************************
750LETS1=SQR(2*M-1)
760LETS3=SQR(2*M-3)
770 LET Z2=(S1-S3)*T6
780 LET A = C1+C1+Z2
790GOSUB1400
800 LET R = S
810 LET A = S3+C1-Z2
820 GOSUB 1400
830LETR=R-S
840 LET A = S1-C1+Z2
850GOSUB1400
860LETR=R+S
870 LET A = S3-C1-Z2
880GOSUB1400
890LETR=R-S
900LETN=1
910FORE=1TOM-1
920LETN=-N
930NEXTE
940LETR1=R1+N*P
950 IF M <= 2 THEN 1005
960LETM=M-1
970GOTO750
980REM**********************************************************
990REM  FIND MINIMA AND MAXIMA AND PRINT THEM
1000REM*********************************************************
1005 LET V = P1
1010 IF ABS(J2)<ABS(J1) THEN 1030
1020 GOTO 1040
```

```
1030 IF ABS(J1)>ABS(R1) THEN 1080
1040 IF ABS(J2)>ABS(J1) THEN 1060
1050 GOTO 1250
1060 IF ABS(J1)<ABS(R1) THEN 1080
1070 GOTO 1250
1080 LET P = J1*J1
1100 IF (X-X1)<>0 THEN 1150
1110REM*****************************************************************
1120REM  SAVE VALUE AT ZERO DB. CAN BE CALCULATED
1130REM*****************************************************************
1140LETZ=P
1150LETP1=R/Z
1160LETD1=4.342945*LOG(P1)
1170REM*****************************************************************
1180REM  PRINT RESULTS FOR ONE DISTANCE VALUE
1190REM*****************************************************************
1200 LET X3 = X-X1
1210 PRINT X3;J1;D1
1220REM*****************************************************************
1230REM  INCREMENT DISTANCE VALUE
1240REM*****************************************************************
1250LETX=X+X1
1260REM*****************************************************************
1270REM  IF THE SPECIFIED DISTANCE HAS BEEN REACHED THEN STOP
1280REM*****************************************************************
1290IFX>X2THEN1340
1300LETM=M1
1310 LET J2=J1
1320 LET J1=V
1330 GOTO 610
1340STOP
1350REM*****************************************************************
1360REM*****************************************************************
1370REM  THIS IS THE SUBROUTINE WHICH COMPUTES THE VALUE OF THE
1380REM  FRESNEL INTEGRAL
1390REM*****************************************************************
1400LETY=1
1410IFA>=0THEN1430
1420LETY=-1
1430LETA=ABS(A)
1440REM*****************************************************************
1450REM  THIS IS THE APPROXIMATION. S IS THE RESULT
1460REM*****************************************************************
1470LETF=(1.570796*A*A)
1480LETA1=(1+.926*A)/(2+1.792*A+3.104*A*A)
1490LETA2=COS(F)/(2+4.142*A+3.492*A*A+6.67*A*A*A)
1500LETS=(T+(M1-M)*T2)*(.5+A1-A2)*Y
1510RETURN
1520END

READY
```

APPENDIX B

Best Results of Programs of Appendix A.

```
RUN


THIS PROGRAM COMPUTES RELATIVE POWER GAIN RESPONSE FOR A FRESNEL
ZONE-PLATE RADAR PROCESSOR.
HEIGHT OF RADAR PLATFORM(KM)?435
VELOCITY OF PLATFORM(KM/S)?7.6
LENGTH OF ANTENNA(M)?3
DEPRESSION ANGLE IN DEGREES?83
CARRIER WAVELENGTH(CM)?6.3
DISTANCE BETWEEN DATA POINTS(M)?1
WHAT IS THE MAXIMUM DISTANCE VALUE YOU WANT CALCULATED(M)?400
THE MAXIMUM NUMBER OF FRESNEL ZONES IS   1534.434
HOW MANY ZONES DO YOU WANT TO PROCESS?3
WHAT FRACTION OF A ZONE SHALL BE ZERO NEAR A ZERO
CROSSING POINT OF THE FUNCTION?.01
WHAT TAPER AT HIGHEST ZONE?1000

    3 FRESNEL ZONES, MINIMA AND MAXIMA ONLY

  X            VOLTAGE          DB.
  0            2664.605            0
 46          -.0658989       -92.1351
 53          -68.31031       -31.82293
 61          -.0940857       -89.04219
111           287.2289       -19.34809
130           6.489162       -52.26888
144          -197.6968       -22.59266
159          -5.389095       -53.88234
179           201.2664       -22.43723
187           191.8311       -22.85427
220           965.3592       -8.818877
248           48.44447       -34.80777
250           49.19543       -34.67416
256           3.249905       -58.27525
276          -839.5714        -10.0315
308            9.42926        -49.0231
322           309.9679       -18.68632
335           183.5064       -23.23963
342           213.6214       -21.91976
353          -12.17728       -46.80165
362          -184.6453       -23.18589
369          -156.1858       -24.63983
381          -312.9868       -18.60214
389          -3.246357       -58.28473
399           450.0165       -15.44809
```

```
RUN


THIS PROGRAM COMPUTES RELATIVE POWER GAIN RESPONSE FOR A FRESNEL
ZONE-PLATE RADAR PROCESSOR.
HEIGHT OF RADAR PLATFORM(KM)?435
VELOCITY OF PLATFORM(KM/S)?7.6
LENGTH OF ANTENNA(M)?3
DEPRESSION ANGLE IN DEGREES?83
CARRIER WAVELENGTH(CM)?6.3
DISTANCE BETWEEN DATA POINTS(M)?1
WHAT IS THE MAXIMUM DISTANCE VALUE YOU WANT CALCULATED(M)?500
THE MAXIMUM NUMBER OF FRESNEL ZONES IS   1534.434
HOW MANY ZONES DO YOU WANT TO PROCESS?4
WHAT FRACTION OF A ZONE SHALL BE ZERO NEAR A ZERO
CROSSING POINT OF THE FUNCTION?.09
WHAT TAPER AT HIGHEST ZONE?110

    4 FRESNEL ZONES, MINIMA AND MAXIMA ONLY

  X              VOLTAGE          DB.
      0         303.1522             0
     44         2.141916      -43.01717
     73         36.87061      -18.29961
     77          36.6786      -18.34496
    103         58.11413      -14.34758
    124         1.311944      -47.27491
    151        -69.43828      -12.80123
    181        -26.51112      -21.16465
    189        -27.63269      -20.80475
    207        -1.172851      -48.24836
    223         25.25049      -21.58782
    234         -1.34592      -47.05283
    251        -69.55984      -12.78604
    264        -51.40128      -15.41374
    277        -68.98771      -12.85778
    291        -.8672529       -50.8703
    320         56.66604      -14.56676
    333         36.65231      -18.35119
    342         46.36211      -16.30995
    352        -2.196907      -42.79698
    362        -58.00701      -14.21514
    373        -42.27375       -17.1118
    379        -46.30113      -16.32138
    389        -.1319876      -67.22256
    399         59.31336      -14.03274
    416          .405031      -57.48345
    427        -16.63895       -25.2107
    437        -10.99958      -28.80569
    445        -14.66707      -26.30634
    453        -.500515      -55.64487
    460         11.03304      -28.77931
    467         7.488306      -32.14554
    477         19.53878      -23.81527
    484        -1.873048      -44.18224
    492        -29.07858      -20.36175
```

```
THIS PROGRAM COMPUTES RELATIVE POWER GAIN RESPONSE FOR A FRESNEL
ZONE-PLATE RADAR PROCESSOR.
HEIGHT OF RADAR PLATFORM(KM)?435
VELOCITY OF PLATFORM(KM/S)?7.6
LENGTH OF ANTENNA(M)?3
DEPRESSION ANGLE IN DEGREES?83
CARRIER WAVELENGTH(CM)?6.3
DISTANCE BETWEEN DATA POINTS(M)?1
WHAT IS THE MAXIMUM DISTANCE VALUE YOU WANT CALCULATED(M)?500
THE MAXIMUM NUMBER OF FRESNEL ZONES IS   1534.434
HOW MANY ZONES DO YOU WANT TO PROCESS?5
WHAT FRACTION OF A ZONE SHALL BE ZERO NEAR A ZERO
CROSSING POINT OF THE FUNCTION?.1
WHAT TAPER AT HIGHEST ZONE?1000000

    5 FRESNEL ZONES, MINIMA AND MAXIMA ONLY

   X            VOLTAGE          DB.
     0          2864509             0
    37          66183.44      -32.72602
    62          641639.7      -12.99518
   111          15996.47      -45.06052
   145           -634363      -13.09425
   173         -6810.316      -52.47766
   222            697095      -12.27517
   247         -3519.318      -58.21184
   257         -65097.35      -32.86974
   270         -1988.469      -63.17063
   275          11190.11      -48.16432
   279          9651.021      -49.44954
   302          510926.3      -14.97384
   319          244372.6      -21.37995
   322            247269      -21.27761
   335         -559.2266      -74.18925
   341         -64011.93      -33.01579
   344         -61901.69      -33.30696
   363         -782678.6      -11.26934
   387          -8153.16      -50.91449
   399          800572.9      -11.07299
   419          13867.06      -46.30132
   431         -332507.1      -18.70499
   439         -267147.9      -20.60597
   446         -323200.9      -18.95156
   455          29602.64       -39.7144
   463          280104.1      -20.19462
   469          244304.4      -21.38238
   476          305772.1      -19.43305
   484         -6219.379      -53.26607
   492         -380326.7      -17.53787
```

```
RUN


THIS PROGRAM COMPUTES RELATIVE POWER GAIN RESPONSE FOR A FRESNEL
ZONE-PLATE RADAR PROCESSOR.
HEIGHT OF RADAR PLATFORM(KM)?435
VELOCITY OF PLATFORM(KM/S)?7.6
LENGTH OF ANTENNA(M)?3
DEPRESSION ANGLE IN DEGREES?83
CARRIER WAVELENGTH(CM)?6.3
DISTANCE BETWEEN DATA POINTS(M)?1
WHAT IS THE MAXIMUM DISTANCE VALUE YOU WANT CALCULATED(M)?500
THE MAXIMUM NUMBER OF FRESNEL ZONES IS   1534.434
HOW MANY ZONES DO YOU WANT TO PROCESS?6
WHAT FRACTION OF A ZONE SHALL BE ZERO NEAR A ZERO
CROSSING POINT OF THE FUNCTION?.1
WHAT TAPER AT HIGHEST ZONE?10

 6 FRESNEL ZONES, MINIMA AND MAXIMA ONLY

  X            VOLTAGE          DB.
  0           31.20314            0
 33           .0829785      -62.65753
 57           8.276024      -11.52753
 99            .080526      -51.76525
115          -2.067473      -23.57517
125          -1.843535      -24.57094
145          -3.256832      -19.62806
168           .0678504      -53.25292
179           .8735763      -31.05795
192           .0167512      -65.40306
197           -.174492      -45.04846
201           .0377407      -58.34776
221           2.880089      -20.69525
235          -.0796908       -51.8558
252          -5.010362      -15.88658
264          -3.916278      -18.02649
276          -4.767808      -16.31759
300           .0020544      -83.63008
308            .517124      -35.61207
314           .0722381      -52.70864
324          -1.236592      -28.03951
338          -.1806236      -44.74824
363          -3.969493      -17.90927
374          -.0072467      -72.68111
399           8.975928      -10.82238
411           .2928056      -40.55238
431          -6.195426      -14.04254
453          -.3001315      -40.33774
463           5.401139      -15.23426
471           3.787652      -18.31656
476           4.105538      -17.61656
484          -.1992027      -43.89806
492          -5.725184      -14.72818
```

```
THIS PROGRAM COMPUTES RELATIVE POWER GAIN RESPONSE FOR A FRESNEL
ZONE-PLATE RADAR PROCESSOR.
HEIGHT OF RADAR PLATFORM(KM)?435
VELOCITY OF PLATFORM(KM/S)?7.6
LENGTH OF ANTENNA(M)?3
DEPRESSION ANGLE IN DEGREES?83
CARRIER WAVELENGTH(CM)?6.3
DISTANCE BETWEEN DATA POINTS(M)?1
WHAT IS THE MAXIMUM DISTANCE VALUE YOU WANT CALCULATED(M)?500
THE MAXIMUM NUMBER OF FRESNEL ZONES IS   1534.434
HOW MANY ZONES DO YOU WANT TO PROCESS?25
WHAT FRACTION OF A ZONE SHALL BE ZERO NEAR A ZERO
CROSSING POINT OF THE FUNCTION?.11
WHAT TAPER AT HIGHEST ZONE?1.1
```

25 FRESNEL ZONES, MINIMA AND MAXIMA ONLY

X	VOLTAGE	DB.
0	9.145535	0
12	.2149646	-32.57685
17	-1.547747	-15.43018
22	.1518383	-35.59656
29	1.548436	-15.42632
37	.0543544	-44.51948
41	-.4490791	-26.17773
46	-.0343155	-48.51438
53	.6506944	-22.95664
60	-.000438	-86.3952
67	-.4206857	-26.74503
77	-.2001015	-33.19919
84	-.2357127	-31.77653
87	-.2345964	-31.81776
100	-.4885958	-25.44519
109	-.0102664	-58.99582
112	.0837145	-40.76817
115	-.0005539	-84.35605
127	-.7452094	-21.77862
133	-.6899236	-22.44816
156	-.9839929	-19.36434
171	-.0100599	-59.17231
176	.1207071	-37.58953
192	-.0026188	-70.86226
193	-.0082257	-60.92071
195	.0007529	-81.68966
220	.9757629	-19.4373
243	-.0146058	-55.93369
274	-.6631379	-22.79211
291	-.0178299	-54.2012
305	.3147213	-29.26566
325	.1899079	-33.65332
341	.4581744	-26.00357
351	.0207563	-52.8812
364	-.7882477	-21.29093
387	.0390306	-47.39609
399	1.049535	-18.80424
413	-.0057485	-64.0331
430	-.5066981	-25.1292
452	.0138221	-56.41273
462	.5355581	-24.64805
481	-.0154136	-55.46609
492	-.9366339	-19.79279

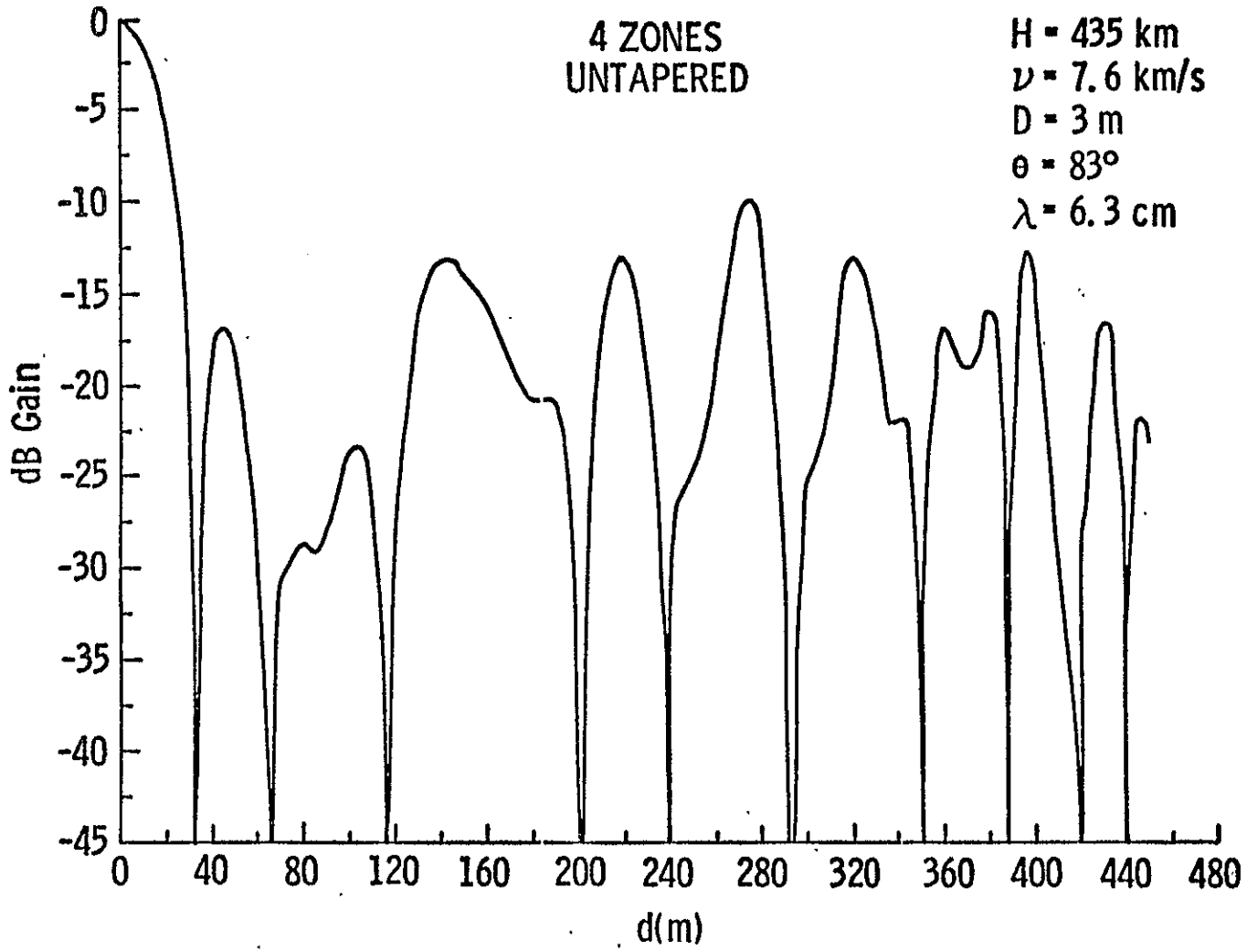
4 ZONES
UNTAPERED
H = 435 km
ν = 7.6 km/s
D = 3 m
θ = 83°
λ = 6.3 cm
dB Gain
0
-5
-10
-15
-20
-25
-30
-35
-40
-45
0
40
80
120
160
200
240
280
320
360
400
440
480
d(m)

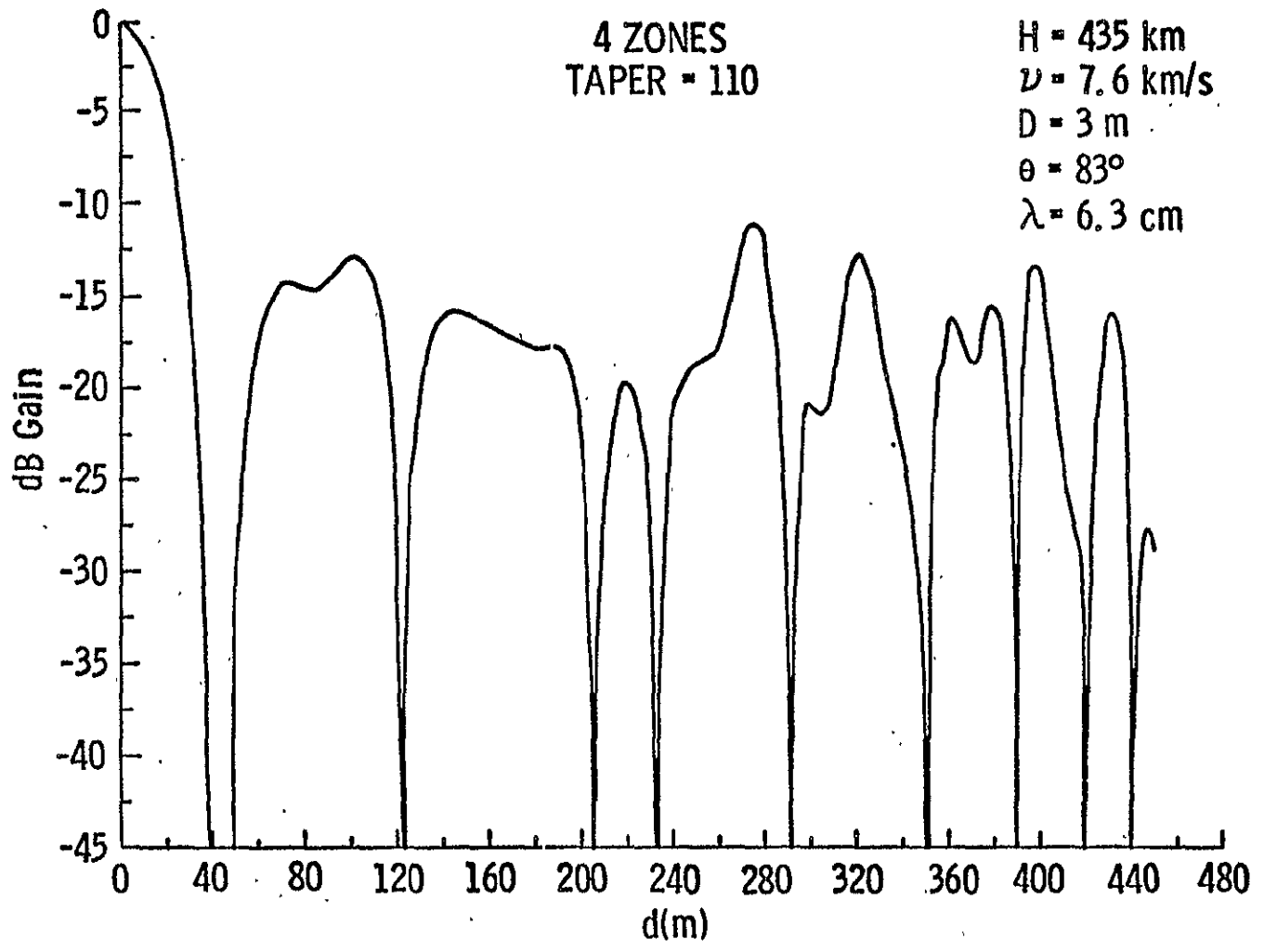

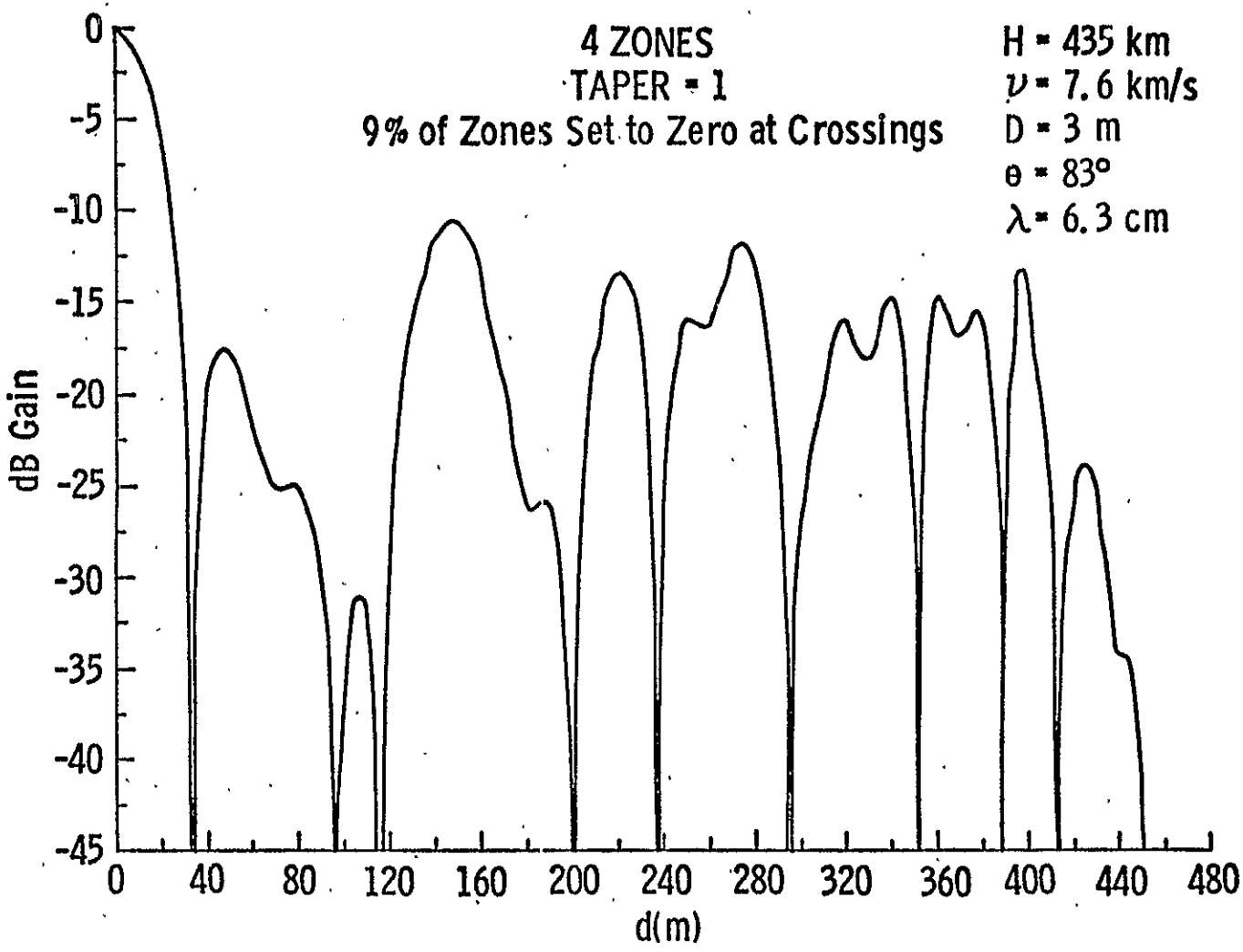
4 ZONES
TAPER = 1
9% of Zones Set to Zero at Crossings
H = 435 km
v = 7.6 km/s
D = 3 m
θ = 83°
λ = 6.3 cm
dB Gain
0
-5
-10
-15
-20
-25
-30
-35
-40
-45
0
40
80
120
160
200
240
280
320
360
400
440
480
d(m)

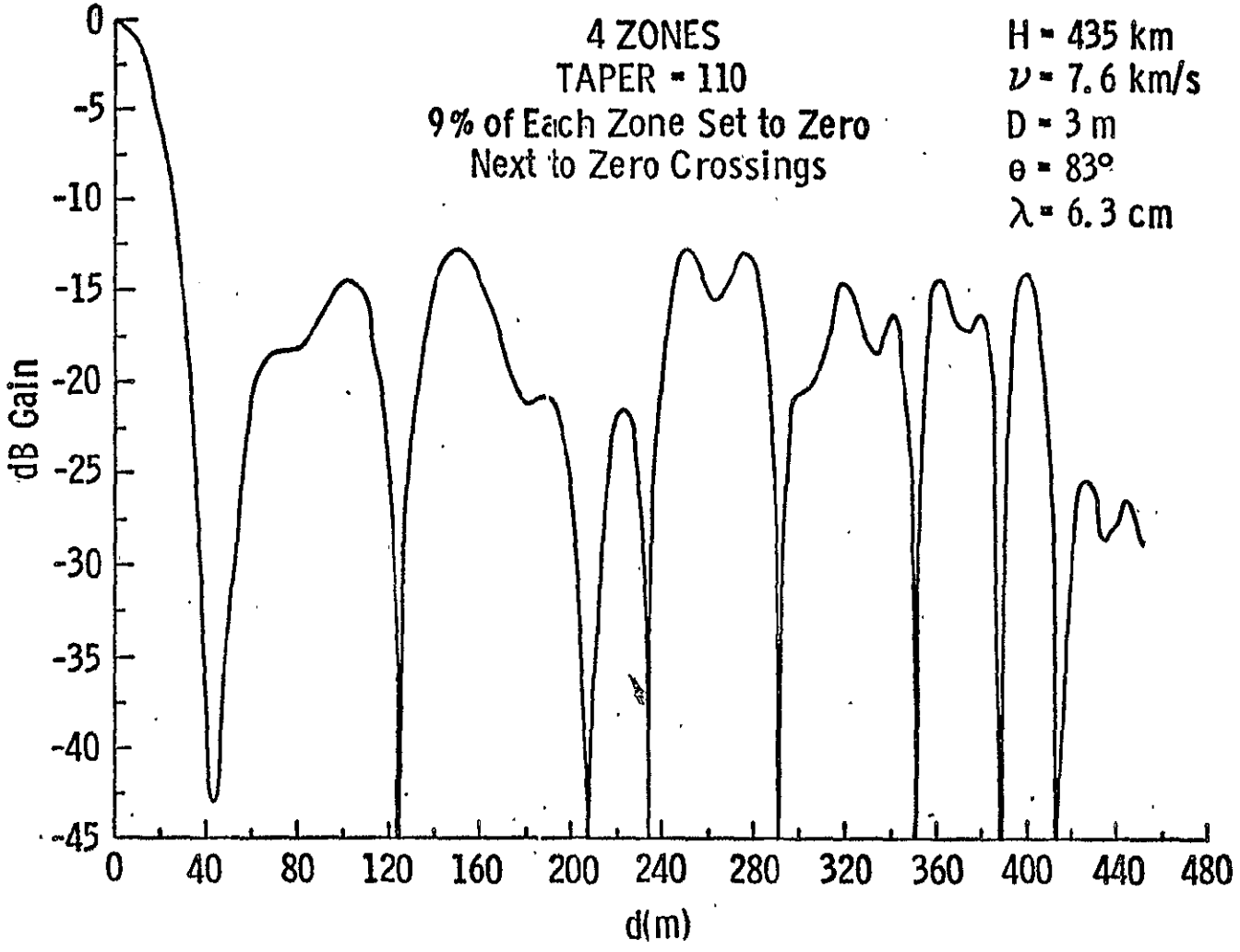

REFERENCES

1. Erickson, Rodney, "Evaluation of the Fresnel Zone-Plate Processor for Applications in Spaceborne Synthetic Aperture Radar," RSL Technical Memorandum 291-7, Remote Sensing Laboratory, University of Kansas Center for Research, Inc., Lawrence, Ks., June 1976.

2. Personal communication with R. K. Moore.

THE UNIVERSITY OF KANSAS SPACE TECHNOLOGY CENTER
Raymond Nichols Hall
2291 Irving Hill Drive—Campus West Lawrence, Kansas 66045

Telephone: 913-864-4836

A POTENTIAL DECREASE IN COMPLEXITY OF THE SAR FFT PROCESSOR

RSL Technical Memorandum 291-10

Rodney Erickson

December 1976

Supported by:

NATIONAL AERONAUTICS AND SPACE ADMINISTRATION
Goddard Space Flight Center
Greenbelt, Maryland 20771

CONTRACT NAS5-22325

ABSTRACT

One method to decrease the memory requirements of the pre-FFT memory in a synthetic aperture radar processor is discussed. This method can potentially reduce the memory requirements by up to one-half. This will substantially reduce the complexity and cost of the memory while requiring only a modest increase in the complexity of controlling circuitry.

A Potential Decrease in Complexity of the SAR FFT Processor

by

Rodney Erickson

1.0 INTRODUCTION

In a previous report,[1] a FFT processor was developed for processing synthetic aperture radar (SAR) data. Like other proposed SAR processors it is quite complex, perhaps to the point of being impractical for some applications. This report examines the pre-FFT memory, a major part of the processor, and demonstrates how its memory requirements could be lessened.

2.0 REDUCING MEMORY REQUIREMENTS OF THE FFT

In the original FFT processor design,[1] two identical memories are required such that, while the contents of one is being fed to the FFT, the other is being filled with new data. This is shown in Figure 1. The memories are composed of numerous CMOS FIFO's which are configured 16 words deep by 4 bits wide. Thus, in their present configuration, they are as shown in Figure 2.

Having two of these memories is wasteful since the equivalent of only one is being used to store data at any one time. The memory configuration in Figure 2 is what shall be called a one dimensional (1D) memory. Here data enters from the left and exits in parallel at the right. As data is read out unused memory appears at the left, growing until the whole memory is empty. A great savings in hardware could be obtained if this unused memory could be used rather than another separate memory.

An alternate memory configuration is proposed which will be called a two dimensional (2D) memory. In this memory there would be two directions of data flow. As data is read out in one direction, data is read in in a perpendicular direction. This is illustrated in

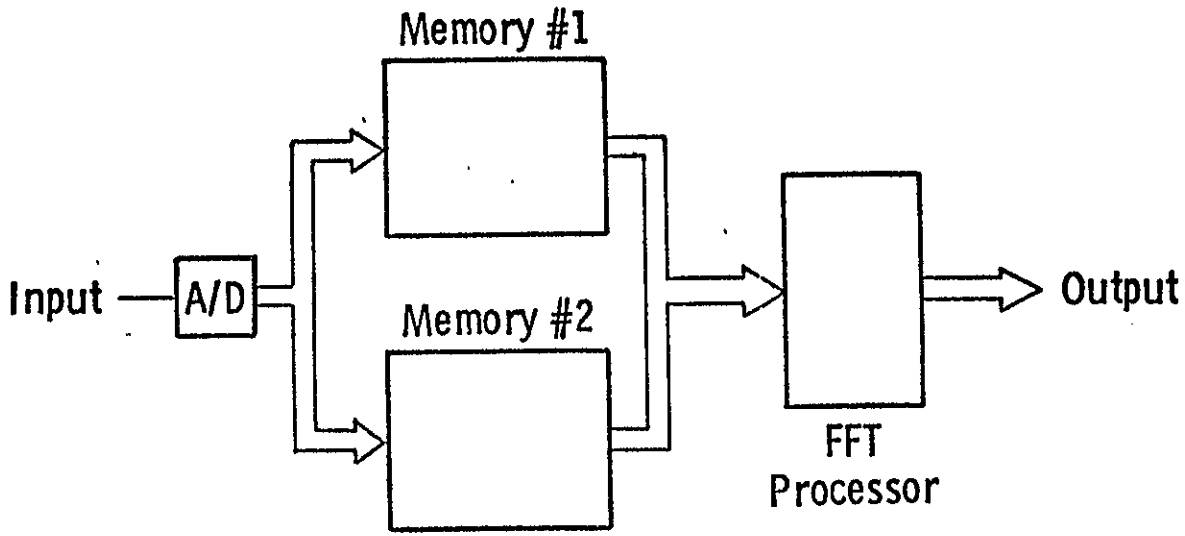

Figure 1.

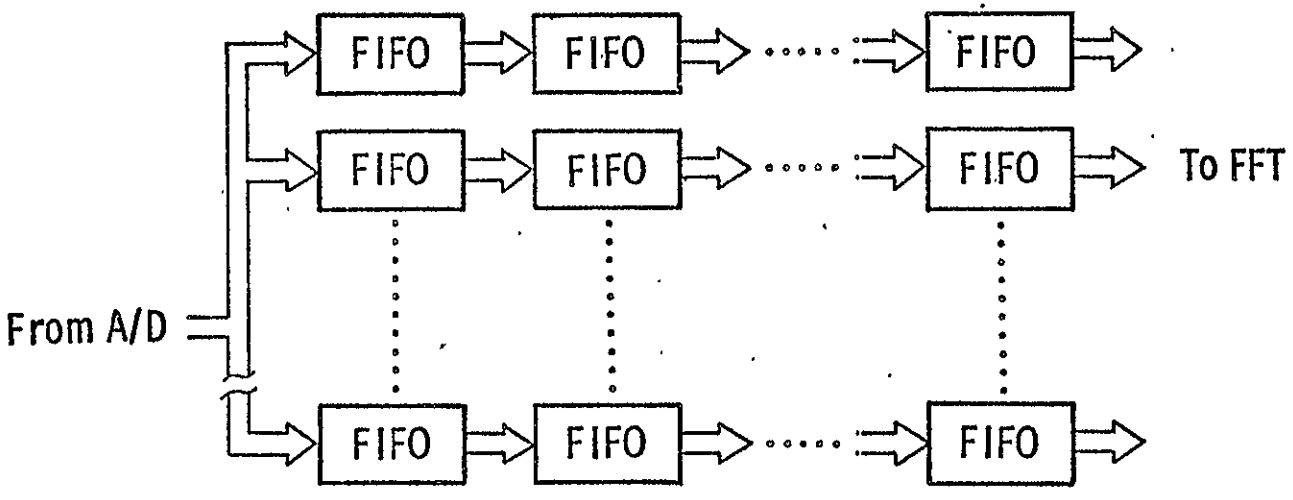

Figure 2.

Figure 3.

In this case data is read out at the right and read in from the top. When all the old data has been read out the read-in and read-out directions will change so that data is read out at the bottom and read in at the left as shown in Figure 4.

It is believed that this type of memory could be configured using the FIFO's. Some additional gating logic will be required but overall the complexity of the processor should decrease substantially. The basic FIFO configuration would become like that shown in Figure 5. Here the FIFO's are shown as four-port devices, i.e., two inputs and two outputs whereas in actuality they are only two-port devices. Some additional gating circuitry must be added to convert the FIFO to a four-port device. In Figure 5 this is assumed to be included in the blocks labeled FIFO. The gating circuitry will be selected such that it will either transfer data from left to right in the figure or from top to bottom.

Because the FIFO's are 16 words deep, either 15 extra FIFO's must be added in each dimension for buffering requirements or the FFT processor speed must be increased temporarily to empty one column (or row) of FIFO's before the first set of new data is read in. Another possibility is to require another FFT processor so that the rate of data withdrawal from the memory is increased.

Maximum memory savings with the two-dimensional memory will be in the case where the original memory configuration is square. If it is not square then the result is the type of memory shown in Figure 6. This figure shows three memory divisions, one which is truly two dimensional and two uni-directional memories. This will still represent a savings over the two separate memory case.

Let SCANSAR[1] be taken as an example. The memory required was originally configured as two 535 by 256 word memories for a total of 547840 words once I and Q storage is taken into account. For the memory configuration of Figure 6, the requirements would be

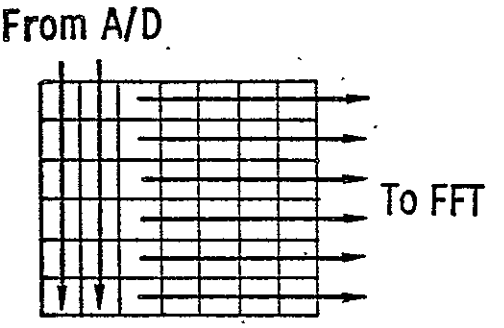

Figure 3.

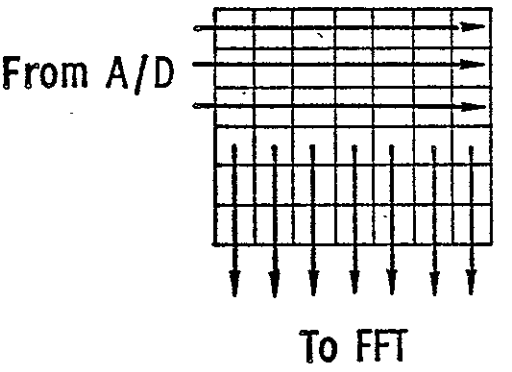

Figure 4.

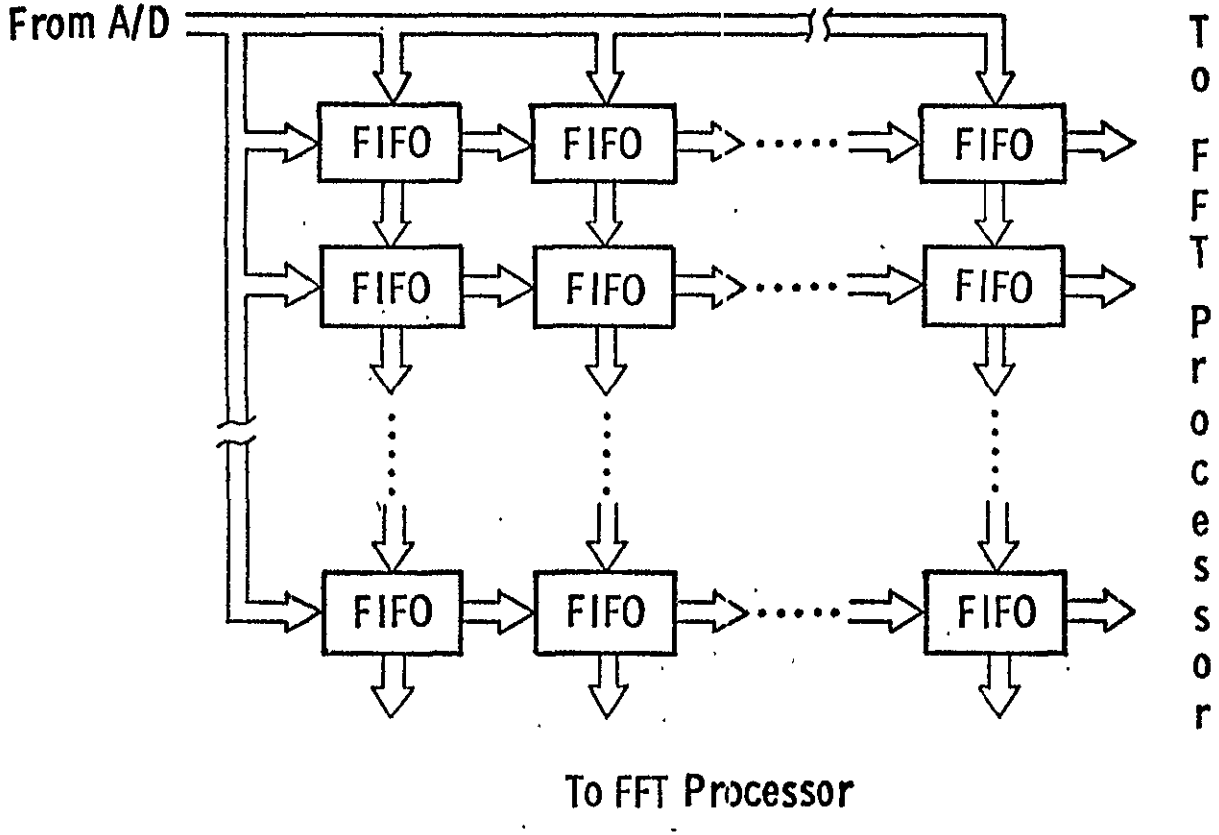
From A/D
FIFO
FIFO
FIFO
FIFO
FIFO
FIFO
FIFO
FIFO
FIFO
To FFT Processor
To FFT Processor

Figure 5.

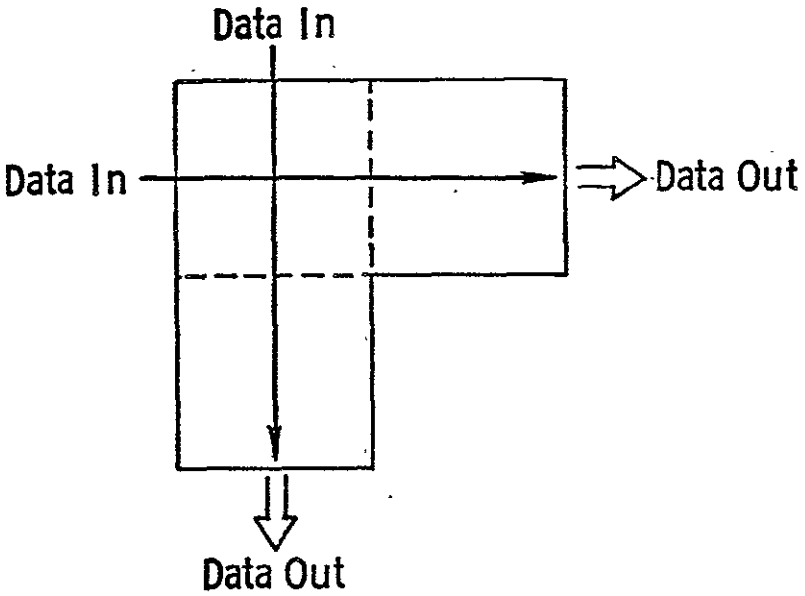

Figure 6.

$2[(256)^2 + 2(256)(279)] = 416768$ 4-bit words. This is a saving of 24% over the two memory case.

Full memory utilization has still not been achieved as 69% of the memory is idle half the time. The addition of a small amount of additional gating circuitry will allow the memory utilization to approach 100%. How this can be done is illustrated in Figure 7 for the case where a memory has 2 x 1 dimensions. 7a shows how the memory can be broken up into two square sub-memories and a data set read into them in the normal way. When the memories are full the data is simultaneously read out column by column from the right-hand side of each sub-memory via port 1 and port 2. This will require either two FFT processors or one processor with twice the speed. As this is done empty memory will appear in the left-most columns of each sub-memory. If these columns are cascaded they will be of adequate length for new data to be read in to them. This is illustrated in Figure 7b for the case where the memory has been refilled and is ready to read the data out. This is actually identical to 7a. Thus it can be seen how efficient memory utilization can be accomplished.

This concept can be extended to a generalized n x m sized memory where n and m are both integer numbers with $n \leq m$. When $\frac{m}{n} \geq 2$ the number of simultaneous, or almost-simultaneous, FFT's required go up dramatically. As seen previously for $\frac{m}{n} = 2$ two simultaneous FFT's are required. For $\frac{m}{n} = 3, 4, 5...$, the same number of simultaneous FFT's will be required. In these instances trading memory for increased processing speed will quickly become uneconomical. On the other hand for the case where $1 \leq \frac{m}{n} < 2$ and the memory is nearly square, the increase in arithmetic rate is not nearly so great. In this case one processor with a faster rate can probably be used.

3.0 CONCLUSION

One method to decrease the memory requirements of the FFT

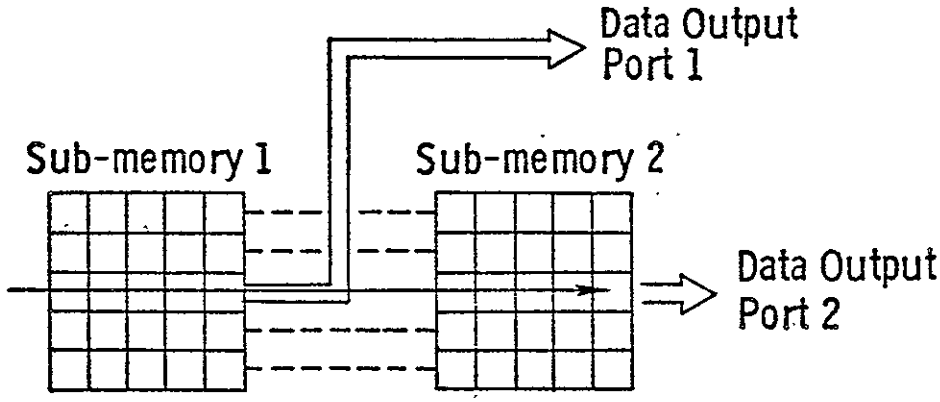

a.

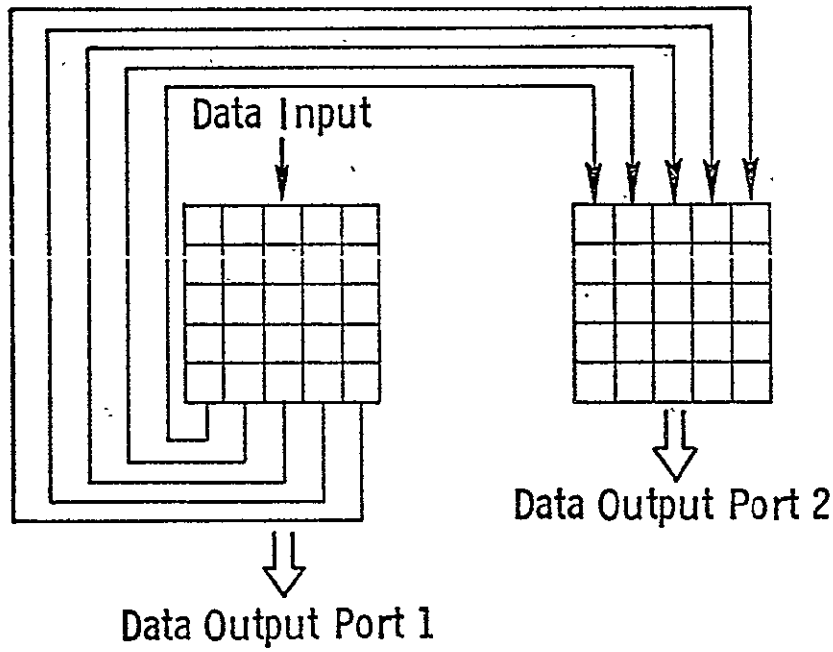

b.

Figure 7.

processor has been examined. If carried to its extreme it will decrease memory requirements by one-half. The trade-off for this reduced memory requirement is a modest increase in controller and gating circuitry and an increase in speed of the FFT's which must be done.

REFERENCES

1. Erickson, Rodney, "Focussed Synthetic Aperture Radar Using FFT," TM 295-9, University of Kansas Center for Research, Inc., Lawrence, Kansas, July, 1976.

CRINC LABORATORIES

Chemical Engineering Low Temperature Laboratory

Remote Sensing Laboratory

Flight Research Laboratory

Chemical Engineering Heat Transfer Laboratory

Nuclear Engineering Laboratory

Environmental Health Engineering Laboratory

Information Processing Laboratory

Water Resources Institute

Technical Transfer Laboratory

Air Pollution Laboratory

Satellite Applications Laboratory

CRINC